Electrostatic and Affinity Enhancements of Protein Partitioning in Two-Phase Aqueous Micellar Systems

by

Hei Ning Henry Lam

B.Sc., Stanford University (1998)
M.Sc., Stanford University (1999)

Submitted to the Department of Chemical Engineering
in partial fulfillment of the requirements for the degree of

Doctor of Philosophy in Chemical Engineering

at the

MASSACHUSETTS INSTITUTE OF TECHNOLOGY

September 2005

Signature of Author .....
Department of Chemical Engineering
15, August 2005

Certified by .....
Daniel Blankschtein
Professor of Chemical Engineering
Thesis Supervisor

Certified by .....
Daniel I. C. Wang
Institute Professor, Professor of Chemical Engineering
Thesis Supervisor

Accepted by .....
Daniel Blankschtein
Chairman, Committee for Graduate Students

Electrostatic and Affinity Enhancements of Protein Partitioning in Two-Phase Aqueous Micellar Systems

by

Hei Ning Henry Lam

Submitted to the Department of Chemical Engineering
on 15 August 2005, in partial fulfillment of the
requirements for the degree of
Doctor of Philosophy in Chemical Engineering

Abstract

This thesis was motivated by the practical need to develop a scalable and cost-effective separation method for low-cost, high-volume protein products. This unmet challenge can potentially be addressed by extraction in two-phase aqueous micellar systems, in which biomolecules can be partitioned in mild, predominantly aqueous environments. The goal of this thesis was to explore various ways of enhancing protein partitioning in two-phase aqueous micellar systems, by the incorporation of electrostatic and affinity interactions, to obtain satisfactory yield and specificity for the purification of industrially relevant hydrophilic proteins.

The electrostatically-enhanced partitioning of the enzyme glucose-6-phosphate dehydrogenase (G6PD) in two-phase aqueous mixed (nonionic/cationic) micellar systems was investigated experimentally and theoretically. The successful enhancement, up to 22-fold, of the partitioning of the negatively-charged G6PD was attained by adding the positively-charged surfactant alkyltrimethylammonium bromide (C_nTAB) to form charged mixed micelles with the phase-forming nonionic surfactant, decyl tetra(ethylene oxide) ($C_{10}E_4$). The effects of the tail length of the positively-charged surfactant on protein denaturation and protein partitioning behavior were also studied. Furthermore, the experimental results were used to validate a predictive theory for electrostatic enhancement.

In the area of affinity enhancement, the affinity-enhanced partitioning of an engineered affinity-tagged protein, CBM9-GFP (Green Fluorescent Protein linked to a carbohydrate-binding module), in two-phase aqueous micellar systems was investigated experimentally and theoretically. The experimental results showed that the partition coefficient of the target protein, CBM9-GFP, can be improved more than 6-fold, by virtue of the affinity interactions, and that the enhancement is specific to the target protein. The system utilized requires only one surfactant, decyl β-D-glucopyranoside ($C_{10}G_1$), which acts simultaneously as the affinity ligand and as the phase-forming surfactant, and as such, has important practical advantages. A novel theoretical framework to describe affinity-

enhanced protein partitioning in two-phase aqueous micellar systems was developed and validated experimentally. In addition, the separation method developed was successfully applied to a real cell lysate. It was found that the protein impurities in the cell lysate do not interfere with the partitioning of the target protein (CBM9-GFP) at industrially relevant concentrations, and that the protein impurities were concentrated away from the target protein. Lastly, the theoretical description developed was used to identify various strategies for improving the affinity-enhanced partitioning of the target protein in two-phase aqueous micellar systems.

Although more work remains to be done before the separation methods studied in this thesis can reach their full potential and be eventually commercialized, this thesis nevertheless represents an essential starting point for future efforts to improve, extend, and commercialize this promising bioseparation method.

Thesis Supervisor: Daniel Blankschtein
Title: Professor of Chemical Engineering

Thesis Supervisor: Daniel I. C. Wang
Title: Institute Professor, Professor of Chemical Engineering

Acknowledgments

No one completes the thesis alone. I would like to express my gratitude to the people who have made this possible.

I would first like to thank Professor Daniel Blankschtein, one of my advisors, for his unwavering support and invaluable mentorship throughout my Ph.D. journey. He taught me the importance of insisting on good-quality research, being attentive to details, and treating people with respect. I thank him for his forgiveness for the many mistakes I have made, for the patience to see me through my struggles, and for the genuine love and care for me as a person. He gave me a positive outlook and made my life here pleasant even in the most trying times.

Professor Daniel. I. C. Wang, also my advisor, deserves the highest of gratitude for his inspiration to me and his valuable input to the thesis. He provided an essential practical perspective and taught me about the importance of having impact for one's research. I would also like to thank him for the good times we had during our group seminars, in which he shared many interesting and insightful personal stories, and for placing me in the excellent internship at Beyond Genomics, Inc., during the summer of 2003.

Professor T. Alan Hatton and Professor Paula T. Hammond, members of my thesis committee, are always supportive and thoughtful. I would like to thank Professor Hatton for his valuable insight in various aspects of my research, and Professor Hammond for her indispensable help in my organic synthesis endeavor.

This thesis would not have been possible if not for the generous help of my collaborators, Mojgan Kavoosi and Professor Charles A. Haynes of the University of British Columbia. I am grateful for their tremendous interest in my work, the efficiency and promptness with which they provided me with materials, and the inspiring exchange of ideas throughout the collaboration.

I next want to thank Professor Daniel T. Kamei, who was the senior graduate student who worked on two-phase aqueous micellar systems when I first came to MIT. Dan was a major reason why I chose this project as my thesis topic in the first place. He patiently

and meticulously taught me all the experimental techniques, down to the smallest details, that were involved in the project. He always had an answer for all my questions, silly or not. Although he and I have only overlapped for about 14 months, the seriousness and integrity with which he approached his work has set an excellent example for me.

I will definitely miss the members of the Blankschtein group. I have enjoyed Isaac's sense of humor and benefited from his words of wisdom. I am grateful for the honor to work with Carlota and Priscila, the charming Brazilian ladies, whom I have to thank for our excellent teamwork. Arthur, my fellow classmate, is always nice and giving, and seems to show an interest in just about everything. I thank Dick for the numerous stimulating intellectual exchanges, and the great times we had in the Vancouver conference. Peter, Hua, Betty, Mike, Vibha were all very friendly and helpful to me when I first started in the group. The younger members of the group: Joe, Saswata, Srinivas, Brian, Jonathan, have made the lab a very lively place. I wish them all the best in their research in the future. I cannot but feel extremely grateful for our friendship and the great memories we had together.

I also have to thank the many postdocs and graduate students in the department who have generously lent a helping hand to my research. My greatest gratitude goes to Dr. Mark A. Johnson, who had volunteered countless hours of his precious time to help me in my painstaking organic synthesis experiments. Mark, who never said a harsh word despite how much I had bothered him, shared my frustration and joy, as if my ill-fated experiments were his own. Dr. Jin Yin of the Wang group always had a smile on his face. He taught me how to do fermentation and showed me many protein assay techniques, and is a good colleague and friend. Dr. Russell Lachance of the Tester group has helped me with some surfactant assay experiments and kindly allowed me to use his equipment. Various members of the Hatton group have also kindly shared their fluorimetry facility with me.

My life at MIT would not have been so enjoyable and memorable without my brothers and sisters in Christ, and many great friends who care for me and cheer me on throughout

my Ph.D. journey. They have made MIT and Boston a home away from home for me. I learned a great deal from all of them, and I look forward to seeing our friendship grow even more as we move on to the next stage of our lives.

No word could express my gratitude to my parents and my brother, who have loved me dearly and have always been supportive and appreciative of whatever I do. Mom and Dad have always given me the freedom to pursue my interest and put me in the best position to succeed. Teddy, my little brother who's not little any more, has shared with me many moments of fun and joy over the years.

I cannot imagine how I would do without my wife, Ruby. She had the unenviable job of cheering me up after every one of my frustrating days at work. In spite of it all, she has always believed in me and given me the strength and confidence I need to keep running until the finish line. I am thankful for her cheerfulness and ever-positive attitude, which has made my world as bright and as lively as it is.

Finally, I would like to acknowledge the financial support provided by the NIGMS/NIH MIT Interdepartmental Biotechnology Training Program (Grant no.5 T32 GM08334), and the Industrial Technology Research Institute of Taiwan.

Contents

List of Figures

List of Tables

Part I

Motivation and Background

Chapter 1

Motivation

Over the past decade, the biotechnology industry has been dominated by low-volume, high-value human health-care products. For these products, the manufacturing cost represents a very small fraction of the selling price, which can range from hundreds of thousands to over a billion dollars per kilogram. It is therefore reasonable that engineering process improvements do not alter the price structure significantly in such cases, and that there has not been an emphasis of research and development for new technologies in downstream processing, that is, in the painstaking task of concentrating and purifying the desired products from a complex mixture harvested from the fermentation host. Typical downstream processes for such products, therefore, are often expensive and, in many cases, inefficient, as attention has been directed to achieving high purity and quality without much regard to cost [1, 2].

However, it can be expected that as the relevant protein engineering technologies mature, more and more high-volume, low-cost bio-based products will find their ways to the market. It is also expected that these products will command a totally different price structure than that of human therapeutics, and that a more cost-effective downstream purification scheme will likely translate into a competitive advantage in the market. In some cases, novel engineering concepts and technologies will be required in order to attain economic viability for these products against their conventional counterparts. Some

examples include bio-based materials such as collagen, nutrition and health products, industrial enzymes, biosurfactants, antibiotics, and commodity chemicals from biological sources [1, 2, 3, 4].

Currently, existing downstream processing schemes typically consist of multiple unit operations, many of which involve chromatographic steps. Understandably, these downstream processing schemes are tailored for high-cost, low-volume products, in which purity and quality are often the only design consideration of the process engineer. Although excellent in achieving purity, such processes are time-consuming, extremely costly, and difficult to scale-up, and depending on the nature of the stationary phase, may require frequent shutdown and column regeneration [1]. Moreover, fouling is a serious problem in almost every chromatographic operation, and cleaning is often a necessary step upstream of the columns to make sure that the feed is free of solid particles or deactivating agents [5]. Typically, membranes are employed in filtration processes to accomplish this task. However, membranes are often expensive, and they are also prone to fouling, and need to be continually replaced or regenerated [6]. This issue, along with the formidable engineering challenge of building and packing large-scale chromatographic columns, makes it necessary for the process engineers to seek alternative ways to concentrate and purify biotechnological products that are cost-effective at a larger scale [1].

Liquid-liquid extraction, on the other hand, is well-known to the chemical engineer as an easy, cost-effective, and scalable separation technique. It can be designed to run continuously without the need of frequent maintenance shutdowns [7]. Unlike chromatography, which depends on the unimpeded flow of liquid through tiny and tortuous paths between solid packings, liquid-liquid extraction is more tolerant to the presence of solid particles in the feed stream. Upstream cleaning and solid removal procedures can therefore be reduced or eliminated. Conventional extraction in the chemical engineering industry, however, makes use of organic-aqueous biphasic systems. This not only requires the use of large amounts of organic solvents, but in the case of biomolecules, may also cause denaturation and loss of activity of the product [8]. Moreover, since hydrophobicity

is the only differentiating parameter in such systems, they are unable to handle biological mixtures, given that these mixtures typically consist mostly of molecules with similar hydrophobicity. Consequently, conventional organic-aqueous extraction systems are often ill-suited for applications involving biomolecules [8]. Luckily, in the past few decades, two-phase aqueous complex-fluid systems have emerged as a promising alternative to organic-aqueous extraction systems. These include two-phase aqueous polymer systems, in which water-soluble polymers, such as poly(ethylene glycol) (PEG) and dextran, are the main ingredients, and two-phase aqueous micellar systems, in which surfactants are utilized to induce phase separation. In both cases, the two immiscible phases formed are predominantly aqueous (over 90% water by weight), with only a small amount of added phase-forming polymers or surfactants, thus providing a mild environment for the delicate biomolecules [8, 9]. It has also been established that these systems, unlike conventional organic-aqueous systems, enable separation based not only on hydrophobicity but also on size. This is particularly important, because in the recovery of useful biomolecules, it is often necessary to remove large particles, for example, other protein impurities, cell debris, and viruses. For example, it is anticipated that these two-phase aqueous complex-fluid systems can potentially replace such expensive operations as membrane filtration for viral clearance [10, 11, 12]. This makes the proposed method very attractive for large-scale industrial purification processes, since these solid-removal operations increase the complexity of the process and add significantly to the cost. Lastly, the capacity of the chromatographic column is limited by the length scale of the stationary phase, which rarely falls below the micrometer range. Polymers and micelles, however, are extremely small, having length scales in the nanometer range. It is therefore expected that these polymer or micellar systems should provide a much higher surface area for interaction, and consequently, a much higher protein capacity [13]. In summary, it is believed that these novel extraction systems can replace and complement the existing chromatographic operations to solve important separation problems in the biotechnology industry.

This thesis was conceived with this great promise in mind. The main focus of the

work presented in the following chapters is to address some of the challenges that exist in applying two-phase aqueous micellar systems to real industrial applications. Some background information on two-phase aqueous micellar systems is provided in Chapter 2, followed by a detailed roadmap and overall organization of the entire thesis in Chapter 3.

Chapter 2

Two-Phase Aqueous Micellar Systems

This chapter provides a pedagogical description of two-phase aqueous micellar systems. Section 2.1 presents an overview of surfactants and their unique behavior in aqueous solutions. Section 2.2 details the formation and characteristics of two-phase aqueous micellar systems. Section 2.3 surveys applications involving the use of two-phase aqueous micellar systems. Lastly, Section 2.4 briefly compares two-phase aqueous micellar systems to the more well-known two-phase aqueous polymer systems.

2.1 Surfactants and Micellization

Surfactants are chemical species that consist of two covalently-attached distinct moieties: a hydrophilic moiety typically referred to as the "head," and a hydrophobic moiety typically referred to as the "tail." Chemically, the "tail" is typically a hydrocarbon, which can be either straight-chained or branched, or in some specialized surfactants, a fluorocarbon. The "head" derives its hydrophilicity from a positive or negative charge (in the case of ionic surfactants), from extensive hydrogen bonding with water (in the case of nonionic surfactants), or from a strong dipole moment (in the case of zwitterionic

surfactants) [14]. Some common surfactants and their chemical structures are shown in Figure 2-1.

Because of their dual nature, surfactants have very unique and useful properties when they are dissolved in water. For example, surfactants tend to adsorb at the air-water interface (if one exists), extending their hydrophobic tails into the air phase to minimize their contact with water. As such, they lower the surface tension of the solution, and are therefore "surface-active." In the bulk water, surfactant molecules exhibit another important property – self-assembly, that is, the formation of macromolecular aggregates known as micelles. This phenomenon of micellization takes place only at surfactant concentrations above a characteristic threshold called the critical micelle concentration (CMC), which varies with the structure of the surfactant and with the solution conditions (temperature, type and concentration of added salt, pH, etc.). In a micelle, surfactant molecules orient themselves such that the hydrophilic heads reside at the surface of the micelle, in contact with the water, and the hydrophobic tails flock to the interior to form the micellar core, away from the water. Furthermore, hydrophobic solutes, ordinarily insoluble in an aqueous medium, exhibit an increased aqueous solubility in the presence of micelles, as these molecules can be accommodated in the hydrophobic micellar core [14]. Because of these unique characteristics, surfactants have important uses in our daily lives as wetting and foaming agents, and as cleansers and emulsifiers [15, 16, 17, 18].

It is important to note that monomeric surfactants, which are freely distributed in the bulk water, exist in chemical equilibrium with the surfactants present in the micelles. In fact, above the CMC, the concentration of monomeric surfactants is closely approximated by the CMC, irrespective of the total surfactant concentration. Accordingly, the CMC can often be loosely interpreted as a "solubility limit" of the monomeric surfactants in water. This typical behavior of a micellar solution is captured in Figure 2-2, where the monomeric surfactant concentration, X_1, is plotted against the total surfactant concentration, X. Below the CMC, all the surfactant molecules exist as monomers, whereas above the CMC, any *additional* surfactant added forms micelles, resulting in a constant

Decyl tetra(ethylene oxide) ($C_{10}E_4$), a nonionic surfactant

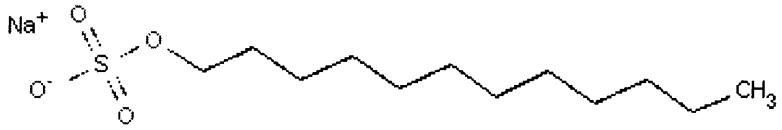

Sodium dodecyl sulfate (SDS), an anionic surfactant

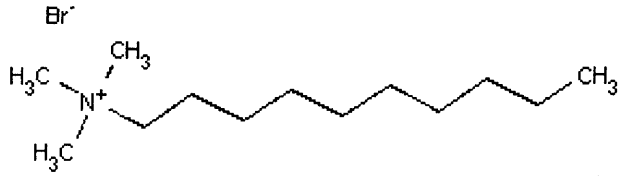

Decyl trimethylammonium bromide (C_{10}TAB), a cationic surfactant

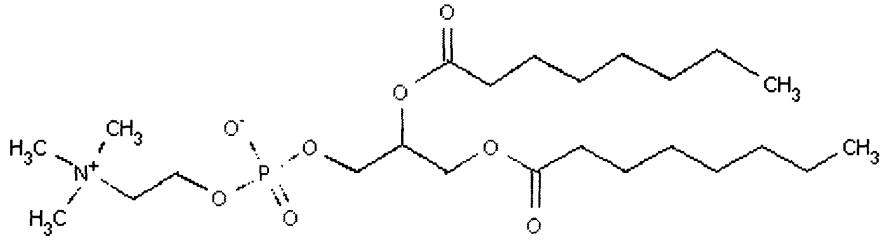

Dioctanoyl phosphatidylcholine (C_8-lecithin), a zwitterionic surfactant

Figure 2-1: Various types of surfactants and their chemical structures.

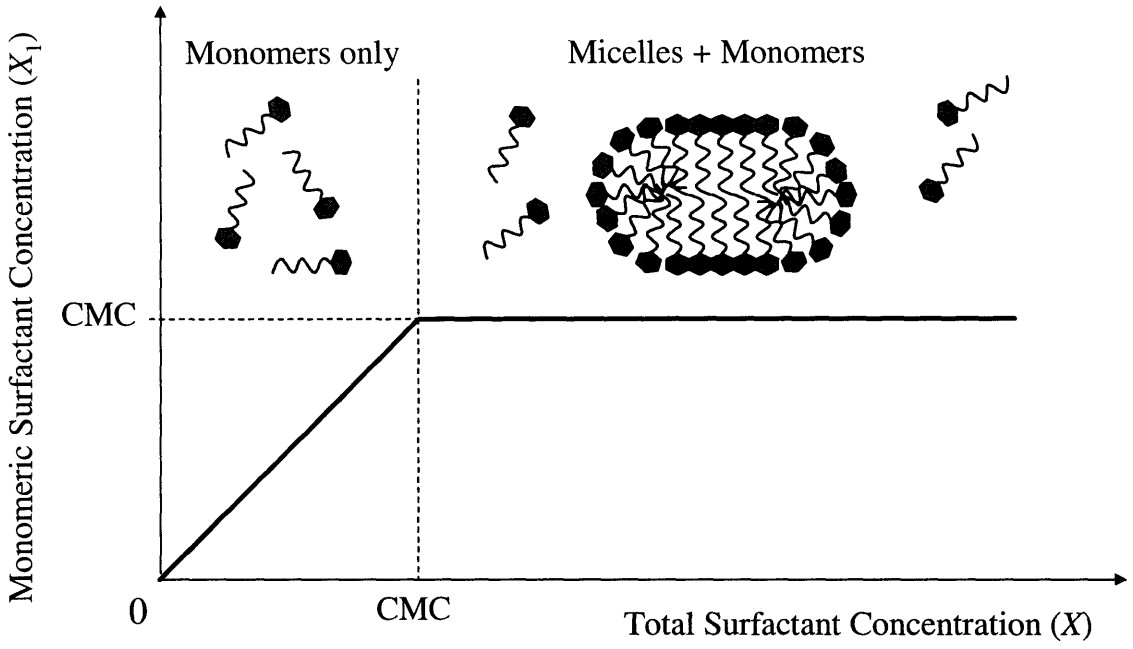

Figure 2-2: A typical plot of the monomeric surfactant concentration (X_1) versus the total surfactant concentration (X) for an aqueous solution of a single surfactant.

monomeric surfactant concentration [14].

Micellization results from a delicate balance of intermolecular forces, including steric, electrostatic, hydrophobic, hydrogen bonding, and van der Waals interactions. In general, the attractive hydrophobic interactions between the hydrophobic tails of the surfactant molecules are opposed by the repulsive steric and/or electrostatic interactions between the hydrophilic heads. The balance of these interactions determine the optimal micelle shape, size, and in the case of mixed surfactant systems, the surfactant composition of the micelle [19]. Depending on the surfactant chemistry and the solution conditions, micelles can take on various shapes and sizes. They can be spherical, in which case there is minimal micellar growth, cylindrical, in which case there is one-dimensional micellar growth, or discoidal or bilayer-like, in which case there is two-dimensional micellar growth. For example, nonionic surfactants of the types used in this thesis to generate two-phase aqueous micellar systems, exhibit one-dimensional growth to form long cylin-

drical micelles. In general, cylindrical and discoidal micelles exhibit size polydispersity. As a result, not all the micelles formed are of the same size. The shapes and sizes of the micelles formed are often critical to their functions; for example, surfactant bilayers are what make up the cell membranes in a living organism [19, 20].

The micellar characteristics and various useful properties of a given surfactant solution can be predicted by a molecular-thermodynamic theory of micellization developed by the Blankschtein group. Specifically, to obtain the optimal micellar characteristics for a given surfactant (or surfactant mixture) and a set of solution conditions, the free-energy change associated with taking a surfactant monomer in water and placing it in a micelle, referred to as the free energy of micellization, g_{mic}, is minimized with respect to various micellar properties, such as the micellar shape, S, the cross-sectional radius of the micellar core, l_c, the surfactant composition of the micelle, α_{mic} (in the case of surfactant mixtures), and the degree of counterion binding, β (in the case of charged surfactant(s)). The free energy of micellization, g_{mic}, is evaluated as a function of these quantities by breaking down the micellization process into a series of well-defined, reversible steps, each contributing to the formation of the micelle. The optimal values for these micellar properties, as well as the optimal value of g_{mic}, resulting from the free energy minimization allows the calculation of useful micellar characteristics, such as the CMC and the average aggregation number of micelles. The predictions from this theory have been shown to be in very good agreement with the experimental data. For more details, the interested reader is referred to the article by Zoeller et al. [21] and the references therein.

2.2 Phase Separation in Aqueous Micellar Solutions

Many micellar solutions, most typically solutions of nonionic and zwitterionic surfactants, exhibit interesting phase behavior. They form a variety of solid and liquid phases depending on the solution conditions [22]. Two-phase aqueous micellar systems form in the so-called "miscibility gap," in which the micellar solution spontaneously separates into

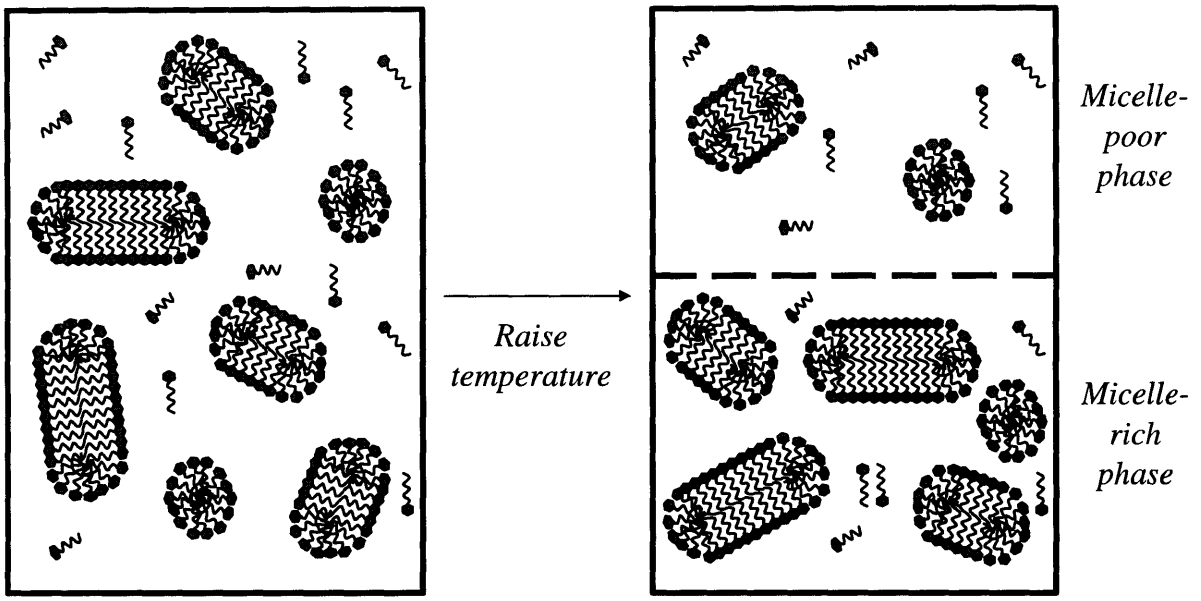

Figure 2-3: Schematic representation of a two-phase aqueous micellar system. In this example, phase separation is induced by an increase in the solution temperature.

two coexisting isotropic liquid phases, one containing a higher concentration of surfactants (referred to as the micelle-rich phase) than the other (referred to as the micelle-poor phase). Schematically, this phenomenon is shown in Figure 2-3.

Figure 2-4 shows the phase diagram of the nonionic surfactant decyl tetra(ethylene oxide), $C_{10}E_4$ (whose structure is shown in Figure 2-1), in the vicinity of the miscibility gap. In Figure 2-4, the coexistence (or binodal) curve, which represents the boundary between the one-phase region and the two-phase region at constant pressure, is shown. In general, depending on the structure of the surfactant, the coexistence curve can either be concave upward (as in Figure 2-4), implying that phase separation can be induced by an increase in temperature, or concave downward, for example, in the case of the zwitterionic surfactant, C_8-lecithin, which exhibits phase separation as the temperature is decreased. The minimum (or maximum) of the coexistence curve is known as the

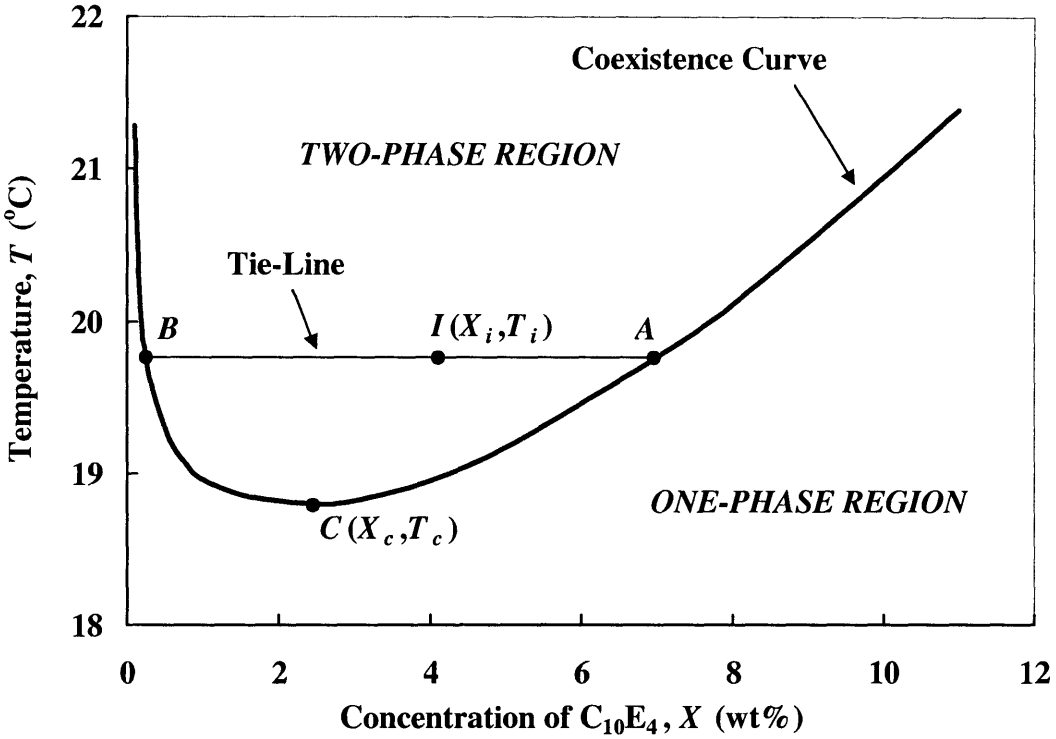

Figure 2-4: The phase diagram of the binary $C_{10}E_4$/water system at a constant pressure of 1 *atm*, adapted from Liu et al., 1996 [25].

lower (or upper) consolute or critical point (Point C in Figure 2-4). The surfactant weight fraction and temperature corresponding to the critical point are known as the critical surfactant concentration, X_c, and the critical temperature, T_c [20, 23, 24].

At the solution conditions represented by the point I in Figure 2-4, the micellar solution spontaneously separates into two coexisting phases. The conditions corresponding to the micelle-rich phase are represented by point A, and the conditions corresponding to the micelle-poor phase are represented by point B, as shown in Figure 2-4. The line BA is referred to as a tie-line. The phase ratio, r, defined as the ratio of the volume of the micelle-rich phase, V_α, to that of the micelle-poor phase, V_β, can be calculated by

the so-called lever-rule:

$$r \equiv \frac{V_\alpha}{V_\beta} = \frac{\overline{BI}}{\overline{IA}} \tag{2.1}$$

which can be obtained by enforcing a material balance on the surfactant species. Both the micelle-rich and the micelle-poor phases remain at the same temperature T_i. Consequently, any phase-separating system prepared at the temperature T_i, regardless of the initial surfactant concentration, will share the same tie-line BA. The phase diagram therefore enables one to determine the surfactant concentrations in each coexisting phase, as well as the phase ratio, given the initial surfactant concentration, X_i, and the temperature, T_i, at which the phase separation takes place. Note that since both the micelle-rich and micelle-poor phase surfactant concentrations are above the CMC, both phases contain micelles as well as monomeric surfactant. The average micellar size and the polydispersity of the micelles are different in the two phases, because as discussed in the Section 2.1, the surfactant concentration can influence micellar size. Nevertheless, both phases are predominantly aqueous, with even the micelle-rich phase containing at least 80% by weight water [10].

The phenomenon of two-phase aqueous micellar systems can be understood in terms of a competition between enthalpic and entropic effects that depends on the solution temperature, as captured in the following equation for the solution Gibbs free energy:

$$G = H - TS \tag{2.2}$$

where G is the solution Gibbs free energy, H is the solution enthalpy, T is the absolute temperature, and S is the solution entropy. The entropic effect favors a single, homogeneous phase, and is expected to increase as the temperature increases, according to Eq. (2.2). The enthalpic effect, which originates from the attractive forces between micelles and is often hydrophobic in nature, favors phase separation. The enthalpic term is often a strong function of the solution temperature as well. For example, the extent of hydrogen bonding between the ethylene oxide groups in C_iE_j-type nonionic

surfactants and water depends strongly on temperature. With increasing temperature and increased thermal motion, the ordered structure of water and the directionality of the hydrogen bonds are weakened, increasing the hydrophobicity of the micelles, and thereby increasing the intermicellar attractions. This explains why aqueous solutions of C_iE_j-type surfactants exhibit a lower consolute point (phase separation occurring as the temperature increases), even though the increasing entropy at higher temperatures favors a single phase [23, 24].

A phenomenological theory has been developed previously in the Blankschtein group to model the phase separation behavior of two-phase aqueous micellar systems [23, 24]. In the context of this theoretical framework, the phase behavior of aqueous surfactant solutions can be modeled in terms of two physically relevant parameters, C (a measure of the strength of the intermicellar attractions), and $\Delta\mu$ (a measure of the tendency for micellar growth). If these two parameters are known as functions of temperature, the coexistence curve can be predicted for any given two-phase aqueous micellar system. The interested reader is referred to the original articles by Blankschtein et al. [23, 24] for a detailed discussion of the theory. The same theory can be generalized to a binary surfactant mixture, with the single intermicellar interaction parameter C replaced by three interaction parameters C_{AW} (reflecting the interactions between surfactant A and water), C_{BW} (reflecting the interactions between surfactant B and water), and C_{AB} (reflecting the interactions between surfactants A and B) [26, 27].

2.3 Applications involving Two-Phase Aqueous Micellar Systems

This section provides a brief review of the important applications of two-phase aqueous micellar systems in liquid-liquid extractions. Examples of applications in the environmental remediation area are described in Section 2.3.1, and applications in the bioseparation area are described in Section 2.3.2. The difference in the physicochemical environments

between the two coexisting micellar phases allows various chemical and biological molecules to partition unevenly between the two phases, thereby enabling an effective separation. Because the onset of phase separation of a micellar solution is often accompanied by a characteristic clouding of the solution, the temperature at which phase separation occurs is often called the "cloud point," and extractions involving two-phase aqueous micellar systems are often called "cloud-point extractions" [8, 13].

2.3.1 Environmental Remediation and Preconcentration of Toxic Compounds for Analysis

Because the two coexisting micellar phases possess hydrophobic domains as part of the micellar cores, these systems can be used to separate molecules based on hydrophobicity. Therefore, two-phase aqueous micellar systems find important applications in the environmental remediation area, where there is often a need to separate and concentrate organic compounds. Cloud-point extraction has comparable or superior effectiveness to conventional organic-aqueous biphasic extractions, and is much more economical, safe, and environmentally friendly, because it does not require a large amount of organic solvents, which are usually toxic and flammable. Furthermore, when compared to conventional organic-aqueous extractions, cloud-point extraction typically requires smaller volumes of the aqueous sample in order to obtain the same sample concentration factor. Many analytical methods offer enhanced sensitivity due to the fact that concentration factors in the range of 10 to 100 are easily obtained with good recoveries using cloud-point extractions [13].

Historically, cloud-point extraction was pioneered by Watanabe and co-workers [28], who utilized this method for the effective extraction of metal ions as hydrophobic metal chelate complexes, which partition to the micelle-rich phase. The commercial surfactants Triton X and PONPE are popular choices for the phase-forming surfactants in these applications. The preconcentration of metal chelates, followed by chromatographic and/or spectrophotometric analysis, is a well-established technique for detecting and quantifying

trace metals in environmental samples. Detection limits of the metal ions of interest can be made as low as several parts per billion or in the nanomolar range [29, 30, 31].

In addition to metal chelates, many organic compounds, due to their hydrophobic character, are also solubilized in the hydrophobic cores of the micelles, and therefore, can be extracted to the micelle-rich phase in a two-phase aqueous micellar system. This also has important application in the area of environmental remediation, where it is often necessary to detect and sometimes remove trace organic toxins from contaminated water. Cloud-point extraction has been employed to successfully concentrate and/or remove important classes of common and dangerous pollutants in an aqueous media, such as phenols [32], polychlorinated biphenyls (PCB) [33], polychlorinated dibenzo-*p*-dioxins (PCDD) [34], polycyclic aromatic hydrocarbons (PAH) [34, 35, 36], and various toxins in many pesticides [37, 38].

2.3.2 Purification and Concentration of Biological Molecules

As stressed in Section 2.2, since the two coexisting micellar phases are both predominantly aqueous, two-phase aqueous micellar systems generally provide a mild and nondenaturing environment for proteins and other biomolecules. Most of the earlier work on protein separation in these systems has exploited differences in hydrophobicity [8, 39, 40, 41]. Bordier was the first to separate proteins using two-phase aqueous nonionic micellar systems. Utilizing the Triton X-114 two-phase aqueous micellar system, Bordier showed that hydrophilic, water-soluble proteins (serum albumin, catalase, ovalbumin, concanavalin A, myoglobin, and cytochrome c) preferentially partition into the micelle-poor phase, while hydrophobic or integral membrane proteins (acetylcholinesterase, bacteriorhodopsin, and cytochrome c oxidase) preferentially partition into the micelle-rich phase [42]. Some practical applications have been developed based on this concept. For example, large-scale purification of pyruvate oxidase from other enzymes, with a recovery of 95% into the micelle-rich phase, has been demonstrated using the Triton X-114 two-phase aqueous micellar system [41]. Two-phase aqueous micellar systems can also be used to purify

platelet compounds, since platelets glycoproteins have been found to partition favorably into the micelle-rich phase, while fibrinogen, albumin, and actin have been observed to partition into the micelle-poor phase [43]. In addition to proteins, two-phase aqueous micellar systems have also been used to separate small hydrophobic molecules from biological sources, such as vitamins [44], hormones [45] and lipids [46].

In the case of hydrophilic, water-soluble proteins, the potential for separating these biomolecules based on size differences was first recognized by the Blankschtein group. When the partitioning behavior of hydrophilic proteins (cytochrome c, ovalbumin, catalase, soybean trypsin inhibitor, and bovine serum albumin) was investigated in the two-phase aqueous micellar system composed of the nonionic surfactant $C_{10}E_4$, it was found that the bigger the protein, the more extremely it partitions into the micelle-poor phase [25, 47, 48]. These experimental findings suggested that for hydrophilic proteins, the observed protein partitioning behavior is driven primarily by repulsive, steric, excluded-volume interactions between the proteins and the micelles. Specifically, because these hydrophilic proteins reside in the aqueous domain outside of the micelles, they partition preferentially to the micelle-poor phase, where they experience less excluded-volume interactions with the micelles. In addition, the protein partitioning behavior can also be understood from an entropy point-of-view, since hydrophilic proteins can sample a greater number of configurations in the micelle-poor phase, due to the larger free volume available. Based on this excluded-volume hypothesis, statistical thermodynamics was used to develop a theory to rationalize the partitioning behavior of hydrophilic proteins [47, 49]. Using the following expression for the protein partition coefficient, K_p, defined as the ratio of the protein concentration in the micelle-rich phase, C_p^α, to that in the micelle-poor phase, C_p^β, that is:

$$K_p = \frac{C_p^\alpha}{C_p^\beta} \tag{2.3}$$

as a quantitative measure of the protein partitioning behavior, the theory shows that K_p is a function of the difference in the surfactant volume fractions between the two coexisting micellar phases, $\Delta\phi$, the hydrodynamic radius of the protein, R_p, and the

cross-sectional radius of the cylindrical micelle, R_0. Specifically,

$$K_p = \exp\left[-\Delta\phi\left(1+\frac{R_p}{R_0}\right)^2\right] \tag{2.4}$$

The theoretical expression in Eq. (2.4) is derived under the assumptions that: (i) the protein behaves like a hard sphere of radius R_p, (ii) the micelles can be represented as infinitely long (from the perspective of the protein) and rigid spherocylinders, (iii) the protein is at a low enough concentration that protein-protein interactions can be ignored, and (iv) the protein and the micelles interact exclusively through repulsive, short-ranged, excluded-volume interactions. Of the various inputs needed in Eq. (2.4), $\Delta\phi$ can be estimated from the surfactant concentrations of each coexisting phase, determined using the phase diagram (see Section 2.2), R_p can either be taken as the hydrodynamic radius measured experimentally or estimated from the three-dimensional structure of the protein, and R_0 can be approximated by the sum of the cross-sectional radius of the micellar core, which can be found using the micellization theory described in Section 2.1, and the head group length, which can be estimated from the known bond lengths and bond angles. With appropriate estimates for these inputs, the theory yields predictions of the protein partition coefficient that are in good agreement with the experimentally measured values for several proteins partitioned in $C_{10}E_4$ two-phase aqueous micellar systems at different temperatures [25, 47, 48]. One can therefore conclude that the partitioning behavior of hydrophilic biomolecules in two-phase aqueous micellar systems is primarily driven by steric, excluded-volume interactions between the biomolecules and the micelles. Since the theory suggests that the bigger the biomolecule, the more uneven its partitioning, one can envision that cloud-point extraction can be very effective in addressing the challenge of concentrating and/or removing viruses, which are much bigger than proteins. The partitioning of viruses, which has important applications in the biotechnology industry, for example, in viral clearance of therapeutic proteins and in vaccine production, was studied extensively by Kamei et al. [10, 11, 12, 50, 51].

In addition to excluded-volume interactions, other modes of interactions between the protein and the micelles can be introduced into two-phase aqueous micellar systems to modulate the partitioning behavior of hydrophilic proteins. For example, electrostatic effects can be incorporated by adding an ionic surfactant, which causes the micelles to become charged. A biomolecule bearing an opposite charge to that of the ionic surfactant can be attracted or "fished" to the micelle-rich phase, thereby enhancing the separation [10, 52]. An excellent separation of lysozyme, a positively-charged protein, and the virus bacteriophage P22 was attained using this method, in which a negatively-charged surfactant, sodium dodecyl sulfate (SDS), was mixed with the phase-forming nonionic surfactant $C_{10}E_4$ to generate the two-phase aqueous mixed (nonionic/anionic) micellar system for extraction [11]. Another mode of interaction that has great potential of enhancing the separation performance of these systems is affinity interactions. Examples of these interactions include antigen-antibody and enzyme-substrate interactions. These strong and highly specific interactions can be exploited in cloud-point extractions to significantly increase the yield and specificity of the separation, provided that the appropriate affinity ligand can be incorporated into the two-phase aqueous micellar system.

It is the goal of this thesis to explore ways of enhancing the partitioning of hydrophilic proteins, both by introducing electrostatic interactions (Part II of this thesis) and affinity interactions (Part III of this thesis).

2.4 Comparison to Two-Phase Aqueous Polymer Systems

A variety of phase separation phenomena have been observed when one or two polymers are dissolved in water, with or without added low-molecular-weight solutes. Two general classes of two-phase aqueous polymer systems have been utilized in separations. The first class corresponds to the cases where the aqueous solubility of a hydrophilic polymer, such as poly(ethylene glycol) (PEG), is reduced by the addition of a solute, such as potassium

sulfate (K_2SO_4) beyond a certain critical concentration, resulting in phase separation. The second class corresponds to cases which exploit incompatibility of two polymers, typically PEG and dextran, in aqueous solutions. In these systems, phase separation results from the unfavorable interaction present when segments of one polymer contact segments of the other polymer [9, 53]. It is beyond the scope of this thesis to review the theories and applications of two-phase aqueous polymer systems, although it may be helpful to contrast two-phase aqueous polymer systems and two-phase aqueous micellar systems with respect to their use in separations. Liu et al. listed the following five important potential advantages of two-phase aqueous micellar systems over two-phase polymer systems [25]:

1. In the simplest case, only a binary surfactant/water mixture is required to generate a two-phase aqueous micellar system, whereas it takes a more complex ternary polymer A/polymer B/water or polymer/salt/water mixture to generate a two-phase aqueous polymer system. The additional thermodynamic degree of freedom in the polymer case makes the systematic study of the phase behavior, and hence of its effect on the partitioning of various types of solutes, more difficult.

2. The self-assembling, labile nature of micelles enables one to control and optimize the partitioning behavior by tuning micellar characteristics, such as micellar shape and size, simply via manipulation of the solution conditions. On the other hand, the unchangeable identity of the polymer molecules does not provide such flexibility.

3. The dual character of the micelles, that is, their ability to simultaneously offer both hydrophilic and hydrophobic environments to solute species, allows the partitioning of molecules based on hydrophobicity. Although some separation based on hydrophobicity can be attained in two-phase aqueous polymer systems by exploiting solute-polymer interactions, this effect is not as pronounced and as general as in two-phase aqueous micellar systems. As a result, two-phase aqueous micellar systems have remained the method of choice for extracting hydrophobic, membrane-

spanning proteins, as well as various organic pollutants and metal chelates.

4. The self-assembling nature of micelles also facilitates the introduction of charged and affinity-based cosurfactants to further improve the performance of the separation in terms of its selectivity and yield. The desired property, whether it be a charged group or an affinity moiety, can be introduced into the micelles simply by mixing surfactants and exploiting the spontaneous self-assembling process. On the other hand, in the case of two-phase aqueous polymer systems, time-consuming organic synthesis procedures are needed to covalently link the desired functional groups to the polymer. It is also easier to introduce multiple functional groups and control the amount of ligands added in two-phase aqueous micellar systems by controlling the composition of the surfactants added to the system. In the polymer case, careful and often difficult synthetic chemistry is needed to achieve these goals.

5. Removal of surfactants after the extraction of solutes can also be facilitated by the self-assembling nature of micelles. For example, one could envision a procedure in which the micelles are disassembled into their constituent surfactant monomers, followed by dialysis to remove the surfactants while retaining the desired biomolecule.

In view of the above advantages, most notably 1 and 4 due to their relevance to the goals of this thesis, two-phase aqueous micellar systems are considered to be a more suitable and promising option than their polymer counterparts, for the investigation of the phenomenon of electrostatic-enhanced and affinity-enhanced extractions.

Chapter 3

Thesis Overview

As discussed in Chapters 1 and 2, the unmet challenge of developing a cost-effective separation method for low-cost, high-volume protein products can potentially be addressed by using extraction in two-phase aqueous micellar systems (cloud-point extraction). Although cloud-point extractions have been utilized in the past to address various separation needs (see Section 2.3), the efficient purification of industrially relevant hydrophilic proteins requires the introduction of new modes of interaction between the proteins and the micelles, in order to obtain desired levels of yield and specificity. With that in mind, the central goal of this thesis is to explore various ways of enhancing protein partitioning in two-phase aqueous micellar systems, by the incorporation of electrostatic and affinity interactions, to purify industrially relevant protein products. In addition to demonstrating proof-of-principle of these methods in enhancing protein partitioning in two-phase aqueous micellar systems, this thesis also seeks to develop a fundamental understanding of the underlying principles behind the phenomena of electrostatically-enhanced and affinity-enhanced partitioning.

The rest of the thesis is organized as follows. Electrostatically-enhanced partitioning is discussed in Part II, consisting of Chapters 4 and 5. Chapter 4 provides an overview of electrostatically-enhanced partitioning in two-phase aqueous micellar systems, and reviews the relevant literature in this area. Chapter 5 reports the experimental and the-

oretical investigation of the electrostatically-enhanced partitioning of an industrially important enzyme, glucose-6-phosphate dehydrogenase (G6PD), using two-phase aqueous mixed (nonionic/cationic) micellar systems. The study presented in Chapter 5 demonstrates proof-of-principle of the electrostatic enhancement of protein partitioning using a positively-charged surfactant. In addition, this study addresses, for the first time, the effect of the charged surfactant tail length on the denaturation of the enzyme G6PD, as well as on the preferential partitioning behavior of G6PD.

Affinity-enhanced partitioning is discussed in Part III, consisting of Chapters 6, 7, 8, and 9. Chapter 6 first provides an overview of affinity-enhanced partitioning in two-phase aqueous micellar systems, and reviews the relevant literature in this area. Chapter 7 presents proof-of-principle of the affinity-enhanced partitioning of an engineered affinity-tagged protein, CBM9-GFP, using two-phase aqueous micellar systems generated by a single surfactant, decyl β-D-glucopyranoside ($C_{10}G_1$). Not only is the system utilized the simplest and easiest to implement among others considered in the past, but it also represents the first successful attempt to achieve significant and specific affinity enhancement in the cloud-point extraction of a protein with a fusion tag that can, in principle, be generally applied to any protein of interest. The simplicity of the system also allowed the development and validation of an original theoretical framework to describe affinity-enhanced partitioning in two-phase aqueous micellar systems. The extraction method developed in Chapter 7 was then tested in terms of its ability to handle a complex protein mixture – a real *E. coli* cell lysate, and the results of this study are presented in Chapter 8. It is successfully proven, for the first time, that affinity-enhanced partitioning in two-phase aqueous micellar systems can indeed be applied to a complex mixture, with predictable results both in terms of the preferential extraction of the target protein and in terms of the simultaneous removal of the protein impurities. In Chapter 9, various possible ways of further improving the partitioning performance by manipulating the original system are investigated and discussed. In addition, the theoretical framework developed in Chapter 7 is utilized to provide important insights into how the separation

method can be optimized.

Lastly, Part IV (Chapter 10) provides a summary of the thesis, as well as discusses possible directions for future research.

Part II

Electrostatically-Enhanced Protein Partitioning in Two-Phase Aqueous Micellar Systems

Chapter 4

Overview

As discussed in Section 2.3.2, electrostatic effects can be exploited to enhance separation of biomolecules in two-phase aqueous micellar systems. Due to the presence of charged amino acid side groups on their surfaces, protein molecules typically carry a net charge, where the sign and the magnitude of the charge depend on the solution pH. Other biomolecules, such as viruses, are also charged, due to the presence of charged proteins on their surfaces. As a result, if one can generate a two-phase aqueous micellar system in which the micelles are charged, the partition coefficient of the charged biomolecules may be manipulated by virtue of the electrostatic interactions that operate between the charged micelles and the charged proteins. This approach was first proposed and implemented by Kamei et al. [10, 11, 52] using two-phase aqueous mixed (nonionic/anionic) micellar systems generated by $C_{10}E_4$ and sodium dodecyl sulfate (SDS), and will be further explored in this thesis. This chapter reviews the key results from the work of Kamei et al. In Section 4.1, the experimental results are reviewed, and in Section 4.2, the theory developed to model electrostatically-enhanced partitioning will be reviewed.

4.1 Electrostatically-Enhanced Protein Partitioning in Two-Phase Aqueous Mixed (Nonionic/Anionic) Micellar Systems

Kamei et al. investigated the partitioning of several proteins, including lysozyme, cytochrome c, ovalbumin, and catalase, in two-phase aqueous mixed (nonionic/anionic) micellar systems generated by the nonionic surfactant $C_{10}E_4$ and the anionic surfactant sodium dodecyl sulfate (SDS) [10, 52]. The $C_{10}E_4$/SDS/buffer system exhibits phase behavior that is similar to that of the single-surfactant $C_{10}E_4$/buffer system, except that the micelles that form are all mixed micelles consisting of both $C_{10}E_4$ and SDS. Therefore, each micelle bears a net negative charge by virtue of the sulfate head groups of the SDS surfactants. If a net positively-charged protein is placed in the $C_{10}E_4$/SDS/buffer system, it is expected to be attracted electrostatically to the micelle-rich phase, where there are a greater number of negatively-charged mixed micelles. Conversely, if a net negatively-charged protein is placed in this system, it is expected to the repelled electrostatically to the micelle-poor phase. As discussed in Section 2.4, a key advantage of this approach is that the self-assembling nature of micelles allows one to decorate the micelles with net negative charges simply by mixing surfactants, without having to perform any synthesis work. The concept of electrostatically-enhanced protein partitioning in two-phase aqueous mixed micellar systems is illustrated schematically in Figure 4-1.

The four proteins (see Table 4.1) were partitioned in both the $C_{10}E_4$/SDS/buffer sys-

Protein	R_p ($\AA$)	**pI**	**Net Charge at pH 7.2**
Lysozyme	19	11.0	Positive
Cytochrome c	16	10.6	Positive
Ovalbumin	29	4.6	Negative
Catalase	52	5.6	Negative

Table 4.1: Proteins partitioned in the $C_{10}E_4$/buffer and in the $C_{10}E_4$/SDS/buffer systems by Kamei et al. [52], with their hydrodynamic radii, R_p, and their isoelectric points, pI.

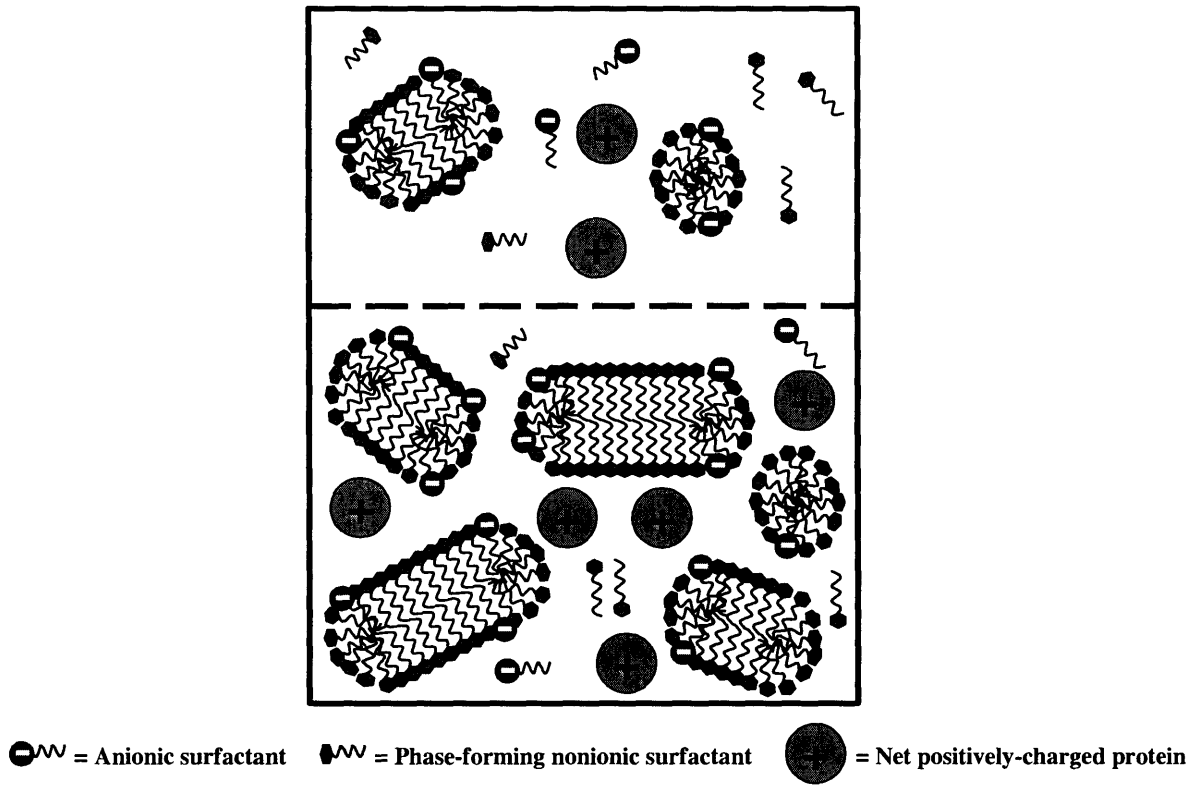

Figure 4-1: Schematic diagram illustrating the concept of electrostatically-enhanced protein partitioning in two-phase aqueous micellar systems. As shown, the target protein bearing a net positive charge is preferentially extracted to the micelle-rich phase, where there are a larger number of net negatively-charged mixed micelles.

tem and the $C_{10}E_4$/buffer system, the latter serving as the control. Since the addition of SDS shifts the phase diagram of the $C_{10}E_4$/buffer system, the partitioning conditions were chosen such that the strength of the excluded-volume interactions remained constant in both experiments. The results revealed that the partition coefficients of the four proteins considered were indeed modified, in the expected direction, when SDS was added at a final concentration of 0.0970 wt% (see Figure 4-2). Specifically, lysozyme and cytochrome c, which are both positively-charged at pH 7.2, were preferentially extracted to the micelle-rich phase compared to the control. On the other hand, ovalbumin and catalase, which are both negatively-charged at pH 7.2, were repelled to the micelle-poor phase compared to the control. The results in Figure 4-2 clearly demonstrated that the $C_{10}E_4$/SDS/buffer system has the capability to modulate the partition coefficients of charged proteins through electrostatic interactions.

Based on these results, the separation of the protein lysozyme from the virus bacteriophage P22 by electrostatically-enhanced partitioning in the two-phase aqueous mixed ($C_{10}E_4$/SDS) micellar system was also demonstrated by Kamei et al. [11]. Using a higher concentration of SDS (0.320 wt%), Kamei et al. were able to increase the partition coefficient of lysozyme from 0.78 ± 0.02 in the control case to 6.7 ± 0.6. Because of the large size of the virus, it partitioned very extremely to the micelle-poor phase, with a partition coefficient of 0.0056 ± 0.0006, by virtue of the strong excluded-volume interactions between the micelles and the virus. Accordingly, an effective one-step separation of lysozyme and bacteriophage P22 was attained, with a 95% yield of lysozyme in the micelle-rich phase, and a 98% yield of bacteriophage P22 in the micelle-poor phase, indicating the great potential of the separation method in applications such as viral clearance [11].

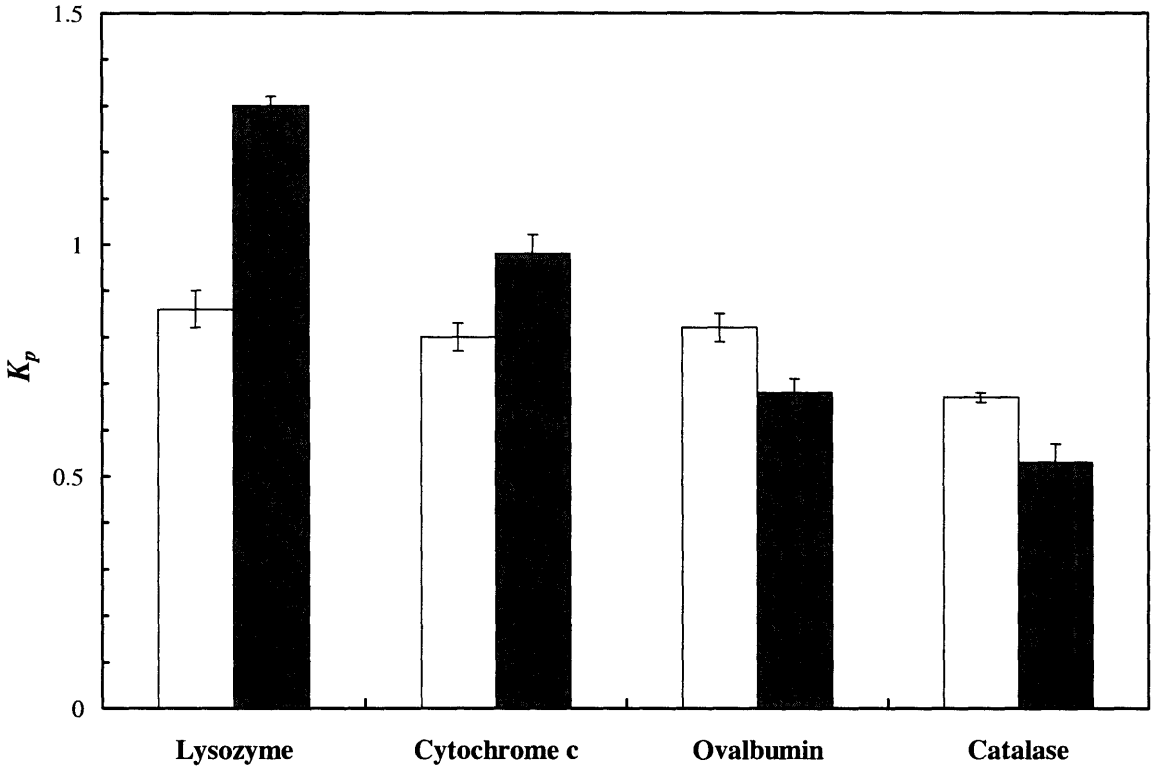

Figure 4-2: Experimentally measured protein partition coefficients (K_p) in the $C_{10}E_4$/buffer system (open bars), and in the $C_{10}E_4$/SDS/buffer system (gray bars) for lysozyme, cytochrome c, ovalbumin, and catalase [52]. The error bars correspond to 95% confidence limits for the measurements.

4.2 Theory of Electrostatically-Enhanced Protein Partitioning

As discussed in Section 2.3, for a hydrophilic protein, the partitioning behavior in two-phase aqueous nonionic micellar systems is primarily driven by excluded-volume interactions, as reflected in Eq. (2.4). However, the partitioning behavior of hydrophilic proteins in two-phase aqueous mixed (nonionic/ionic) micellar systems cannot be predicted using Eq. (2.4) alone, because electrostatic interactions operating between the charged proteins and the charged mixed micelles were not accounted for in the derivation of Eq. (2.4). Therefore, a detailed protein partitioning theory that incorporates both excluded-volume and electrostatic interactions was developed recently [52], based on a molecular-thermodynamic theory of mixed surfactant micellization developed earlier [21, 54]. In the context of the new theory, the partition coefficient of a hydrophilic protein in two-phase aqueous mixed (nonionic/ionic) micellar systems can be expressed as follows [52]:

$$K_p = K_p^{EV} K_p^{elec} \tag{4.1}$$

where K_p^{EV} denotes the excluded-volume contribution to the protein partition coefficient, and is given by Eq. (2.4), and K_p^{elec} denotes the electrostatic contribution to the protein partition coefficient. Essentially, the two contributions to the protein partition coefficient are decoupled and can be modeled separately. Kamei et al. derived an expression for K_p^{elec} by modeling the free energy associated with the electrostatic interactions between the charged micelles and the charged proteins in each coexisting micellar phase:

$$K_p^{elec} = \exp\left\{\frac{-\epsilon_w R_p}{2R_0^2 k_B T}\left[\left(\Psi_{mic,\alpha}^2 + \Psi_p^2\right) I_\alpha \phi_\alpha - \left(\Psi_{mic,\beta}^2 + \Psi_p^2\right) I_\beta \phi_\beta\right]\right\} \tag{4.2}$$

where ϵ_w is the dielectric constant of water, k_B is the Boltzmann constant, T is the absolute temperature, $\Psi_{mic,x}$ is the electrostatic potential at the surface of each micelle

in phase x [micelle-rich (α) or micelle-poor (β)], Ψ_p is the electrostatic potential at the surface of the protein, and I_x is an integral over the entire volume of phase x reflecting electrostatic interactions between a charged mixed micelle and a charged protein in phase x, given by the following expression [52]:

$$I_x = \int_R^\infty \left\{ \frac{2\Psi_{mic,x}\Psi_p}{\Psi_{mic,x}^2 + \Psi_p^2} \ln\left[\frac{1+\exp\left(-\kappa d(r)\right)}{1-\exp\left(-\kappa d(r)\right)}\right] + \ln\left[1-\exp\left(-2\kappa d(r)\right)\right] \right\} r dr \qquad (4.3)$$

where κ is the inverse of the Debye-Hückel screening length based on the buffer salt ions in the hypersolvent, $d(r) = (r - R_p - R_0)$ is the distance from the surface of the micelle to the surface of the protein, and r is the radial distance from the cylindrical micelle axis of symmetry. The lower limit of integration in Eq. (4.3), R_{min}, corresponds to the minimum radial distance between the micelle cylindrical axis and the center of the protein, and is given by the sum of the protein hydrodynamic radius, R_p, the micelle cross-sectional radius, R_0, and the distance of closest approach between the micelle and the protein, d_{min}, that is, by:

$$R_{min} = R_p + R_0 + d_{min} \qquad (4.4)$$

Equations (4.1) through (4.4) were derived based on the following assumptions: (i) the difference in the excess Gibbs free energy associated with the electrostatic interactions between the proteins and the micelles can be approximated by the corresponding difference in the excess internal energy, (ii) the charges are smeared on the micellar surface, as well as on the protein surface, enabling them to be modeled as uniformly-charged cylinders and spheres, respectively, (iii) the effect of the end-caps of the cylindrical micelles can be ignored, and (iv) only pairwise micelle-protein interactions need to be considered. To simplify the mathematical complexities, an approximation commonly used to treat this particular geometry was also employed: the cylindrical micelles are approximated as uniformly-charged, infinite flat plates, when evaluating the electrical double

layer interaction potentials [52].

The expressions for the electrical potentials $\Psi_{mic,x}$ ($x = \alpha$ or β) and Ψ_p (both in the cgs system of units) are given below [52]:

$$\Psi_{mic,x} = \frac{4\pi\sigma_x}{\epsilon_w \kappa} \tag{4.5}$$

and

$$\Psi_p = \frac{4\pi\sigma_p R_p}{\epsilon_w (1 + \kappa R_p)} \tag{4.6}$$

where σ_x is the surface charge density of each micelle in phase x, and σ_p is the surface charge density of the protein. The surface charge density of a protein can be calculated by modeling it as a sphere, and then estimating its net charge using the Henderson-Hasselbalch equation.

The surface charge density of each micelle in phase x was calculated according to the following equation [10]:

$$\sigma_x = \frac{\alpha_{mic} Z e l_{c,x}^2}{2 l_{ionic} \left[(1 - \alpha_{mic}) V_{tail,nonionic} + \alpha_{mic} V_{tail,ionic} \right]} \tag{4.7}$$

where Z is the valence of the ionic surfactant, e is the electronic charge, $l_{c,x}$ is the mixed micelle core radius in phase x, $l_{ionic,x}$ is the length of an ionic surfactant molecule in each micelle in phase x, $V_{tail,nonionic}$ and $V_{tail,ionic}$ are the volumes of the hydrophobic tails of the nonionic and the ionic surfactants, respectively, and α_{mic} is the micelle composition of the ionic surfactant in terms of moles, which is defined as follows:

$$\alpha_{mic} = \frac{[S_{ionic}]_{mic}}{[S_{ionic}]_{mic} + [S_{nonionic}]_{mic}} \tag{4.8}$$

where $[S_{ionic}]_{mic}$ and $[S_{nonionic}]_{mic}$ are the molar concentrations of the ionic surfactant, and of the nonionic surfactant, respectively, in the micelles. Equations (4.2) through (4.8) enable the prediction of the electrostatic contribution to the protein partition coefficient,

K_p^{elec}, given various molecular characteristics of the protein and the micelles that can be estimated or computed. The theoretical model described above has been validated using the experimental results obtained by Kamei et al. [52], and is further validated in the experimental investigation presented in the next chapter (Chapter 5).

Chapter 5

Partitioning of G6PD in Two-Phase Aqueous Mixed (Nonionic/Cationic) Micellar Systems

5.1 Introduction

Section 4.1 reviewed the successful attempt by Kamei et al. at enhancing the separation of lysozyme, a positively-charged protein, from the virus bacteriophage P22, by adding the negatively-charged surfactant, SDS, to form the two-phase aqueous mixed ($C_{10}E_4$/SDS) micellar system [11]. In this chapter, the same concept is implemented for a negatively-charged protein, glucose-6-phosphate dehydrogenase (G6PD), with SDS replaced by a *positively-charged* surfactant belonging to the alkyl trimethylammonium bromide (C_nTAB) family. The purpose of the work presented here is three-fold: (i) to develop an effective method to purify G6PD, an important enzyme in great demand, (ii) to demonstrate proof-of-principle of the method of electrostatically-enhanced partitioning in two-phase aqueous micellar systems in the case of a negatively-charged protein, and to verify the applicability of the theory reviewed in Section 4.2, and (iii) to investigate the effect of the tail length of the surfactant on the protein partitioning behavior, as well

as on the denaturation of the protein.

Glucose-6-phosphate dehydrogenase (EC.1.1.1.49) is the first enzyme of the pentose phosphate pathway. It catalyzes the oxidation of glucose-6-phosphate using $NADP^+$ and/or NAD^+ yielding pentose phosphates for nucleotides synthesis, as well as NADPH / NADH for reductive biosynthesis and protection from oxidative stress [55, 56, 57]. G6PD is ubiquitous in nature, being found in almost all animal tissues, plants, and microorganisms. In most species, G6PD has a subunit with a molecular weight of 50–60 kDa, corresponding to approximately 500 amino acid residues. G6PD is normally dimeric or tetrameric [57]. (The *Leuconostoc mesenteroides* G6PD, which is the one used in this work, is a dimer.) This enzyme is of great interest as an analytical reagent, being used in various quantitative assays, including the measurement of creatin kinase activity for diagnosis of heart and skeletal-muscle diseases, the measurement of hexose concentrations, and as a marker for enzyme immunoassays [58]. Unfortunately, the industrial purification of the hydrophilic enzyme G6PD has been carried out in multiple-step processes that consist of such expensive techniques as affinity chromatography and ion-exchange chromatography [59, 60, 61]. As a result, the cost of this enzyme as an analytical grade reagent is very high, and therefore, finding a simpler and more economical technique for the purification of G6PD is highly desirable. With this in mind, it is envisioned that electrostatically-enhanced partitioning in two-phase aqueous micellar systems, similar to the attempt described in Section 4.1, may provide a promising alternative, or complement, to the conventional chromatography-dominated separation schemes.

G6PD has an isoelectric point of 4.6, implying that at physiological pH, G6PD is negatively-charged. While it is possible, as described in Section 4.1, to use an anionic surfactant, such as SDS, to manipulate the partition coeffiicient of G6PD by electrostatic repulsion, it is counterproductive to do so, because such repulsion will drive G6PD into the micelle-poor phase, where most impurities will reside, due to excluded-volume effects (see Section 2.3.2). Instead, it is more desirable to concentrate G6PD in the micelle-rich phase, away from the majority of the impurities which reside in the micelle-poor

phase. Hence, the approach adopted here is to introduce a positively-charged surfactant to create a two-phase aqueous mixed (nonionic/cationic) micellar system for the partitioning of the negatively-charged protein G6PD. The family of cationic surfactants, alkyl trimethylammonium bromide (C_nTAB), where n is the number of carbon atoms in the hydrophobic tail of the surfactant, will be used for this purpose. These cationic surfactants were chosen because they are very common, well-understood, and available commercially. Like SDS, the anionic surfactant used in the partitioning experiments described in Section 4.1, the C_nTAB surfactants do not phase-separate by themselves, and therefore, need to be mixed with $C_{10}E_4$ to generate two-phase aqueous mixed micellar systems.

However, it is not immediately clear what the optimal tail length of the C_nTAB surfactant should be, for the purpose of introducing a positive charge to the micelles. Although the charge is the same for all C_nTAB surfactants (that is, +1), it is expected that the partitioning behavior of the protein, as well as the overall recovery of active protein, will depend strongly on the tail length of the C_nTAB surfactant. The tail length of the surfactant is an important factor which affects several aspects of the system. First, it affects the mixed micellization process, and ultimately the composition (and hence, the charge density) of the mixed micelles formed. Second, the presence of the C_nTAB surfactant affects the overall phase behavior of the mixed micellar system, as is commonly observed [10], the extent of which depends on the identity of the surfactant. Third, the tail length of the surfactant is also a critical factor affecting the extent of denaturation (if any) of the protein that comes in contact with it. Although it is well known that ionic surfactants can bind to proteins and induce denaturation, this effect has been shown to depend on the type and concentration of the ionic surfactant [62, 63]. Nevertheless, possible protein denaturation effects during the partitioning of charged proteins in two-phase aqueous charged mixed micellar systems were not investigated in the previous studies by Kamei et al, which are reviewed in Section 4.1. It is therefore very important to investigate the effects of the tail length of the C_nTAB surfactant on

the partitioning behavior, including potential denaturation effects, of the enzyme G6PD.

In the following sections, the partitioning of the enzyme G6PD in $C_{10}E_4/C_n$TAB two-phase aqueous mixed micellar systems is investigated, both experimentally and theoretically. Section 5.2 describes the materials and methods used in this study. In Section 5.3, the partitioning of the protein G6PD in a few selected $C_{10}E_4/C_n$TAB two-phase aqueous mixed micellar systems is presented and compared to the appropriate control cases where no charged surfactant was added. The experimental conditions for the partitioning were selected such that the enzyme G6PD retains a reasonable level of activity following partitioning for 3 h. The denaturating effects of the C_nTAB surfactants with different tail lengths on the enzyme G6PD were quantified in terms of the overall recovery of G6PD activity. To understand how the tail length of the cationic surfactant affects the phase behavior, the phase diagrams of the mixed micellar systems consisting of $C_{10}E_4$ and C_nTAB ($n = 8, 10$,and 12) were determined, and then are presented in Section 5.3.2. Lastly, the experimentally measured protein partition coefficients are compared to the theoretically predicted values in Section 5.3.4 .

5.2 Materials and Methods

5.2.1 Materials

The nonionic surfactant decyl tetra(ethylene oxide) (C E , lot no. 6011) was purchased from Nikko Chemicals (Tokyo, Japan). The cationic surfactants octyltrimethylammonium bromide (C TAB, lot no. OGK01) and decyltrimethylammonium bromide (C TAB, lot no. OGI01) were purchased from TCI-America (Portland, OR). The cationic surfactant dodecyltrimethylammonium bromide (C TAB, lot no. 63H0519), glucose-6-phosphate dehydrogenase from *Leuconostoc mesenteroides* (lot no. 50K8612), glucose 6-phosphate (lot no. 40K7014), and β-nicotinamide adenine dinucleotide phosphate (β-NADP+, lot no. 80K7046) were all purchased from Sigma (St. Louis, MO). The other reagents were all of analytical grade. All these materials were used as received.

All solutions were prepared at pH 7.2 using a solution of 16.4 mM disodium phosphate and 1.82 mM citric acid (derived from McIlvaine's buffer [64]) in water purified through a Millipore Milli-Q ion-exchange system (Bedford, MA). The glassware used in all the experiments were washed in a 50 : 50 ethanol:1M sodium hydroxide bath for at least 24 hours, followed by a 1M nitric acid bath for at least 24 hours, then rinsed copiously with Milli-Q water, and finally dried in an oven.

5.2.2 Determination of G6PD Concentrations by Enzymatic Assay

The determination of G6PD concentrations in aqueous surfactant solutions was based on a well-established enzymatic assay [65], with some modifications to match the conditions of the G6PD partitioning experiments. In particular, McIlvaine's buffer was utilized instead of Tris buffer, and the temperature was lowered from 25 $°C$ to 15 $°C$ to prevent phase separation during the assay. The activity of G6PD was measured by determining the rate of NADPH formation, which absorbs ultraviolet light at 340 nm. One G6PD unit was defined as the amount of enzyme that catalyzes the reduction of 1 mol of $NADP^+$ per minute under the assay conditions. The amounts of each reagent mixed in the spectrophotometer cell were as follows: 900 μL of pH 7.2 McIlvaine's buffer, 20 μL of a 250 mM glucose 6-phosphate solution, 5 μL of a 131 mM $NADP^+$ solution, and 20 μL of a sample containing G6PD. The spectrophotometric measurements were performed immediately after the sample addition, using a Shimadzu UV-160U spectrophotometer.

5.2.3 Determination of Cationic Surfactant Concentrations by Titration

The concentration of the cationic surfactant present in each coexisting micellar phase was determined based on a two-phase titration method, described by Tsubouchi et al. [66]. Instead of a pH 6 phosphate buffer solution used in the original protocol, pH 6

McIlvaine's buffer was utilized, since this buffer was also utilized in the G6PD partitioning experiments. Briefly, the sample was added to a 200 mL Erlenmeyer flask containing 5 mL of buffer solution, two drops of tetrabromophenolphthalein ethyl ester indicator (0.2% solution in ethanol), and 1 mL of 1,2-dichloroethane. The mixture was titrated with a 10 mM sodium tetraphenylborate solution, with intermittent shaking by hand to ensure equilibrium between the organic (1,2-dichloroethane) and the aqueous phases. In the absence of tetraphenylborate titrant, the indicator tetrabromophenolphthalein ethyl ester forms an ion pair with the cationic surfactant ion, in which the indicator is in the dissociated form (blue, max 610 nm). Throughout the titration, a complex between the cationic surfactant ion and the tetraphenylborate added is formed, with the indicator returning to its nondissociated form. When one drop of excess titrant is added, the dichloroethane phase changes to a faint yellow color, due to the presence of the indicator only in the nondissociated form (max 410 nm). Therefore, the cationic surfactant concentration can be determined from the amount of sodium tetraphenylborate added, with a color change from sky blue to faint yellow in the organic phase signaling the endpoint of the titration.

5.2.4 G6PD Partitioning in Two-Phase Aqueous Micellar Systems

Buffered solutions, each with a total volume of 3 mL, were prepared in graduated 10-mL test tubes by the addition of the desired amounts of C E , C_nTAB (n = 8, 10, or 12), and G6PD. Since the enzymatic assay for the determination of G6PD concentration is very sensitive, the final concentration of G6PD was 0.0068 wt%. The solutions were well mixed and equilibrated at 4 $°C$ in order for each solution to exhibit a clear and homogeneous single phase. Subsequently, the solutions were placed in a thermo-regulated device, previously set at the desired temperature. Solutions were maintained at that temperature for 3 h to attain partitioning equilibrium, since previous experiments had indicated that the partitioning behavior after 3 h is essentially the same as that observed after 21 h (see

Section 5.3.1). After partitioning equilibrium was attained, the two coexisting micellar phases formed were withdrawn separately with great care, using syringe and needle sets, and the enzyme concentration in each phase was determined as described above. Each G6PD partitioning experiment was repeated at least 3 times to verify reproducibility.

5.2.5 Mapping the Coexistence Curves of the $C_{10}E_4/C_nTAB$/ Buffer Systems

To better understand the G6PD partitioning behavior in the two-phase aqueous mixed ($C_{10}E_4/C_nTAB$) micellar systems, and to be able to implement the recently developed theoretical framework of protein partitioning [52], knowledge of the concentrations of both the nonionic and the cationic surfactants in each coexisting micellar phase was required. The concentrations of the cationic surfactants in each coexisting micellar phase can be determined by titration (see Section 5.2.3). To obtain the concentrations of the nonionic surfactant in each coexisting micellar phase, the coexistence curves for the various $C_{10}E_4/C_nTAB$/buffer systems were mapped out, at the same temperatures utilized in the G6PD partitioning experiments. The coexistence curve represents the boundary separating the one-phase region from the two-phase region. As one traverses this boundary from the one-phase region to the two-phase region, the solution becomes turbid, signaling the onset of phase separation. For a $C_{10}E_4/C_nTAB$/buffer micellar system at a given temperature and fixed pressure, the coexistence curve can be represented as a $C_{10}E_4$ concentration vs. C_nTAB concentration phase diagram, shown schematically in Figure 5-1. In Figure 5-1, a surfactant composition represented by point A, which is within the two-phase region, will exhibit phase separation, and the compositions of the resulting top and bottom micellar phases correspond to points B and C, respectively. The dashed line connecting points B and C is referred to as a tie-line, and any surfactant composition represented by points on the same tie-line will exhibit phase separation having the same top and bottom phase surfactant compositions (that is, the same B and

C points), but having different volumes of the top and bottom phases [53]. Therefore, if one knows the equilibrium concentrations of cationic surfactant in the top and bottom phases of a two-phase system at that particular temperature and pressure (that is, the x-coordinates of points B and C in Figure 5-1), one can read off the concentrations of the nonionic surfactant in the top and bottom phases (that is, the y-coordinates of points B and C in Figure 5-1) from the experimentally determined coexistence curve.

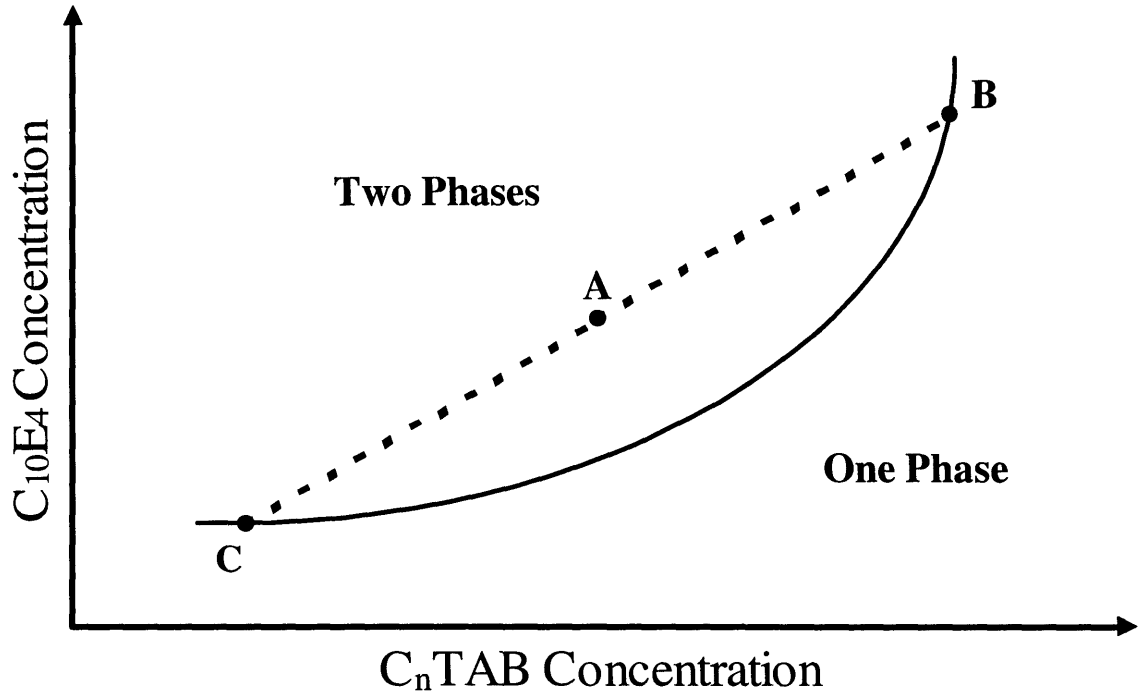

Figure 5-1: Schematic representation of a phase diagram for a two-phase aqueous mixed ($C_{10}E_4/C_nTAB$) micellar system at fixed temperature and pressure. The solid line represents the coexistence curve, separating the one-phase region from the two-phase region. The dashed line represents a tie-line, where any solution composition located on this segment, such as point A, will undergo phase separation, resulting in a top phase corresponding to the point B composition and a bottom phase corresponding to the point C composition.

To map a coexistence curve, the procedure described previously by Kamei et al. [52], which is similar to the one employed to measure coexistence curves for two-phase

aqueous polymer systems [53], was utilized. This procedure makes use of the fact that the coexistence curve marks the transition between a clear (one-phase) and a turbid (two-phase) solution, observable by the naked eye. A few grams of a concentrated buffered $C_{10}E_4$ solution were first equilibrated at the desired temperature in a thermo-regulated device where it was turbid. A solution of known concentration of C_nTAB (n = 8, 10, or 12) in buffer was added, dropwise, until the solution cleared. The concentrations of C_nTAB and $C_{10}E_4$ were then calculated based on the initial concentration of $C_{10}E_4$ and the amount of C_nTAB solution added. The resulting concentrations of $C_{10}E_4$ and C_nTAB correspond to the coordinates of one point on the coexistence curve at that particular temperature, characterizing the transition from a two-phase region to a one-phase region. A known mass of the buffer was then added until the solution again became turbid, indicating a surfactant composition in the two-phase region. The C_nTAB solution was again added, dropwise, until the solution cleared, and the concentrations of C_nTAB and $C_{10}E_4$, corresponding to the coordinates of another point on the coexistence curve, were calculated. The above procedure was repeated until sufficient points on the coexistence curve, typically 25 to 35 points, were determined. By connecting the two points on the experimentally mapped coexistence curve, corresponding to the cationic surfactant concentrations in each coexisting phase of the system, measured using the titration method discussed above, a tie-line is obtained which should pass through the point corresponding to the experimental G6PD partitioning condition for the respective system at the respective temperature.

5.3 Results and Discussion

5.3.1 G6PD Partitioning in the $C_{10}E_4/C_n$TAB/Buffer Systems

The G6PD partitioning behavior was studied in the $C_{10}E_4/C_n$TAB/buffer systems for the three cationic surfactants examined ($n = 8, 10$, and 12), at the same initial conditions, to determine which system is more effective for the purpose of purifying the enzyme. The

partitioning experiments were conducted at a temperature of 26.7 $°C$, a total surfactant concentration of 128 mM, and a solution surfactant composition, α_{sol}, of 0.035. The solution surfactant composition is defined as:

$$\alpha_{sol} = \frac{[C_nTAB]}{[C_nTAB] + [C_{10}E_4]} \tag{5.1}$$

where square brackets denote molar concentrations. This set of experimental conditions was based on preliminary experiments with C_{12}TAB in which an α_{sol} value higher than 0.035 led to a severe loss of the G6PD activity (data not shown). For this first set of experiments, the effect of the partitioning time on the equilibrium attained by the system was determined. Specifically, the partitioning of G6PD was carried out over 3 h and 21 h, for the three systems studied ($C_{10}E_4$/C_nTAB/buffer; n = 8, 10, and 12) (see Figure 5-2).

According to the results presented in Figure 5-2, a partitioning time of 3 h was found to be sufficient for the three systems to reach equilibrium, since no significant difference was found between the values of the G6PD partition coefficients, K_{G6PD}, measured after 3 h and after 21 h. Based on this finding, a partitioning time of 3 h was adopted in all the subsequent experiments. The highest G6PD partition coefficient, K_{G6PD} = 4.4, was attained in the $C_{10}E_4$/C_{12}TAB/buffer system, followed by K_{G6PD} = 1.8 in the $C_{10}E_4$/C_{10}TAB/buffer system, and the lowest one, K_{G6PD} = 0.10, in the $C_{10}E_4$/C_8TAB/buffer system (see Figure 5-2). Based on these findings, the $C_{10}E_4$/C_{12}TAB/buffer system generated stronger electrostatic attractions with the enzyme G6PD than the two other systems examined. To understand this behavior, knowledge of the compositions of the two coexisting micellar phases in each system is necessary, and therefore, the trend observed in Figure 5-2 in the K_{G6PD} values will be discussed later in Section 5.3.2.

On the other hand, the G6PD activity balances for partitioning times of 3 h and of 21 h, presented in Figure 5-3, reveal that G6PD is more stable in the $C_{10}E_4$/C_8TAB/buffer system (103% for t = 3 h, 96% for t = 21 h), followed by the $C_{10}E_4$/C_{10}TAB/buffer

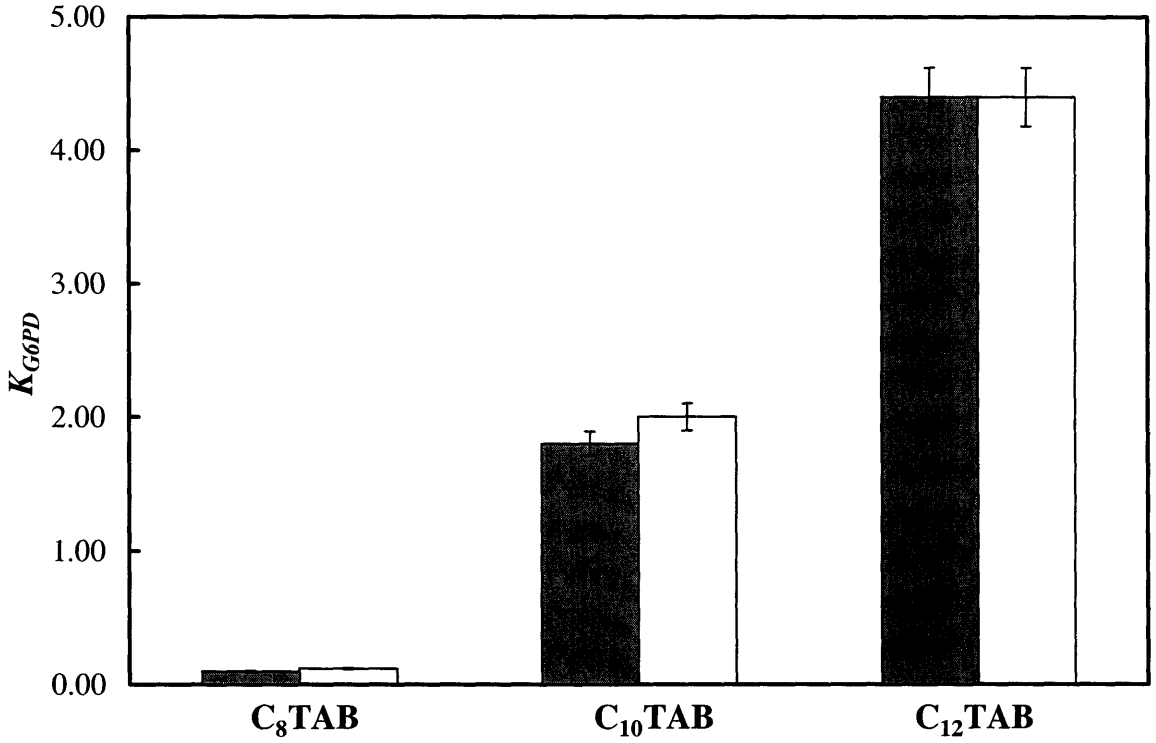

Figure 5-2: Experimentally measured G6PD partition coefficients (K_{G6PD}) in two-phase aqueous mixed ($C_{10}E_4/C_n$TAB) micellar systems carried out at a temperature T = 26.7 $°C$ and at a solution composition α_{sol} = 0.035 for C_8TAB, C_{10}TAB, and C_{12}TAB surfactants. The gray bars and open bars correspond to partitioning times of 3 h and 21 h, respectively. The error bars represent 95% confidence limits for the measurements.

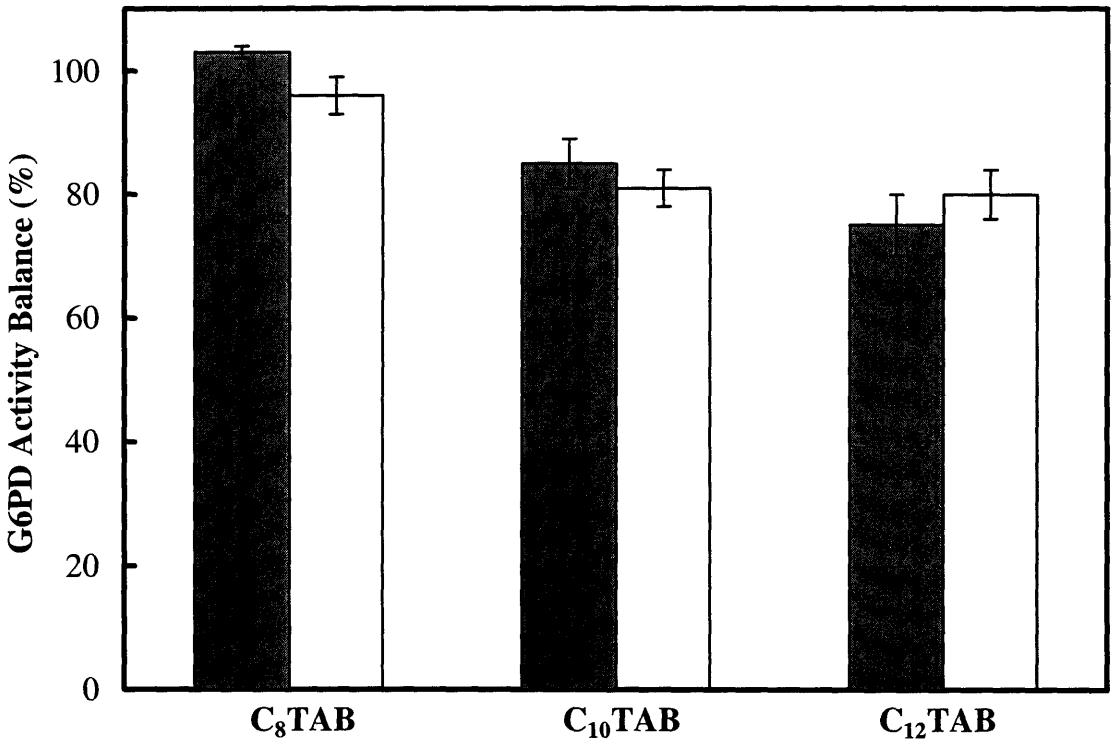

Figure 5-3: G6PD activity balance results for the G6PD partitioning experiments in the two-phase aqueous mixed ($C_{10}E_4/C_n$TAB) micellar systems carried out at a temperature $T = 26.7\ ^{\circ}C$ and at a solution composition $\alpha_{sol} = 0.035$ for C_8TAB, C_{10}TAB, and C_{12}TAB. The gray bars and the open bars correspond to partitioning times of 3 h and 21 h, respectively. The error bars represent 95% confidence limits for the measurements.

system (85% for $t = 3\ h$, 81% for $t = 21\ h$), and finally by the $C_{10}E_4/C_{12}TAB$/buffer system (75% for $t = 3\ h$, 80% for $t = 21\ h$), where the G6PD activity balance is defined as follows:

$$\text{G6PD Activity Balance} = \frac{[G6PD]_\alpha V_\alpha + [G6PD]_\beta V_\beta}{[G6PD]_i V_i} \times 100\% \tag{5.2}$$

where $[G6PD]_\alpha$, $[G6PD]_\beta$, and $[G6PD]_i$ are the G6PD concentrations in the top phase, in the bottom phase, and in the G6PD solution initially added to the system, respectively, and V_α, V_β, and V_i are the volumes of the top phase, the bottom phase, and the G6PD solution initially added to the system, respectively. The trend in G6PD stability observed in Figure 5-3 can be understood based on the mechanism of protein denaturation induced by ionic surfactants. It is generally accepted that the denaturation of proteins by ionic surfactants results from a combination of electrostatic and hydrophobic interactions [67]. In an aqueous solution containing protein and ionic surfactant, the ionic surfactant monomers first bind electrostatically to oppositely-charged residues at the protein surface (site-specific binding), and induce an expansion of the protein structure. This expansion, in turn, allows more interactions of the surfactant hydrophobic tails with the protein nonpolar interior (nonspecific, cooperative binding), and leads to protein unfolding and loss of its secondary structure. In this second stage, the surfactant molecules aggregate to form micellar structures that interact with proteins [68]. Some studies of the binding of small molecules, particularly of fatty acids and surfactants, to albumin indicate that the hydrophobic, nonspecific interactions may be stronger than the electrostatic ones, but that the electrostatic interactions are nevertheless significant, since uncharged hydrocarbon chains have a lower binding affinity to the protein [69]. Therefore, consistent with the trend observed in the data shown in Figure 5-3, cationic C_nTAB surfactants having a shorter hydrocarbon tail (smaller n value) are expected to be less denaturing to proteins (G6PD) due to weaker nonspecific cooperative (hydrophobic) interactions. It is important to point out that the noncharged surfactant $C_{10}E_4$ is not expected to interfere with the electrostatic binding ability of the C_nTAB surfactants, thus not changing the

trend in denaturation induced by the C_nTAB surfactants [68].

Based on the G6PD activity balance results shown in Figure 5-3, additional partitioning experiments were carried out in the $C_{10}E_4/C_n$TAB/buffer systems (n = 8 and 10) at higher concentrations of C_8TAB and C_{10}TAB, in an attempt to further increase the values of K_{G6PD} for these two systems while maintaining an acceptable level of G6PD activity. The best partitioning results in each case, corresponding to the highest solution compositions utilized (α_{sol} = 0.20 for C_8TAB and α_{sol} = 0.06 for C_{10}TAB), are presented in Figure 5-4. For these experiments, the temperature had to be increased to attain phase separation. Specifically, a temperature of 30.0 $°C$ was used for the $C_{10}E_4/C_{10}$TAB/buffer system, and a temperature of 30.5 $°C$ was used for the $C_{10}E_4/C_8$TAB/buffer system. The G6PD activity balances for these two experiments were about 75%, similar to the result of the G6PD partitioning experiment with C_{12}TAB shown in Figure 5-3.

The G6PD partitioning results shown in Figures 5-2 and 5-4 indicate that, for both the C_{10}E4/C_8TAB/buffer system and the $C_{10}E_4/C_{10}$TAB/buffer system, increasing the cationic surfactant concentration results in higher G6PD partition coefficients while still maintaining the same G6PD activity balance as in the $C_{10}E_4/C_{12}$TAB/buffer system (Figure 5-3). When compared to the other two systems (n = 10 and 12), the $C_{10}E_4/C_8$TAB/buffer system, even with an α_{sol} value as high as 0.20, does not generate sufficiently strong electrostatic attractions between the positively charged $C_{10}E_4/C_8$TAB mixed micelles and the net negatively charged enzyme G6PD to significantly improve the partitioning of the enzyme to the top, mixed micelle-rich phase, resulting in a K_{G6PD} value of 1.3 (see Figure 5-4). On the other hand, an α_{sol} value of 0.06 in the $C_{10}E_4/C_{10}$TAB/buffer system results in the highest G6PD partition coefficient observed (K_{G6PD} = 7.7; see Figure 5-4).

One should note that it is always possible to maintain a higher G6PD activity balance in any of the three $C_{10}E_4/C_n$TAB/buffer systems examined by adding less cationic surfactant, at the expense of attaining lower K_{G6PD} values. To better understand the practical advantage of adding more cationic surfactant, Table 5.1 lists the values of the G6PD

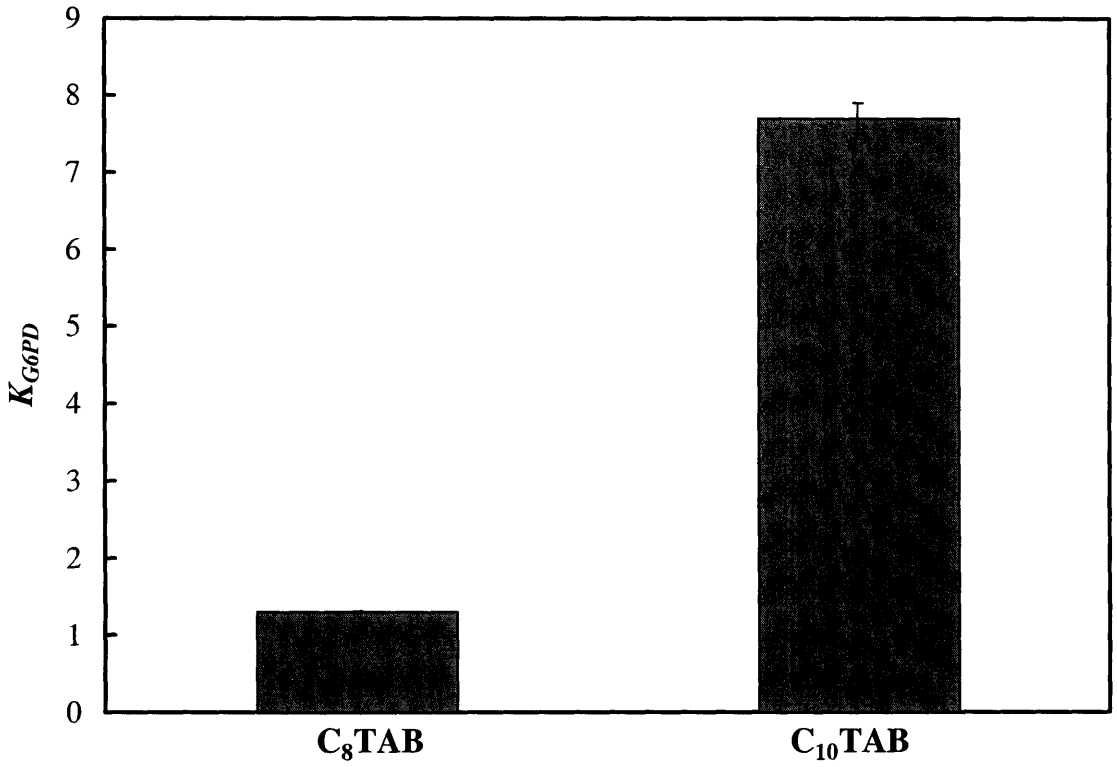

Figure 5-4: Experimentally measured G6PD partition coefficients (K_{G6PD}) in the $C_{10}E_4/C_8TAB$/buffer system carried out at a temperature $T = 30.5\ ^\circ C$ and at a solution composition $\alpha_{sol} = 0.20$, and in the $C_{10}E_4/C_{10}TAB$/buffer system carried out at a temperature $T = 30.0\ ^\circ C$ and at a solution composition $\alpha_{sol} = 0.06$. The error bars represent 95% confidence limits for the measurements.

yield in the micelle-rich phase ($Y_{G6PD,\alpha}$) for each condition examined, where $Y_{G6PD,\alpha}$ is defined as follows:

$$Y_{G6PD,\alpha} = \frac{[G6PD]_\alpha V_\alpha}{[G6PD]_i V_i} \times 100\% \tag{5.3}$$

As can be seen in Table 5.1, the $C_{10}E_4/C_{10}TAB$/buffer system at $\alpha_{sol} = 0.06$ provides a better balance between the denaturing effect of $C_{10}TAB$ on G6PD and the electrostatic attractions between the positively-charged $C_{10}E_4/C_{10}TAB$ mixed micelles and the net negatively-charged enzyme G6PD, with a $Y_{G6PD,\alpha}$ value of 71%. Table 5.1 also reveals that the higher stability of G6PD in the $C_{10}E_4/C_{10}TAB$/buffer system at $\alpha_{sol} = 0.035$ does not compensate for the lower K_{G6PD} value of 1.8, resulting in a relatively low $Y_{G6PD,\alpha}$ value of 48% at this condition.

System	$T(°C)$	α_{sol}	$Y_{G6PD,\alpha}$ (%)
$C_{10}E_4/C_8TAB$/buffer	26.7	0.035	2.5
$C_{10}E_4/C_{10}TAB$/buffer	26.7	0.035	48
$C_{10}E_4/C_{12}TAB$/buffer	26.7	0.035	60
$C_{10}E_4/C_8TAB$/buffer	30.5	0.200	49
$C_{10}E_4/C_{10}TAB$/buffer	30.0	0.060	71

Table 5.1: Yield of G6PD in the micelle-rich phase for the various $C_{10}E_4/C_nTAB$/buffer systems ($n = 8, 10$, and 12) and conditions examined.

5.3.2 Mapping the Coexistence Curves of the $C_{10}E_4/C_nTAB$/ Buffer Systems

To better understand the partitioning behavior of G6PD, it is necessary to know the compositions of the top and bottom phases of the three $C_{10}E_4/C_nTAB$/buffer systems examined. For this purpose, coexistence curves were mapped out for all the two-phase aqueous mixed micellar systems examined, at the same temperatures utilized in the G6PD partitioning experiments, and the experimental tie-lines were obtained based on the C_nTAB concentrations determined by titration (see Section 5.2). Figure 5-5 shows the

experimentally measured coexistence curves and tie-lines for the $C_{10}E_4/C_8TAB$/buffer system, at 26.7 $°C$ and 30.5 $°C$. Figure 5-6 shows the experimentally measured coexistence curves and tie-lines for the $C_{10}E_4/C_{10}TAB$/buffer system, at 26.7 $°C$ and 30.0 $°C$. Figure 5-7 shows the experimentally measured coexistence curve and tie-line for the $C_{10}E_4/C_{12}TAB$/buffer system, at 26.7 $°C$.

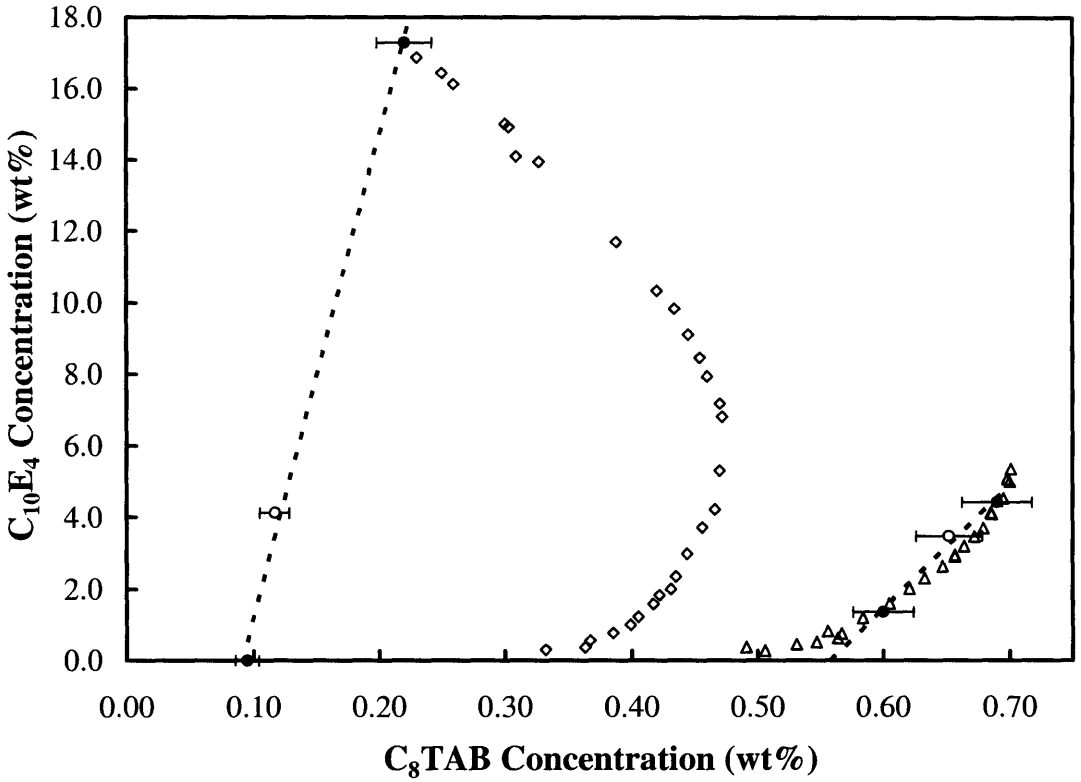

Figure 5-5: Experimentally determined coexistence curves of the $C_{10}E_4/C_8TAB$/buffer system at 26.7 $°C$ ($\Diamond$) and at 30.5 $°C$ ($\triangle$), with their respective tie-lines, represented by the dashed lines. The intersections of the tie-lines with the coexistence curves ($\bullet$) were obtained based on the C_8TAB concentrations determined for the top and bottom phases. The open circles ($\circ$) represent the initial conditions at which G6PD was partitioned for this system. The error bars represent 95% confidence limits for the C_8TAB concentration measurements.

In each coexistence curve, the filled circles correspond to the compositions of the top and bottom phases of the partitioning experiment carried out in the same system and

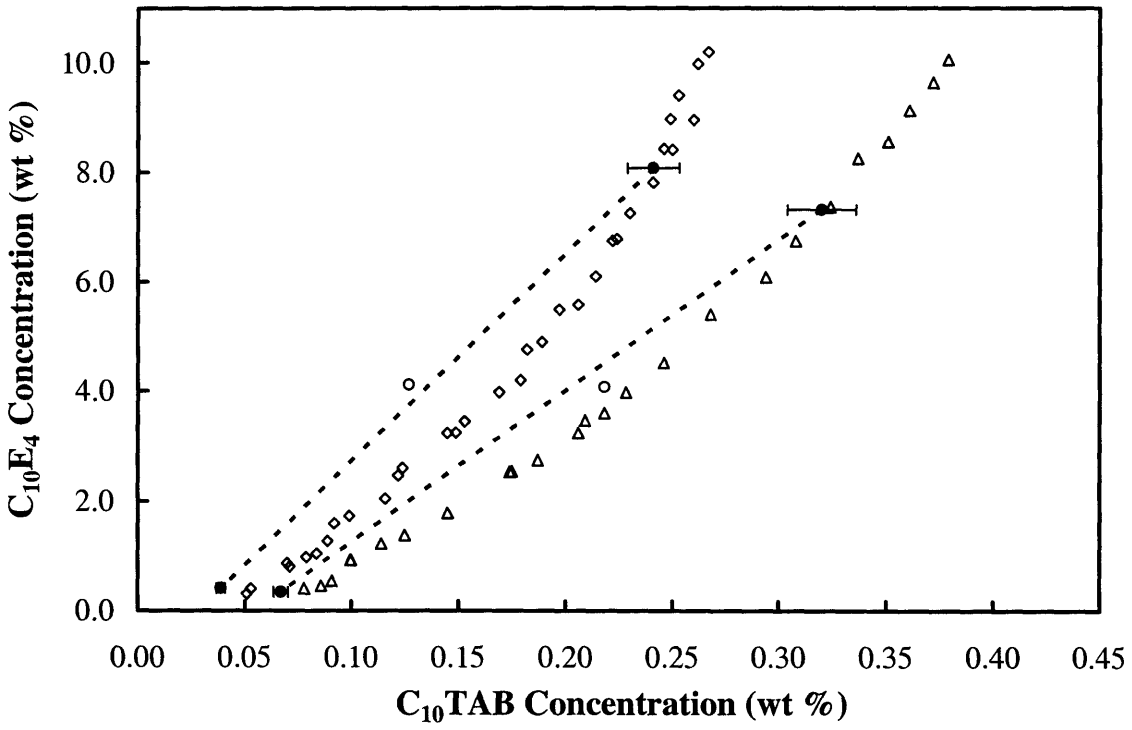

Figure 5-6: Experimentally determined coexistence curves of the $C_{10}E_4/C_{10}$TAB/buffer system at 26.7 $°C$ ($\Diamond$) and at 30.0 $°C$ ($\triangle$), with their respective tie-lines, represented by the dashed lines. The intersections of the tie-lines with the coexistence curves ($\bullet$) were obtained based on the C_{10}TAB concentrations determined for the top and bottom phases. The open circles ($\circ$) represent the initial conditions at which G6PD was partitioned for this system. The error bars represent 95% confidence limits for the C_{10}TAB concentration measurements.

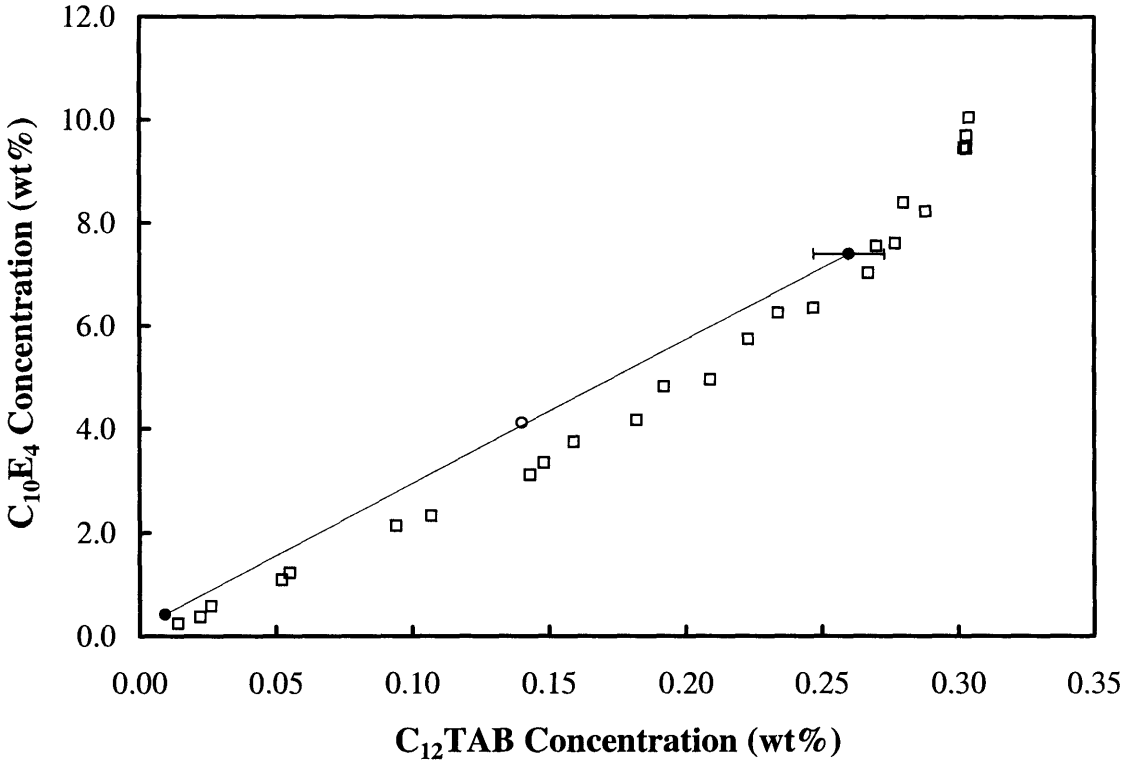

Figure 5-7: Experimentally determined coexistence curve of the $C_{10}E_4/C_{12}TAB$/buffer system at 26.7 $°C$ (□), with the respective tie-line, represented by the dashed line. The intersections of the tie-line with the coexistence curve (•) were obtained based on the $C_{12}TAB$ concentration determined for the top and bottom phases. The open circle (○) represents the initial condition at which G6PD was partitioned for this system. The error bars represent 95% confidence limits for the $C_{12}TAB$ concentration measurements.

at the same temperature that the coexistence curve was mapped out. The dashed line connecting these points is a tie-line, and the open circle corresponds to the overall initial solution composition of the partitioning experiment. As can be seen, there is good agreement between the compositions of the top and bottom phases and the initial solution composition for each partitioning experiment, since in each case, the tie-line obtained passes through the point corresponding to the initial solution composition, within the experimental uncertainty. Table 5.2 lists the experimentally determined partition coefficients (K_{G6PD}) and the differences in surfactant concentrations between the top and bottom phases of the three $C_{10}E_4/C_nTAB$/buffer systems examined, obtained based on the phase diagrams in Figures 5-5, 5-6, and 5-7. As shown in Table 5.2, the partition coefficient of G6PD increases from 1.3 to 7.7 with an increase in the difference in the cationic surfactant concentrations between the top and bottom phases, $\Delta[C_nTAB]$ from 0.09 to 0.25, highlighting the important role of the electrostatic attractions on the G6PD partitioning behavior. Note, however, that for the $C_{10}E_4/C_8TAB$/buffer system at $\alpha_{sol} = 0.035$, although $\Delta[C_nTAB] = 0.13$ is higher than the corresponding value of $\Delta[C_nTAB] = 0.09$ for $\alpha_{sol} = 0.20$, a smaller partition coefficient value of 0.10 is attained (see Table 5.2). This extremely small K_{G6PD} value of 0.10 obtained for the $C_{10}E_4/C_8TAB$/buffer system at $\alpha_{sol} = 0.035$ results from the large excluded-volume effect observed at this condition, which is clearly reflected in the difference in total surfactant concentrations between the top and bottom phases ($\Delta[C_{10}E_4 + C_nTAB] = 17.43\%$, see Table 5.2). Therefore, to attain the optimal G6PD partition coefficient, it is necessary to consider both the electrostatic and the excluded-volume effects.

5.3.3 G6PD Partitioning in the $C_{10}E_4$/Buffer System

To decouple the effects of the electrostatic attractions and the excluded-volume interactions on the G6PD partition coefficient, and also to probe the strength of the electrostatic attractions between the net negatively-charged enzyme G6PD and the positively-charged mixed $C_{10}E_4/C_nTAB$ micelles, G6PD was partitioned in the $C_{10}E_4$/buffer system at con-

System	T ($^{\circ}C$)	α_{sol}	K_{G6PD}	$\Delta[C_{10}E_4 + C_nTAB]$ (wt%)	$\Delta[C_nTAB]$ (wt%)
$C_{10}E_4/C_8TAB$/buffer	26.7	0.035	0.1	17.43	0.13
$C_{10}E_4/C_8TAB$/buffer	30.5	0.200	1.3	3.16	0.09
$C_{10}E_4/C_{10}TAB$/buffer	26.7	0.035	1.8	7.86	0.20
$C_{10}E_4/C_{12}TAB$/buffer	26.7	0.035	4.4	7.40	0.25
$C_{10}E_4/C_{10}TAB$/buffer	30.0	0.060	7.7	7.22	0.25

Table 5.2: Experimentally determined partition coefficients (K_{G6PD}), and differences in total surfactant concentrations $\Delta[C_{10}E_4 + C_nTAB]$, and in cationic surfactant concentrations $\Delta[C_nTAB]$, between the top and bottom phases of the $C_{10}E_4/C_nTAB$/buffer systems ($n = 8, 10$, and 12) examined.

ditions where the excluded-volume interactions operating between the micelles and the enzyme G6PD were the same as those in the mixed micellar systems examined. Considering that the predicted cross-sectional radii (R_0) of the cylindrical mixed micelles were, for all the experiments, similar to that of the $C_{10}E_4$ cylindrical micelles, and that the G6PD hydrodynamic radius (R_p) is fixed, the excluded-volume interactions can be maintained constant if $(\phi_\alpha - \phi_\beta)$ is kept at a fixed value [see Eq. (2.4)]. Accordingly, the excluded-volume interactions can be maintained constant by partitioning G6PD in the $C_{10}E_4$/buffer system at a temperature that corresponds to a tie-line having the same $(\phi_\alpha - \phi_\beta)$ value observed in the $C_{10}E_4/C_nTAB$/buffer system under consideration. With this in mind, we utilized the $C_{10}E_4$/buffer system coexistence curve obtained by Kamei et al. [52], since we used $C_{10}E_4$ from the same lot. Figure 5-8 shows a comparison between the experimentally determined partition coefficients in the $C_{10}E_4$/buffer system (open bars) and in the $C_{10}E_4/C_nTAB$/buffer systems (gray bars). As can be seen in Figure 5-8, in all cases, the measured K_{G6PD} values in the $C_{10}E_4/C_nTAB$/buffer systems are significantly higher than those in the corresponding $C_{10}E_4$/buffer system, thus demonstrating that the net negatively-charged enzyme G6PD is indeed attracted electrostatically to the top, mixed micelle-rich phase, which contains a greater number of positively-charged $C_{10}E_4/C_nTAB$ mixed micelles. Note that even in the case of C_8TAB-1, corresponding to the $C_{10}E_4/C_8TAB$/buffer system at $\alpha_{sol} = 0.035$, the K_{G6PD} value is 2.5 times

higher in the presence of the cationic surfactant, increasing from 0.04 to 0.1. Note also, that a K_{G6PD} value of 7.7 (22 times larger) is obtained in the case of C_{10}TAB-2, corresponding to the $C_{10}E_4/C_{10}$TAB/buffer system at $\alpha_{sol} = 0.06$. The experimental G6PD partitioning results shown in Figure 5-8 clearly demonstrate that electrostatic attractions contribute significantly to the preferential partitioning of the enzyme G6PD to the top, mixed micelle-rich phase.

5.3.4 Theoretical Prediction of K_{G6PD} Accounting for Excluded-Volume and Electrostatic Interactions

In Figure 5-9, the partition coefficients measured in the $C_{10}E_4/C_{10}$TAB/buffer systems and the $C_{10}E_4/C_{12}$TAB/buffer systems are compared with those predicted using the partitioning theory reviewed in Section 4.2. The theoretical K_{G6PD} values were calculated using a number of input parameters, including the micelle compositions $\alpha_{mic,\alpha}$, and $\alpha_{mic,\beta}$. The values of ϕ_α and ϕ_β were obtained based on the sum of the measured $C_{10}E_4$ concentration and the measured C_nTAB concentration, corresponding to the top and bottom phases, respectively, extracted from the coexistence curves as shown in Figures 5-5, 5-6, and 5-7. A molecular-thermodynamic theory of mixed surfactant micellization [21, 54] was utilized to predict α_{mic} in each phase of the two-phase aqueous micellar systems, at the conditions studied. Note that the partitioning theory was not utilized for the $C_{10}E_4/C_8$TAB/buffer system because, based on predictions for the compositions of the top and bottom phases (data not shown), the C_8TAB monomers are present at significant concentrations, while in the two other cationic systems, the C_nTAB ($n = 10$ and 12) monomer concentrations can be neglected relative to the C_nTAB ($n = 10$ and 12) concentrations in the $C_{10}E_4/C_n$TAB mixed micelles. Furthermore, the difference in the C_8TAB monomer concentrations between the top and bottom phases in the $C_{10}E_4/C_8$TAB/buffer system is also significant. The theory presented in the Section 4.2 does not account for electrostatic effects associated with the cationic surfactant monomers, since it was de-

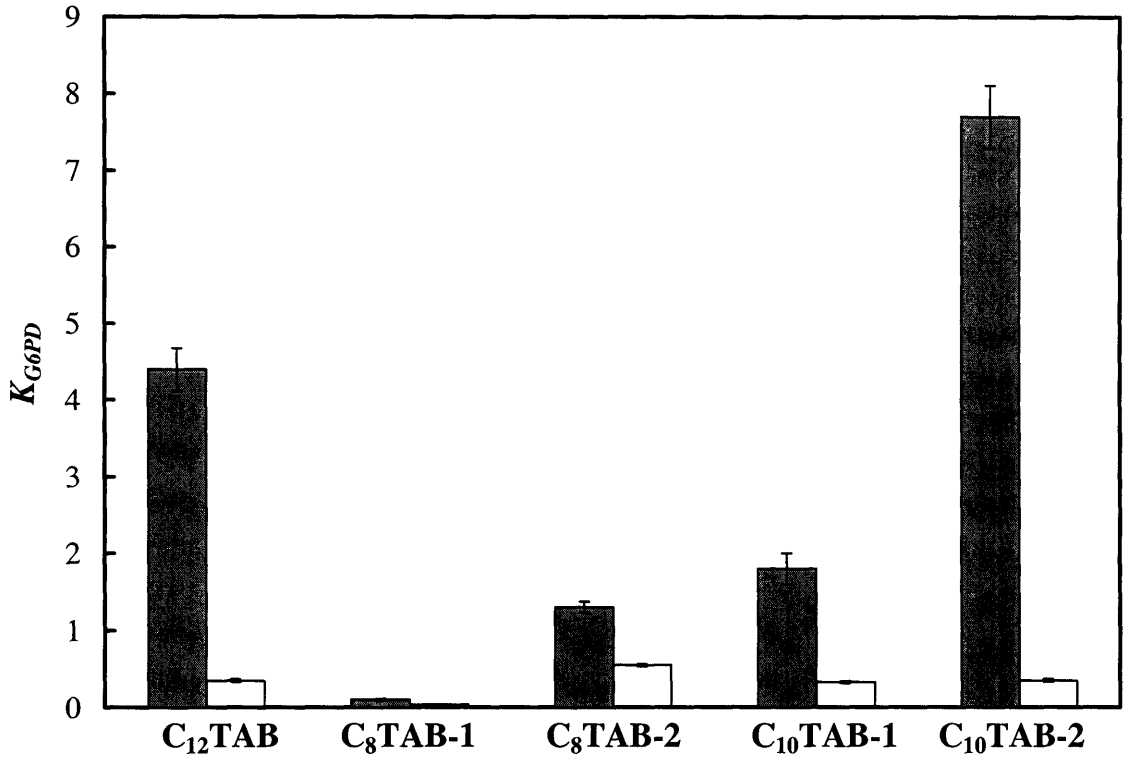

Figure 5-8: Experimentally measured G6PD partition coefficients (K_{G6PD}) in the $C_{10}E_4/C_nTAB$/buffer systems (gray bars) and the corresponding ones in the $C_{10}E_4$/buffer system (open bars), keeping the excluded-volume effect constant, for the $C_{10}E_4/C_{12}TAB$/buffer system, $\alpha_{sol} = 0.035$ (denoted as $C_{12}TAB$), for the $C_{10}E_4/C_8TAB$/buffer system, $\alpha_{sol} = 0.035$ (denoted as C_8TAB-1) and $\alpha_{sol} = 0.20$ (denoted as C_8TAB-2), and for the $C_{10}E4/C_{10}TAB$/buffer system, $\alpha_{sol} = 0.035$ (denoted as $C_{10}TAB$-1) and $\alpha_{sol} = 0.06$ (denoted as $C_{10}TAB$-2). The net negatively-charged enzyme G6PD is attracted to the top, mixed micelle-rich phase, relative to the case without C_nTAB, as reflected by the K_{G6PD} values in the presence of C_nTAB being higher than those attained without C_nTAB. The error bars represent 95% confidence limits for the measurements.

veloped for surfactant systems in which the ionic surfactant monomer concentrations are comparable in the top and bottom phases, or are negligible relative to the micellar concentrations of the ionic surfactant in each coexisting micellar phase [52]. To utilize the theory in the $C_{10}E_4/C_8TAB$/buffer system, a new term associated with the electrostatic attractions between the net negatively-charged proteins and the positively-charged C_8TAB monomers needs to be incorporated into the excess free energy model used to characterize each phase. However, this generalization of the original theory is beyond the scope of this thesis.

As can be seen in Figure 5-9, the theoretically predicted protein partition coefficients (open bars) are in reasonable quantitative agreement with the experimentally measured ones (gray bars). Considering the reasonable quantitative agreement between theory and experiment observed in Figure 5-9, and the previous similar quantitative agreement obtained by Kamei et al. [52], the protein partitioning theory reviewed in Section 4.2 can serve as a useful tool to establish practical guidelines to optimize protein separations in two-phase aqueous mixed (nonionic/ionic) micellar systems.

5.4 Conclusions

The partitioning behavior of the enzyme glucose-6-phosphate dehydrogenase (G6PD) in two-phase aqueous mixed (nonionic/cationic) micellar systems was investigated, both experimentally and theoretically. The cationic surfactants C_nTAB ($n = 8, 10$,and 12) were mixed with the nonionic surfactant $C_{10}E_4$ to form mixed $C_{10}E_4/C_nTAB$ micelles which have sufficient positive charge to attract the net negatively-charged enzyme G6PD to the top, mixed micelle-rich phase, while not significantly denaturing the enzyme. The measured G6PD partition coefficients in the $C_{10}E_4/C_nTAB$/buffer systems were at least 2.5 times larger than those in the corresponding $C_{10}E_4$/buffer system, clearly demonstrating that the net negatively-charged enzyme G6PD is indeed attracted electrostatically to the top, mixed micelle-rich phase, which contains a greater number of positively-

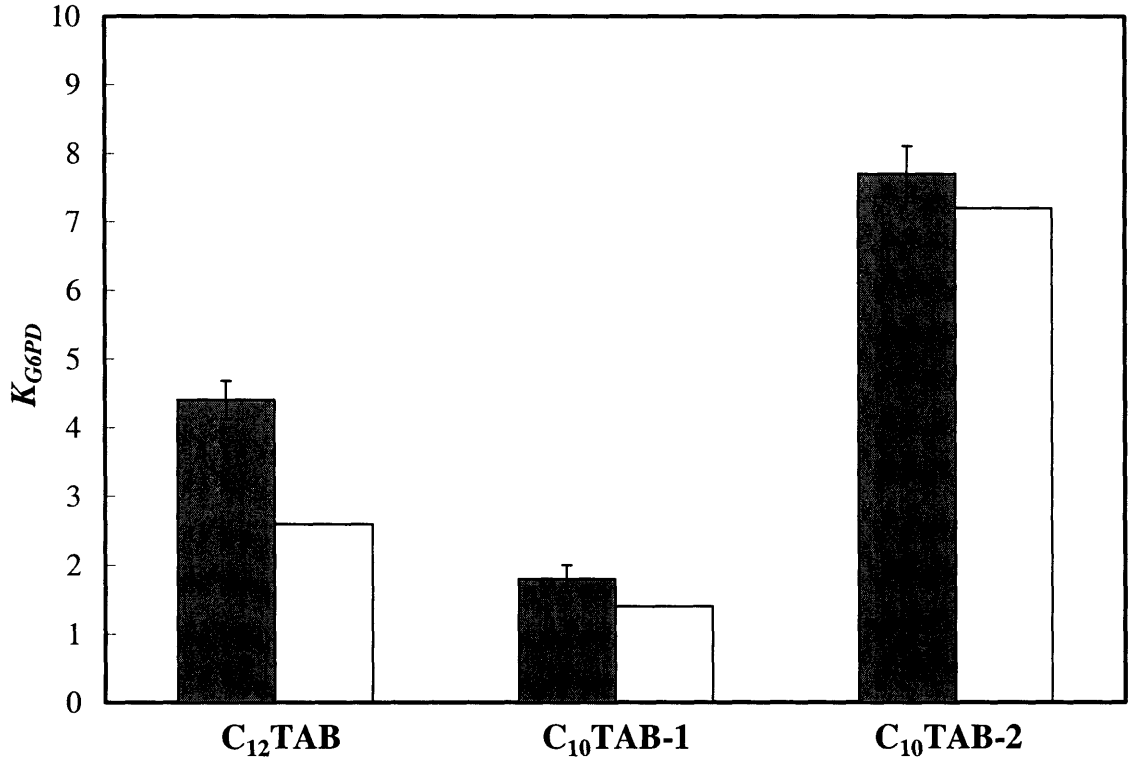

Figure 5-9: Comparison between the experimentally measured (gray bars) and the theoretically predicted (open bars) G6PD partition coefficients (K_{G6PD}) in the $C_{10}E_4/C_{10}$TAB/buffer system with an $\alpha_{sol} = 0.035$ (denoted as C_{10}TAB-1) and an $\alpha_{sol} = 0.06$ (denoted as C_{10}TAB-2), and in the C_{10}E4/C_{12}TAB/buffer system with an $\alpha_{sol} = 0.035$ (denoted as C_{12}TAB). The error bars represent 95% confidence limits for the measurements.

charged $C_{10}E_4/C_nTAB$ mixed micelles. The $C_{10}E_4/C_{12}TAB$/buffer system generated stronger electrostatic attractions, resulting in the highest K_{G6PD} value when using the same amount of cationic surfactant. However, for the $C_{10}E_4/C_8TAB$/buffer system and the $C_{10}E_4/C_{10}TAB$/buffer system, it was possible to increase the amount of cationic surfactant without inducing severe denaturation of G6PD, and as a result, the G6PD partition coefficients also increased. In particular, the $C_{10}E_4/C_{10}TAB$/buffer system provided the highest G6PD partition coefficient ($K_{G6PD} = 7.7$), increasing the G6PD partitioning to the top phase about 22 times more than that obtained in the $C_{10}E_4$/buffer system, and resulting in a G6PD yield in the top phase of 71%. The results presented in this chapter using two-phase aqueous mixed micellar systems compare favorably with previous results obtained utilizing two-phase aqueous polymer systems. For example, Alred et al. [70] reported a G6PD partition coefficient value of about 0.75 in the $EO_{20}PO_{80}$/Dextran T500 two-phase aqueous polymer system. In addition, increases in the G6PD partition coefficient from about 0.005 to about 0.03, using unbound triazine dyes as affinity ligands in two-phase aqueous PEG/phosphate systems, were reported by Bhide et al. [71]. A recently developed molecular-thermodynamic theory combining mixed micelle formation and protein-micelle interactions was utilized to predict G6PD partition coefficients in two-phase aqueous mixed (nonionic/cationic) micellar systems. The theoretically predicted G6PD partition coefficients were found to be in reasonable quantitative agreement with the experimentally measured ones, thus demonstrating the practical utility of the theory in guiding the implementation of optimal protein separation strategies. In conclusion, two-phase aqueous mixed (nonionic/cationic) micellar systems can be considered as a new promising alternative for the purification of G6PD. Among the three two-phase aqueous mixed micellar systems studied, the $C_{10}E_4/C_{10}TAB$/buffer system was found to be best suited for the purification of G6PD, providing an optimal balance between denaturation effects and electrostatic attractions.

Part III

Affinity-Enhanced Protein Partitioning in Two-Phase Aqueous Micellar Systems

Chapter 6

Overview

While electrostatic interactions can effectively modulate the partitioning behavior of charged proteins and enhance their separation, as demonstrated in Part II, another promising avenue to enhance protein partitioning in two-phase aqueous micellar systems makes use of affinity interactions. This chapter provides an overview of the concept of affinity-enhanced partitioning and of the relevant literature on this subject. Section 6.1 surveys various types of affinity interactions and their roles in bioseparations. Section 6.2 lists the design requirements for selecting an appropriate type of affinity interaction to be used in two-phase aqueous micellar systems. In Section 6.3, previous attempts to exploit affinity interactions to enhance partitioning in two-phase aqueous micellar systems are reviewed and evaluated.

6.1 Specific Bioaffinity and its Role in Bioseparations

Affinity interactions are the basis for molecular recognition in many biological processes, and as such, they are highly specific between the particular binding partners. To be able to operate between very dilute species in biological systems, affinity interactions are also typically very strong, with dissociation constants approaching the femtomolar

range in the strongest binders. The protein avidin, for example, binds the vitamin biotin with a dissociation constant of approximately 1×10^{-15} M [72]. Some common examples of bioaffinity interactions include enzyme-substrate binding in enzymatic reactions, antigen-antibody binding in immune response, and hormone-receptor binding in signal transduction [73]. Generally, the tight binding results from numerous simultaneous interactions (electrostatic, hydrogen-bonding, or hydrophobic) between the binding sites of the two binding partners. The remarkable specificity stems from the unique configuration and the orientation of these interactions in the three-dimensional space for each different pair of binders [73, 74].

In the context of bioseparations, affinity interactions allow the isolation of a particular target biomolecule of interest by exposing a mixture containing that biomolecule to its specific binding partner, often referred to as the ligand. Ideally, because of the high specificity of the affinity interaction, the ligand will bind to the target biomolecule and to the target biomolecule only, while leaving the impurities behind, thus allowing the efficient isolation of the target biomolecule. To be able to collect the bound target biomolecule separately from the impurities, the ligand is typically immobilized to a stationary phase through covalent linkage (as in affinity chromatography), or captured and concentrated away from the impurities in a different phase (as in affinity extraction) [75]. Although affinity chromatography remains the most well-known and popular choice in the laboratory and in the biotechnology industry among affinity-based separations, other novel schemes of affinity-based separations, aimed at better scalability and greater cost-effectiveness for large-volume products, have also been developed. These include affinity precipitation [76], affinity ultrafiltration [77], affinity extraction into reverse micelles [78], magnetic separation using ligands immobilized on magnetic particles [79], and affinity extraction in two-phase aqueous polymer systems [80].

Since the first affinity-based separation was reported in 1951, when Campbell et al. purified an antibody by attaching its corresponding antigen to cellulose [75], affinity-based separations, especially affinity chromatography, have become commonplace in the

laboratory and in the biotechnology industry. There have been innovations in the design and development of the stationary phase, the ligand, the immobilization or capture method, and more recently, the target binding moiety on the biomolecule [72, 81]. This last innovation, which makes use of molecular cloning techniques to artificially introduce affinity moieties to proteins (often known as "fusion tags"), is especially worth mentioning, since it greatly enhances the applicability of affinity-based separations to practically all proteins for which the corresponding coding genes are available [82]. The variety of affinity interactions being exploited for bioseparations has also grown to be very diverse. Table 6.1 provides a non-exhaustive list of the common types of affinity interactions being exploited in bioseparations [82]. Many commercially available purification kits for proteins have been developed based on the affinity interactions listed in Table 6.1

Ligand	**Target protein or target fusion tags**
Glutathione (GSH)	Glutathione-S-transferase (GST) tag
Transition metal chelates	Polyhistidine tag
Maltose	Maltose binding domain (MBD)
Biotin	Strepavidin / avidin
Antibodies	Antigenic epitopes
Lectins	Glycoproteins
Calmodulin	Calcium-dependent kinases
Triazine dyes	Nucleotide-binding proteins
Heparin	Lipoproteins

Table 6.1: Common types of affinity interactions exploited in bioseparations.

6.2 Selection of the Affinity Ligand

In spite of the great variety of affinity tags available in the market, the development of an effective separation method based on extraction in two-phase aqueous micellar systems remains a formidable challenge. The success of the method depends on the careful selection of the surfactants and the conditions under which the extraction takes place. The surfactant, or surfactant mixture, needs to play a dual role: first, it must form

two-phase aqueous micellar systems under convenient solution conditions, and second, it must possess the affinity ligand as part of its head group, so that the micelles are decorated with binding sites for the tagged protein. Ideally, one would like to use a single surfactant that serves both roles, but in the absence of such an option, mixing two surfactants, one having phase-forming ability and the other bearing the affinity ligand, is the next best alternative. The two options are illustrated in Figure 6-1.

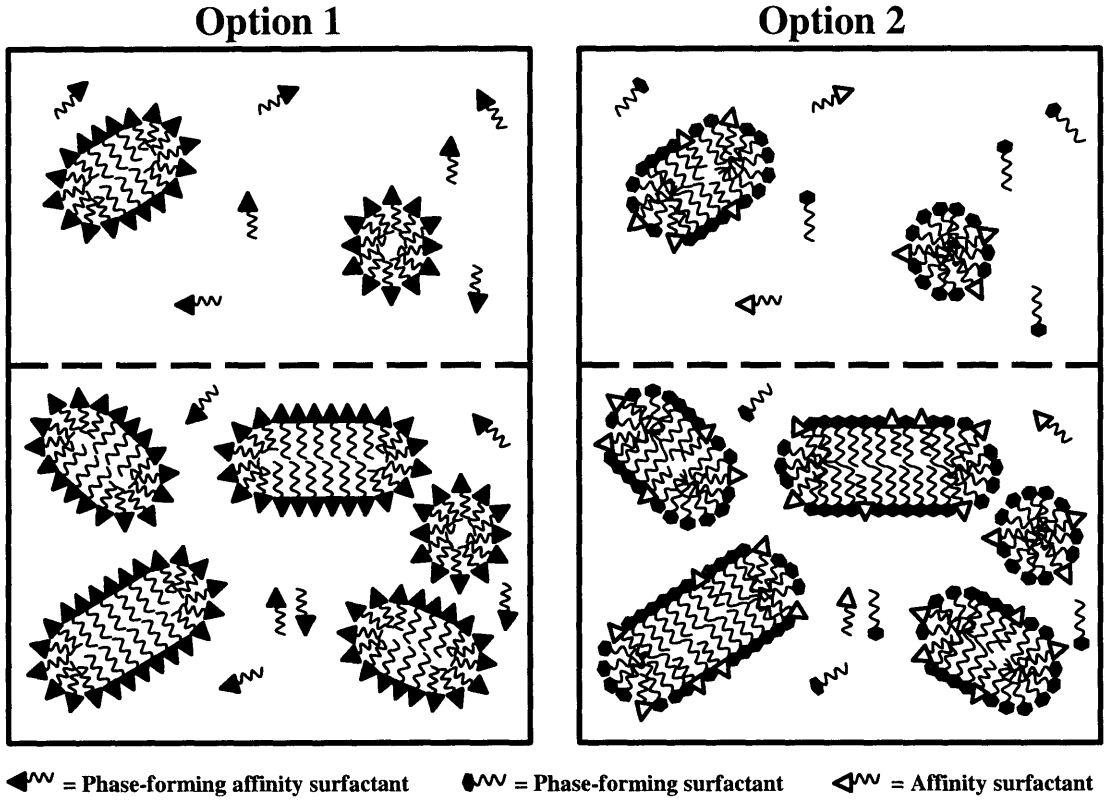

Figure 6-1: Schematic diagram illustrating the two options for incorporating affinity interactions into two-phase aqueous micellar systems. Option 1: The affinity surfactant is able to form two-phase aqueous micellar systems by itself. No mixing is needed. Option 2: The affinity surfactant is unable to form two-phase aqueous micellar systems by itself. It must be mixed with another phase-forming surfactant to create two-phase aqueous micellar systems.

Some important criteria for choosing the appropriate type of affinity interactions to

be used in the proposed cloud-point extraction scheme are listed below.

1. The affinity tag should either be uniquely present in the native protein to be purified, or should be capable of being fused to the protein to be purified by molecular engineering with relative ease. For the method to be generally applicable to all proteins of interest, the latter is preferable to the former. The chosen affinity interaction should not be widely observed in many native proteins, in order to maximize the specificity of the separation.

2. If an engineered protein tag is used, it is imperative that it be reasonably small (economical for the host to produce), highly stable to both thermal and proteolytic degradation, and should not interfere with the normal production and functioning of the target protein.

3. The affinity interactions with the tag should be strong, to maximize the yield and specificity of the separation. In addition, one would like to have the ability to "turn off" the affinity interactions after the extraction is completed, in order to recover the purified protein and recycle the surfactant. This can potentially be achieved by changing the solution conditions (e.g., pH, ionic strength), or by adding a competitive inhibitor, but it should be done in such a way that it does not harm the target protein or contaminate the product with undesirable species.

4. The affinity surfactant should be readily available. It is highly desirable that it be available commercially in purified form and reasonably priced. If not, one would like to have a simple and effective organic synthesis procedure that can be employed to produce the affinity surfactant in large quantities and at high purity, perhaps by derivatizing an existing commercial surfactant. The affinity surfactant should be stable, non-toxic, soluble in water, and non-denaturing to proteins.

5. The affinity surfactant must either phase-separate by itself within a convenient temperature range, or form mixed micelles with another phase-forming surfactant

without disrupting phase separation.

Of the five criteria listed above, criteria 1, 2 and 3 are common to all affinity-based separation methods, and can be satisfied by utilizing existing, proven tag-ligand pairs in other affinity-based separations. Criteria 4 and 5 are unique to affinity-enhanced cloud-point extractions, and together they pose significant challenges to finding an appropriate tag-ligand pair for the proposed separation method. Specifically, the ligand must be in the form of a surfactant, with the binding moiety being all or part of the hydrophilic head, which plays a significant role in the micellization and phase separation process. Consequently, the design problems of identifying a ligand with the desired binding properties, and of creating and optimizing the two-phase aqueous micellar system for separation, are intrinsically coupled. In Section 6.3, some of the previous attempts to implement affinity-enhanced extractions in two-phase aqueous micellar systems are reviewed and evaluated in the context of the criteria listed above. In Chapter 7, the successful proof-of-principle, as well as the theoretical modeling, of affinity-enhanced partitioning in a two-phase aqueous micellar system using a novel sugar-binding fusion tag is presented.

6.3 Past Attempts to Implement Affinity-Enhanced Extractions in Two-Phase Aqueous Micellar Systems

While there have been many attempts to incorporate affinity interactions in two-phase aqueous *polymer* systems [83, 80, 84], there have been relatively few attempts to incorporate affinity interactions in two-phase aqueous micellar systems. The most likely reason for the disparity is the longer history of two-phase aqueous polymer systems and the resulting higher degree of familiarity with the corresponding extraction method among researchers. However, as noted in Section 2.4, there are important advantages of two-phase aqueous micellar systems over their polymer counterparts, especially with regard

to incorporating affinity interactions. In this section, a few selected reports on incorporating affinity interactions in two-phase aqueous micellar systems will be reviewed and evaluated.

Saitoh et al. [85] reported the affinity extraction of avidin in a two-phase aqueous mixed micellar system, generated by mixing a phase-forming zwitterionic surfactant 3-(nonyldimethylammonio)propylsulfate (C_9APSO_4) and a biotinylated phospholipid, which acts as the affinity cosurfactant. The reported recovery of avidin in the micelle-rich phase was 10% in the absence of, and 88% in the presence of, 5.0 $wt\%$ of the biotinylated surfactant (corresponding to avidin partition coefficients of 0.41 and 22.5, respectively), clearly demonstrating the dramatic enhancing effect of the affinity interactions between avidin and the biotinylated surfactant. On the other hand, it was also noted by the authors that the reported method will not be suitable for large-scale extraction, because the elution condition for a biotin-bound avidin is very harsh (pH 1.5 and 6 M guanidinium chloride), which makes the recovery of the protein and the recycling of the surfactant very difficult. Another protein, hexokinase, having an affinity for glucose, was also extracted in two-phase aqueous mixed micellar systems, generated by mixing the nonionic surfactant Triton X-114, or the zwitterionic surfactant C_9APSO_4, with octyl β-D-glucopyranoside (C_8G_1), which acts as the affinity cosurfactant. A significant improvement in the recovery of hexokinase (from 12% to 58%) in the micelle-rich phase was reported in the C_9APSO_4 system, but not with the Triton X-114 system, at an optimal C_8G_1 composition of 20 $wt\%$. There was, however, little explanation or rationalization of the observed results, perhaps due to a lack of understanding of the phase behavior of mixed micellar solutions, as well as of how the affinity interactions affect the partitioning behavior of the protein. The method described by Saitoh et al. is also not generally applicable to other proteins of interest, since the affinity interactions being exploited are unique for the proteins studied.

Linder et al. [86] studied the partitioning of a hydrophobized protein in two-phase aqueous micellar systems generated by the C E surfactants. A fusion protein, EGIc-

HFBI, where EGIc is the catalytic domain of the enzyme cellulase endogluconase I, and HFBI is hydrophobin I derived from the fungus *Trichoderma reesei.* Hydrophobin I is a surface-active protein that has hydrophobic patches on its surface, thereby conferring some hydrophobic character to the otherwise hydrophilic protein EGIc. As such, HFBI acts as a tag that distinguishes the target protein from other protein impurities. EGIc-HFBI was shown to partition strongly to the micelle-rich phase ($K_p > 20$), whereas the unmodified EGIc prefers the micelle-poor phase ($K_p = 0.7$), suggesting that the hydrophobin tag HFBI indeed causes the fusion protein to favor the micelle-rich phase where there is a much greater available volume of hydrophobic micellar cores. To recover the protein, the micelle-rich phase was subsequently extracted with isopropanol, which stripped the surfactant from the fusion protein, enabling the surfactant to be recycled. In subsequent studies, Selber et al. [87] also demonstrated that the EGIc-HFBI can be purified by this method from *T. reesei* cell lysate, both at a small scale of 10 mL and at a large scale of 1200 L, although the partitioning of the protein in the presence of the cell lysate is much less extreme (K_p between 3.8 and 11) than with the purified protein, and there was considerable variation in partitioning performance among different fermentation batches. Although the concept of using a hydrophobizing tag has some important advantages over more conventional affinity tags, there are also some serious drawbacks. Obviously, the most important advantage is that there is no need for a special affinity surfactant; any two-phase aqueous micellar systems can be used to separate based on hydrophobicity. However, because of its peculiar nature, the hydrophobin tag is also quite likely to affect the production and trafficking of the fusion protein in the host cell (although the authors did not report such issues with EGIc-HFBI). The isopropanol extraction needed to recover the protein is also prone to denature some delicate proteins. Moreover, since the hydrophobized protein will be partially buried inside the micelles, it may have a significant and often unpredictable effect on the micellization and the phase behavior, as reflected in the observed phase behavior reported in Linder et al. [86]. This not only poses problems with respect to process control, but it also makes any attempt to

model and understand the partitioning behavior very difficult. As with other attempts to incorporate affinity interactions in cloud-point extractions, a quantitative understanding of the phase behavior and of the protein partitioning behavior appears to be lacking.

In conclusion, while the results discussed above are certainly illuminating and encouraging, there remain significant challenges to be addressed, both in the design and optimization of the extraction system, as well as in developing a fundamental understanding of the phenomenon of affinity-enhanced protein partitioning in two-phase aqueous micellar systems.

Chapter 7

Affinity-Enhanced Protein Partitioning in Decyl β-D-Glucopyranoside ($C_{10}G_1$) Two-Phase Aqueous Micellar Systems

7.1 Introduction

As discussed in Chapter 6, affinity interactions can be incorporated to improve the separation performance of cloud-point extractions. Figure 7-1 shows a schematic diagram illustrating the concept of affinity-enhanced protein partitioning. In affinity-enhanced protein partitioning, a protein of interest that possesses an affinity tag is preferentially extracted to the micelle-rich phase, where more affinity ligands are available. If impurities, such as cell debris, viruses or other proteins, are also present, they are simultaneously removed to the micelle-poor phase, where they experience less excluded-volume interactions from the micelles. Hence, affinity-enhanced protein partitioning represents a

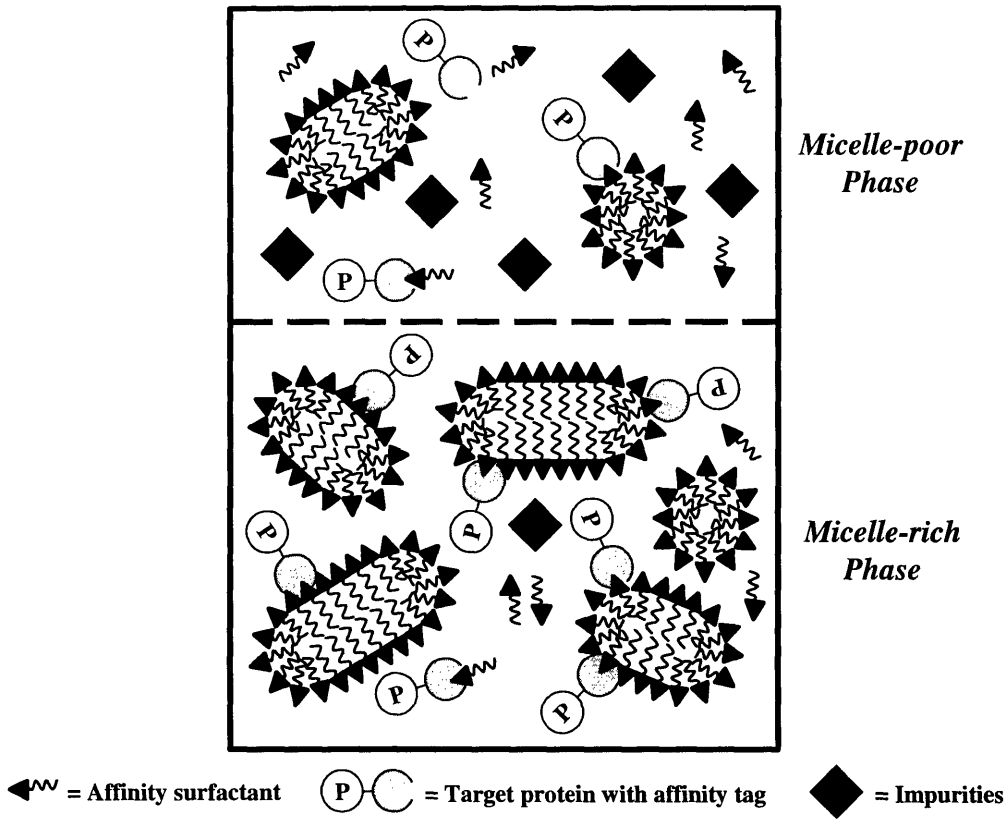

Figure 7-1: Schematic diagram illustrating the concept of affinity-enhanced protein partitioning in two-phase aqueous micellar systems. As shown, the target protein bearing the affinity tag is preferentially extracted to the micelle-rich phase, while impurities are concentrated in the micelle-poor phase.

mechanism by which the target protein can be isolated and concentrated away from the impurities in a mixture.

In this chapter, the proof-of-principle of that concept will be demonstrated experimentally using a novel affinity tag that is particularly suitable for cloud-point extractions. In addition, a detailed theoretical description of affinity-enhanced protein partitioning will be presented and validated using the experimental results. It will become clear that the proposed method introduced in this Chapter addresses some of the shortcomings of the previous attempts made in this area, as discussed in Section 6.3.

As stressed in Section 6.2, although there are numerous protein-based affinity tags [82], and many are commercially available [88], few offer the desirable qualities needed for them to be utilized in two-phase aqueous micellar systems. A novel fusion tag derived from the C-terminal family 9 carbohydrate-binding module (CBM) of xylanase 10A from *Thermotoga maritima* [89] is a promising choice. It binds specifically to the reducing ends of cellulose, as well as to various monosaccharides and disaccharides, a property that is currently unique to this CBM. Measured association constants for binding range from $10^3\ M^{-1}$ for monosaccharides to $10^6\ M^{-1}$ for disaccharides and oligosaccharides [90]. The use of CBM9 as a robust affinity tag for the one-step chromatographic purification of a protein using an inexpensive cellulosic resin has recently been demonstrated [91]. Kavoosi and coworkers [91] have engineered a fusion between CBM9 and the N-terminus of the Green Fluorescent Protein (GFP) from the jellyfish, *Aquorin victoria* [92, 93]. The natural fluorescence of GFP offers a convenient and direct means of tracking and quantifying the target protein throughout the bioseparation.

The fluorescent property of GFP, combined with the sugar-binding affinity of the CBM9 tag, makes the CBM9-GFP fusion protein an appealing choice for the design and study of affinity-enhanced extractions in two-phase aqueous micellar systems. This is because the corresponding affinity surfactants, which belong to the nonionic surfactant family of alkyl polyglucosides (abbreviated as C_iG_j, where i is the number of carbon atoms in the surfactant hydrophobic tail group, and j is the number of glucose moieties in the surfactant hydrophilic head group), are available commercially in large quantities and are also relatively well known [94]. Being nonionic, the C_iG_j surfactants are also known to be mild and usually non-denaturing to proteins. Octyl β-D glucopyranoside (C_8G_1), for example, is widely used to solubilize and crystallize membrane-bound proteins (see, for example, [95]). Another interesting and useful feature of the C_iG_j surfactants is their ability to exhibit cloud-point phase separation within convenient temperature ranges. This implies that the affinity surfactant, by itself, can be used to generate two-phase aqueous micellar systems. In previous attempts to incorporate affinity ligands

into two-phase aqueous micellar systems, including those cited above [85, 96], surfactant mixtures were used, because the surfactant with the affinity moiety is usually not capable of forming two-phase aqueous micellar systems. As a result, another phase-forming surfactant, such as $C_{10}E_4$, must be mixed with the affinity cosurfactants that target the biomolecules. In our case, because C_iG_j can act simultaneously as the affinity ligand and as the phase-forming surfactant, mixing with another phase-forming surfactant is not necessary. Using a binary C_iG_j/water system instead of a ternary system, the experimental protocols are greatly simplified. For example, with one fewer thermodynamic degree of freedom, it is significantly simpler to determine the surfactant concentrations in the two coexisting micellar phases by mapping the phase diagram using the cloud-point method (see Section 7.2). More importantly, the simpler two-phase aqueous micellar system also facilitates the development of a theoretical framework to model and rationalize affinity-enhanced partitioning in two-phase aqueous micellar systems. This is because the current theoretical capabilities to model single surfactant systems are considerably more advanced, and the resulting theoretical predictions of various relevant micellar physicochemical properties are more accurate and reliable.

In view of all the advantages indicated above, a novel two-phase aqueous micellar system consisting of a single surfactant – decyl β-D glucopyranoside ($C_{10}G_1$), which acts both as the phase-forming surfactant and as the affinity surfactant, was created. The effective extraction of the fusion protein CBM9-GFP into the micelle-rich phase of this system was subsequently demonstrated, and conclusive proof that the affinity interactions are indeed responsible for the observed extraction behavior was provided. In addition, a simple theoretical framework to model the phenomenon of affinity-enhanced partitioning in two-phase aqueous micellar systems was developed.

7.2 Materials and Methods

7.2.1 Materials

The *Escherichia coli* strain BL21 (DE3) and the expression vector pET28a were obtained from Novagen (Madison, WI). The vector pGFPuv encoding the GFP protein was purchased from Clontech (Palo Alto, CA). Restriction endonucleases Nhe I and Not I were obtained from New England Biolabs (Beverly, MA). T4-DNA ligase was obtained from Roche Molecular Biochemicals (Laval, Quebec). Perloza MT100 cellulose-based chromatography resin and Ni^{2+}-NTA Sepharose IMAC resin were purchased from Iontosorb Inc. (Czech Republic) and Novagen (Madison, WI), respectively. Kanamycin and all other chemicals used for molecular cloning and protein production were obtained from Sigma (St. Louis, MO).

The nonionic surfactant decyl β-D-glucopyranoside ($C_{10}G_1$, lot no. 012K5028), and all other reagents used in the partitioning experiments, including D-glucose and the buffer salts, were purchased from Sigma (St. Louis, MO). All these materials were of analytical grade, and were used as received. All solutions for the partitioning experiments were prepared at pH 7.2 using a solution of 16.4 mM dissodium phosphate and 1.82 mM citric acid (derived from McIlvaine's buffer [64]) in water purified through a Millipore Milli-Q ion-exchange system (Bedford, MA). The glassware used in all the experiments was washed in a 50 : 50 ethanol : $1M$ sodium hydroxide bath for at least 24 h, then in a $1M$ nitric acid bath for at least 24 h, rinsed with copious amounts of Milli-Q water, and finally dried in an oven.

7.2.2 Cloning of GFP and CBM9-GFP

All cloning procedures were performed according to standard molecular biology techniques [97]. The GFP coding region was amplified from the commercial vector pGFPuv. A Nhe I restriction site (underlined in the DNA sequence below) was introduced at the 5' end of the GFP coding region using the oligonucleotide 5'-TTGCTAGCAAGCTTATGAG

TAAAGGAGAAGA-3' as primer. A Not I restriction site (underlined in the DNA sequence below) was placed at the 3' end using the oligonuleotide 5'-ATTGCGGCCGCTCA TTATTTGTACAGCTCATCCAT-3' as primer. The PCR protocol was carried out as described in Kavoosi et al. [91]. The resulting GFP coding region was digested with Nhe I and Not I and ligated into the pET28a vector using standard reaction conditions (16 $°C$ for 16 h). The pET28a vector places a hexahistidine affinity tag at the N-terminus of GFP. The resulting pET28-GFP expression vector was then sequence-verified and used for the production of GFP, following transformation of *E. coli* strain BL21.

The cloning of the fusion protein CBM9-GFP was carried out as described in Kavoosi et al. [91].

7.2.3 Protein Production and Purification

Protein production was carried out as described in Kavoosi et al. [91]. In brief, overnight cultures of *E. coli* strain BL21 harboring the pET28-GFP plasmid or the pET28-CBM9-GFP plasmid [91] were diluted 100-fold in tryptone-yeast extract-phosphate (TYP) medium supplemented with 50 $\mu g/mL$ of kanamycin. Cells were grown at 37 °C to a cell density (OD_{600nm}) of about 1.0, and protein production was induced with the addition of isopropyl-1-thio-β-D-galactoside (IPTG) to a final concentration of 0.3 mM. Incubation was continued for an additional 10 to 12 h at 30 $°C$. The cells were harvested by centrifugation at $8,500 \times g$ for 20 minutes at 4 $°C$, resuspended in high salt buffer (1 M NaCl, 50 mM potassium phosphate, pH 7.0), and ruptured by two passages through a French pressure cell at a pressure of $21,000$ $lb\ in^{-2}$. Cell debris was removed by centrifugation at $27,000 \times g$ for 30 minutes at $4°C$. CBM9-GFP and GFP were affinity-purified from the clarified cell extract by cellulose affinity chromatography on Perloza MT100 chromatography resin with a nominal particle diameter distribution of 50 to 80 μm [91], and by immobilized-metal affinity chromatography (IMAC) on Ni^{2+}-NTA Sepharose IMAC resin (according to the manufacturer's instructions), respectively.

7.2.4 Determination of CBM9-GFP and GFP Concentrations by Fluorimetry

The determination of CBM9-GFP and GFP concentrations in aqueous surfactant solutions was carried out by fluorimetry in a QuantaMaster luminescence spectrofluorometer (Photon Technology International, Inc., NJ). The excitation wavelength at 395 nm and the emission wavelength at 508 nm were used for both proteins. Calibration curves were determined using prepared solutions of known protein concentrations and surfactant concentrations that matched those of the micelle-rich or the micelle-poor phases. It was observed that the calibration curves were linear at the protein concentrations investigated. The accuracy of the assay was confirmed by measuring the protein concentrations in both phases and determining the overall material balance on the protein.

7.2.5 Determination of the $C_{10}G_1$/Buffer Phase Diagram by the Cloud-Point Method

The phase diagram of $C_{10}G_1$ in buffer was measured by the cloud-point method [47, 98]. Briefly, buffered solutions of $C_{10}G_1$ of known concentrations were prepared and placed in a transparent thermo-regulated device whose temperature was controlled to within 0.02 $°C$. A magnetic stirrer was used to ensure temperature and concentration homogeneity. The temperature was first lowered such that the solution exhibited a single, clear phase. Then, the temperature was raised slowly, and the temperature at which the solution first became cloudy, indicating the onset of phase separation, was noted as T_u. As soon as clouding was observed, the temperature was lowered slowly until the solution became clear again at a temperature T_d. The cloud-point temperature was taken to be the average of T_u and T_d. The procedure was repeated a few times for each data point to ensure reproducibility. The total (monomeric and micellar) $C_{10}G_1$ concentrations in each coexisting phase can be read off the phase diagram by noting the intersections of the operating tie-line and the fitted coexistence curve (see Figure 7-2).

7.2.6 Partitioning GFP and CBM9-GFP in $C_{10}G_1$ Two-Phase Aqueous Micellar Systems

Buffered solutions, each with a total volume of 3 mL, were prepared in graduated 10-mL test tubes. The concentrations of 0.05 g $C_{10}G_1/g$ total, and 0.002 mg CBM9-GFP/g total (0.038 μM) or 0.001 mg GFP/g total (0.038 μM) were used. In order to "tune" the affinity interactions between the protein and the surfactant through competitive inhibition, D-glucose was also added at various concentrations, ranging from 0.02 to 10 mg glucose/g total. The solutions were well mixed and equilibrated at 4 $°C$ in order for each solution to exhibit a clear and homogeneous single phase. Subsequently, the solutions were placed in a thermo-regulated device, previously set at the temperature of 29 $°C$. The observed phase ratio at this temperature was 1 : 1, which also confirmed the accuracy of the phase diagram measured (see Figure 7-2), since a surfactant concentration of 0.05 g $C_{10}G_1/g$ total lies at the mid-point of the tie-line at 29 $°C$. Solutions were maintained at that temperature for at least 6 h to attain partitioning equilibrium. It was observed that the partitioning behavior after 6 h was essentially the same as that observed after 12 h (results not shown). After partitioning equilibrium was attained, the two coexisting micellar phases formed were withdrawn separately with great care, using syringe and needle sets, and the protein concentration in each phase was determined as described above. Each partitioning experiment was repeated at least three times to verify reproducibility.

7.3 Results and Discussion

7.3.1 Mapping the $C_{10}G_1$/Buffer Phase Diagram

The phase diagram of the $C_{10}G_1$/buffer system is presented in Figure 7-2. As shown, the cloud-point method yields a coexistence curve similar in shape to those corresponding to other more common two-phase aqueous nonionic micellar systems, such as those formed

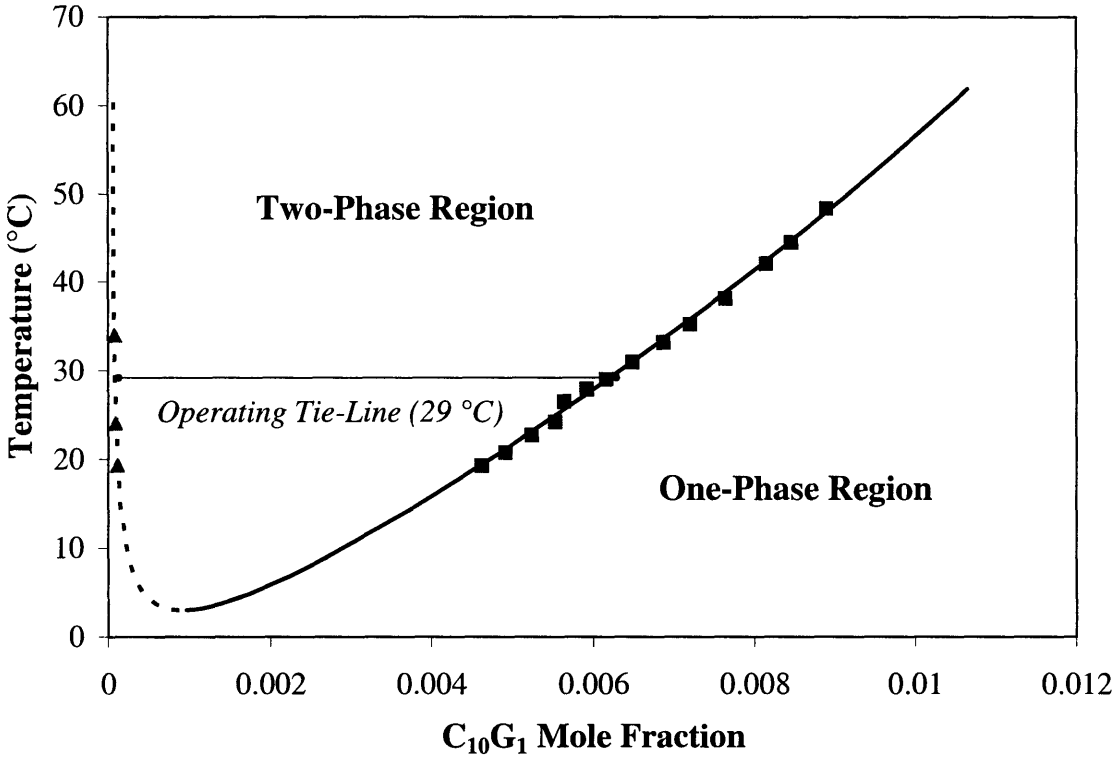

Figure 7-2: Phase diagram of the $C_{10}G1$/buffer system. The solid squares (■) and the solid triangles (▲) represent experimentally measured cloud points corresponding to the micelle-rich branch and the micelle-poor branch, respectively, of the coexistence curve. The errors for the cloud points are about 0.1 $°C$ (within the size of the symbols). The solid line (——) and the dotted line (– –) represent the best-fit of the experimental cloud points using the theory described in Section 7.4.1. The two-phase region, the one-phase region, and the operating tie-line at 29$°C$ are indicated.

by the alkyl poly(ethylene oxide) (C_iE_j) family of surfactants. The cloud-point temperature corresponding to the micelle-poor (left) branch changes much more rapidly with increasing surfactant concentration than that corresponding to the micelle-rich (right) branch. For that reason, it was difficult to obtain more data points for the micelle-poor branch. Only the cloud points within the temperature range between 18 $°C$ and 50 $°C$ were determined, because this range adequately spans the partitioning condition of interest. To generate an appropriate fit through the data points, a micellar phase-separation theory previously developed by the Blankschtein group was utilized [23, 24]. For a detailed description of the theory and the fitting procedure used, see Section 7.4.1.

To ensure that the phase diagram does not change with the addition of protein or glucose, a similar procedure was employed to measure the cloud points of surfactant solutions at the highest concentrations of protein and glucose encountered in this study. It was found that the presence of the protein or of glucose does not alter the phase diagram appreciably (results not shown).

7.3.2 CBM9-GFP Partitioning in $C_{10}G_1$ Two-Phase Aqueous Micellar Systems

The results of the CBM9-GFP partitioning experiments are best summarized in Figure 7-3, in which the measured protein partition coefficients, K_p, are plotted against the added glucose (acting as the inhibitor, I) concentrations. The addition of glucose enables one to "turn off" the affinity interactions between the protein, CBM9-GFP, and the $C_{10}G_1$ surfactants, thereby establishing a baseline at which no affinity interactions are operative. As shown, the baseline protein partition coefficient (at a high glucose concentration of 55 mM) is 0.473 ± 0.005, and the maximum protein partition coefficient (at zero glucose concentration) is 3.1 ± 0.2, which represents more than a six-fold increase in the K_p value.

These results have the following practical implications. First, the effectiveness of the concept of affinity-enhanced partitioning in this simple two-phase aqueous micellar system was clearly demonstrated, since the tagged CBM9-GFP protein was extracted

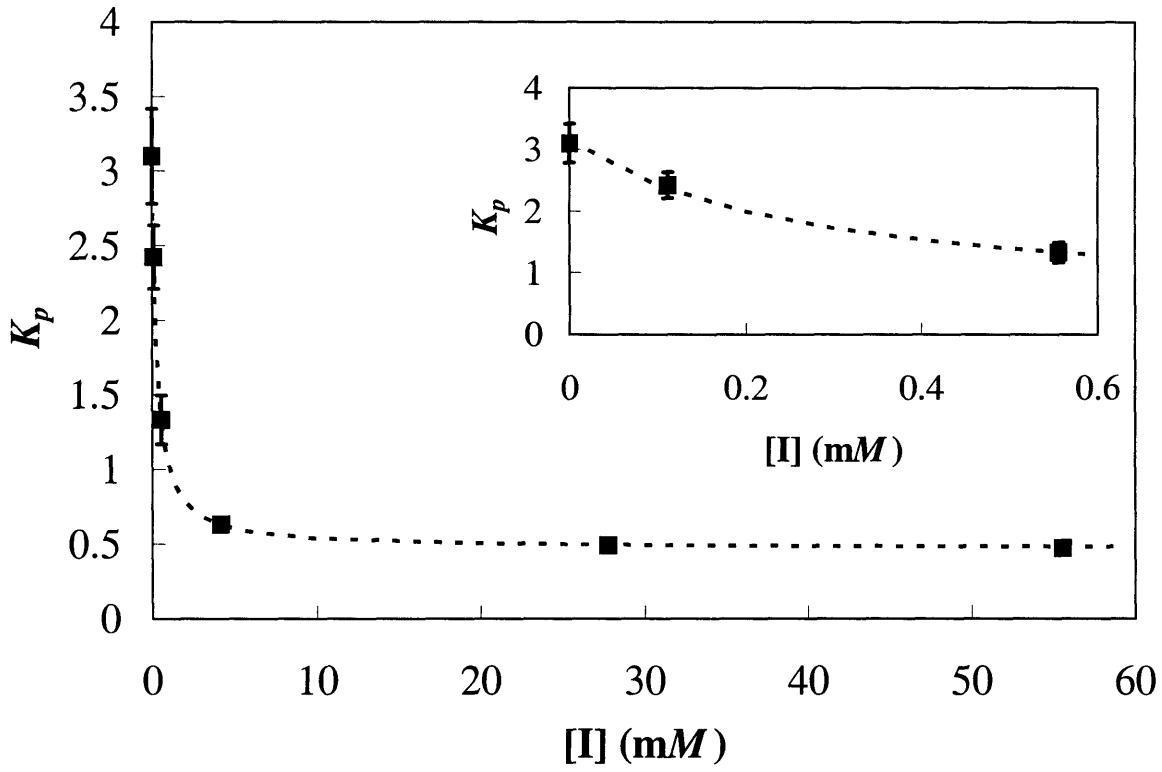

Figure 7-3: Experimentally measured CBM9-GFP partition coefficients, K_p, shown as solid squares (■) in $C_{10}G_1$ two-phase aqueous micellar systems at a temperature of 29.0 °C, at different glucose (inhibitor) concentrations, [I]. The error bars represent 95% confidence intervals obtained from triplicate measurements. The surfactant and protein concentrations were held constant at 0.05 g $C_{10}G_1/g$ total and 0.002 mg CBM9-GFP/g total, respectively. The dotted line (– –) represents the theoretically predicted K_p values, with $K_{mon} = 800\ M^{-1}$, $K_{mic} = 36\ M^{-1}$, and $K_I = 8000\ M^{-1}$. The inset represents a magnification of the graph at the low glucose concentrations.

into the micelle-rich phase ($K_p > 1$), despite the opposing tendency of the excluded-volume effects, which serve to drive any biomolecule into the micelle-poor phase based on its size [47, 48, 49]. In a real separation, this suggests that the tagged protein can be separated from any other large contaminating molecules present in the system. Second, as evident in the remarkable decrease in protein partition coefficient when the affinity interactions are inactivated by the addition of excess glucose, the preference of the protein for the micelle-rich phase in the absence of glucose must be due to the specific affinity interactions between the protein and the surfactant. This suggests that the CBM9 tag is responsible for the partitioning behavior of the protein, implying that the method is, in fact, general as long as the tag is attached to the desired target protein of interest. Third, after the initial extraction step to remove the contaminants in a real separation, it is possible to detach the protein from the surfactant, as well as to back-extract the protein into the micelle-poor phase, simply by adding a small amount of glucose, a safe and inexpensive reagent. This eluting procedure, which has no detrimental effect on the ligand, represents a simple and generic means to recover the extracted protein and recycle the surfactant-ligand.

7.3.3 GFP Partitioning in $C_{10}G_1$ Two-Phase Aqueous Micellar Systems

To further confirm that the observed enhancement in the partitioning of CBM9-GFP shown in Figure 7-3 results from the specific affinity interactions between the surfactant $C_{10}G_1$ and the CBM9 domain, the unmodified GFP in the $C_{10}G_1$ two-phase aqueous micellar system was also partitioned under the same conditions. The protein partition coefficient of GFP was found to be 0.660 ± 0.003, in the absence of glucose. This implies that GFP, unlike CBM9-GFP, partitioned preferentially into the micelle-poor phase ($K_p < 1$), in line with the expectation that in the absence of other interactions, the excluded-volume interactions between the protein and the micelles will tend to drive the protein into the micelle-poor phase based on its size [47, 48, 49]. Note that since GFP is

a smaller protein (26 kDa) than CBM9-GFP (53 kDa), it is expected to be less excluded sterically from the micelle-rich phase than CBM9-GFP, resulting in a less extreme (closer to unity) protein partition coefficient compared to the baseline protein partition coefficient of CBM9-GFP. This is precisely what was observed experimentally, with K_p(GFP) $= 0.660 > K_p$(CBM9-GFP, baseline) $= 0.473$.

7.4 Theoretical Considerations

As stressed in Section 7.1, for the proposed affinity-enhanced separation method to gain acceptance among process engineers, it is of paramount important to develop a fundamental understanding of the phenomenon of affinity-enhanced partitioning in two-phase aqueous micellar system. To this end, a simple and intuitive model for affinity-enhanced partitioning in two-phase aqueous micellar system is developed and presented in this section. The model developed should shed light on the underlying physics that governs protein partitioning, and should facilitate the rational design and optimization of the new separation method by process engineers.

7.4.1 Fitting the Coexistence Curve

The experimentally measured cloud points of the $C_{10}G_1$/buffer system can be fitted to yield a continuous coexistence curve, as shown in Figure 7-4, by using a theory describing phase separation in aqueous surfactant solutions in the dilute regime was developed previously by the Blankschtein group [23, 24]. The procedure described below allows the researcher to validate cloud-point measurements and interpolate between data points properly.

In the context of the theoretical framework described by Blankschtein et al. [23, 24], the phase equilibria of aqueous surfactant solutions can be modeled in terms of two physically relevant parameters, C (a measure of the strength of the intermicellar attractions), and $\Delta\mu$ (a measure of the tendency for micellar growth). If these two parameters

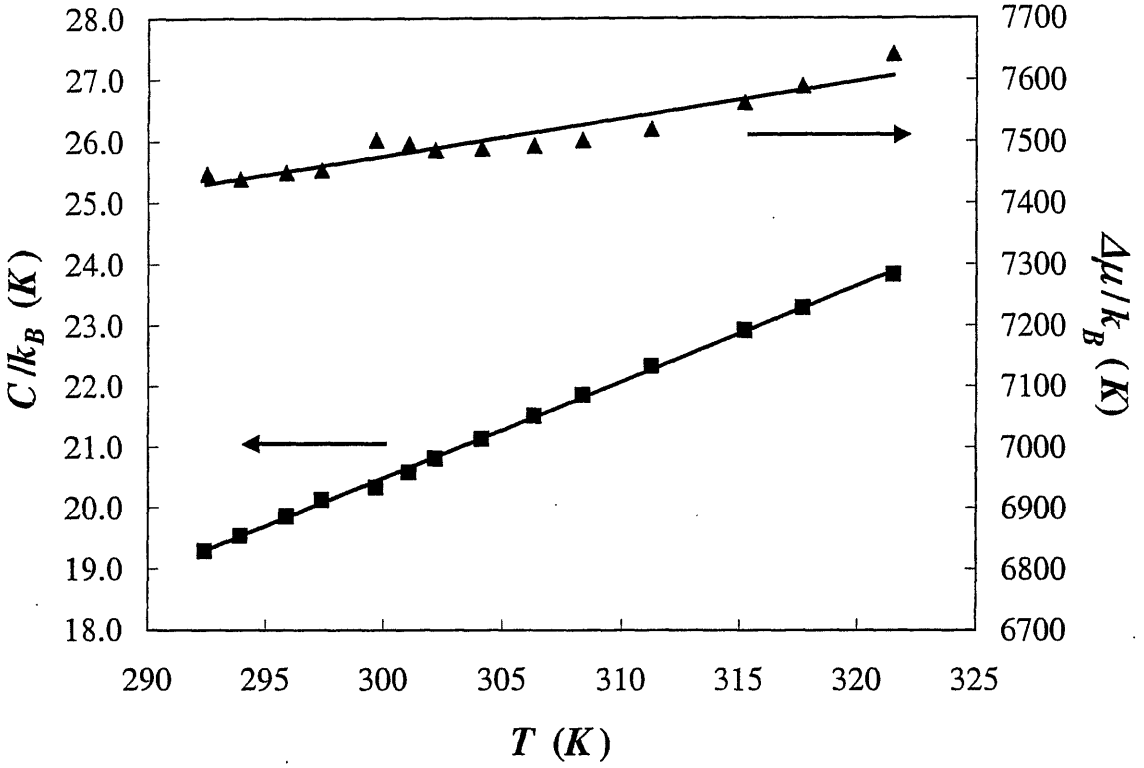

Figure 7-4: The intermicellar interaction parameter, C (■), and the micellar growth parameter, $\Delta\mu$ (▲), versus the absolute temperature, T, as calculated from the experimentally measured cloud points, using Eqs. (7.1) and (7.2). The errors, as calculated from the errors of the cloud-point measurements, are within the size of the symbols. The two solid lines (——) represent linear regressions of the data points.

are known as a function of temperature, the coexistence curve can be predicted for any given two-phase aqueous micellar system. The interested reader is referred to the original papers by Blankschtein et al. [23, 24] for a detailed discussion of the theory.

The coexistence curve of the $C_{10}G_1$/buffer system was generated by calculating C and $\Delta\mu$ from the experimentally measured cloud points, and determining their respective dependence on temperature by regression. The parameters C and $\Delta\mu$ are calculated at a few temperatures using the following expressions [23]:

$$C(Y,Z) = \frac{k_B T}{\gamma}\left[1 + \frac{3\gamma - 2}{3}\right]\left[2\left(\sqrt{Y} + \sqrt{Z}\right)^2 - 3\sqrt{YZ}\right] \tag{7.1}$$

and

$$\Delta\mu(Y,Z) = k_B T \ln\left(\frac{\left[6/(3\gamma - 2)\right]^2}{YZ\left(\sqrt{Y} + \sqrt{Z}\right)^6}\right) \tag{7.2}$$

where Y and Z are the surfactant mole fractions in the micelle-poor and in the micelle-rich phases, respectively, k_B is the Boltzmann constant, T is the absolute temperature, and γ is the ratio of the effective volume of a surfactant molecule to that of a water molecule. The value of γ was taken to be 17.8 for $C_{10}G_1$, which was obtained by taking the ratio of the molecular weight of $C_{10}G_1$ (320 g/mol) to that of water (18 g/mol), in order for it to be consistent with the assumption that the molar volume of the micellar solution is the same as that of water. To actually utilize Eqs. (7.1) and (7.2), one needs to know the values of Y and Z at the same temperature. Since the data points on the micelle-rich and micelle-poor branches do not necessarily match in temperature, for each data point (Z,T) in the micelle-rich branch, the corresponding micelle-poor phase surfactant concentration at the same temperature, $Y(T)$, was calculated by using a quadratic interpolation of the data points on the micelle-poor branch. The values of C and $\Delta\mu$ were calculated at different temperatures and plotted in Figure 7-4.

As shown in Figure , both parameters, C and $\Delta\mu$, fit reasonably well to a straight line in T, similar to that found in the case of another phase-forming nonionic surfactant, $C_{12}E_6$, as reported by Blankschtein et al. [24]. The linear regression analysis yields:

$$C(T)/k_B = 0.1579T - 26.88 \qquad (T \text{ in } K) \tag{7.3}$$

and

$$\Delta\mu(T)/k_B = 6.062T + 5658 \qquad (T \text{ in } K) \tag{7.4}$$

The micelle-rich and micelle-poor surfactant concentrations for any given temperature can then be obtained by solving Eqs. (7.1) and (7.2) simultaneously for Y and Z, using the values of C and $\Delta\mu$ given in Eqs. (7.3) and (7.4). The coexistence curve generated in this manner represents the best-fit to the experimental data. The solid and dotted lines in Figure 7-2 were calculated in this manner. As shown, the theory predicts a theoretical lower consolute (critical) point at a temperature of 3.0 $°C$ and at a surfactant mole fraction of 0.0009. It is also noted that the temperature dependence of C and $\Delta\mu$ in Eqs. (7.3) and (7.4) follow the trends expected in the case of two-phase aqueous micellar systems exhibiting a lower consolute (critical) point, as discussed in Blankschtein et al. [24].

7.4.2 Modeling the Excluded-Volume Contribution to the Protein Partition Coefficient

The partitioning behavior of a protein in a two-phase aqueous micellar system can be quantified in terms of the protein partition coefficient, K_p. If K_p is known, other relevant performance indicators of the separation, such as the yield and the concentration factor, can be calculated [11, 53]. In order to acquire a fundamental understanding of the phenomenon of affinity-enhanced partitioning in two-phase aqueous micellar systems, as well as to rationalize the protein partitioning behavior that we observed, a theoretical framework to model the protein partition coefficient was developed.

In the absence of affinity interactions, it has been shown previously that the partitioning of hydrophilic proteins, such as CBM9-GFP, can be modeled adequately in terms of steric considerations [47, 48, 49]. Specifically, since hydrophilic proteins tend to remain in the aqueous domain external to the micelles when placed in two-phase aqueous micellar systems, their partitioning behavior is a function of the difference in free volumes between the two coexisting micellar phases. In that case, larger biomolecules partition more extremely into the micelle-poor phase where they experience less repulsive excluded-volume (EV) interactions with the micelles. This behavior is captured in the following theoretical

expression for K_p, derived earlier by our group based on statistical-mechanical arguments [47, 48, 49]:

$$K_p^{EV} = \exp\left[-\Delta\phi\left(1+\frac{R_p}{R_0}\right)^2\right] \tag{7.5}$$

where $\Delta\phi$ is the difference in surfactant volume fractions between the micelle-rich and the micelle-poor phases, R_p is the effective hydrodynamic radius of the protein treated as a hard-sphere, and R_0 is the cross-sectional radius of the cylindrical micelles. Comparisons of the predictions of Eq. (7.5) with experimental K_p values have shown that Eq. (7.5) indeed provides quantitative estimates of the protein partition coefficients in systems where only excluded-volume interactions operate.

However, when other types of protein-surfactant interactions, such as electrostatic or affinity interactions, operate, the contributions of such interactions to partitioning must be accounted for, in addition to the excluded-volume contribution. Recently, Kamei et al. developed a detailed protein partitioning theory that incorporates both excluded-volume and electrostatic interactions [52], in order to model the protein partitioning behavior in two-phase aqueous mixed (nonionic/ionic) micellar systems. In the context of the new theory, the partition coefficient of a hydrophilic protein can be expressed as follows:

$$K_p = K_p^{EV} K_p^{elec} \tag{7.6}$$

where K_p^{EV} denotes the excluded-volume contribution to the protein partition coefficient, and is given by Eq.(7.5), and K_p^{elec} denotes the electrostatic contribution to the protein partition coefficient. The excluded-volume interactions and the electrostatic interactions are thus decoupled, and can be modeled separately.

In the same spirit, we propose here that the protein partition coefficient in the presence of affinity interactions can similarly be written as follows:

$$K_p = K_p^{EV} K_p^{aff} \tag{7.7}$$

where K_p^{aff} is the affinity contribution to partitioning. According to Eq. (7.7), it is

expected that when the affinity interactions are absent or inactivated, $K_p^{aff} = 1$ and $K_p = K_p^{EV}$.

7.4.3 Modeling the Affinity Contribution to the Protein Partitioning Coefficient

The protein-surfactant affinity interactions can be modeled as binding reactions, characterized by appropriate equilibrium binding, or association, constants. A similar approach was utilized in the past to model affinity-enhanced partitioning in two-phase aqueous polymer systems [99, 100]. However, unlike polymers, surfactants exist as both micellar aggregates and as monomers in two-phase aqueous micellar systems. Consequently, one should consider two competing binding reactions in the case of a protein-surfactant solution, as follows:

$$P + S_{mon} \rightleftharpoons PS_{mon} \tag{7.8}$$

and

$$P + S_{mic} \rightleftharpoons PS_{mic} \tag{7.9}$$

where P denotes the protein, S_{mon} denotes a monomeric surfactant, PS_{mon} denotes a protein-monomeric surfactant complex, S_{mic} denotes a surfactant molecule in a micelle (referred to hereafter as a micellar surfactant), and PS_{mic} denotes a protein-micellar surfactant complex. The corresponding association constants are defined as follows:

$$K_{mon} = \frac{[PS_{mon}]}{[P]\,[S_{mon}]} \tag{7.10}$$

and

$$K_{mic} = \frac{[PS_{mic}]}{[P]\,[S_{mic}]} \tag{7.11}$$

where square brackets denote concentrations in molar units. Note that we have assumed that the activity coefficients associated with the various components are unity under dilute conditions, and that mole fractions can be replaced by molar concentrations, which is justified given that the molar volume of the solution is approximately equal to that of water.

A few comments are in order regarding the theoretical formulation discussed above. First, the stoichiometry of the protein-surfactant binding was assumed to be 1 to 1, which is consistent with the fact that CBM9 has a single sugar binding pocket [90]. Second, the monomeric surfactants and the micellar surfactants were treated as different entities. Indeed, surfactants coexist as both monomers and micellar aggregates in aqueous solutions of surfactants above the critical micelle concentration (CMC). The monomeric surfactants are distributed in the bulk water, more or less without geometric constraints. On the other hand, micellar surfactants are tightly packed in micelles. Accordingly, from the protein's perspective, the ability to bind to a monomeric surfactant or to a micellar surfactant will not generally be the same, which implies that K_{mon} and K_{mic} may be different. In fact, it is reasonable to expect K_{mon} to be much greater than K_{mic}, due to the following consideration. While the glucosyl head group of a surfactant monomer is more or less fully exposed for binding with the protein, the head group of a micellar surfactant molecule is partially blocked by its immediate neighbors in the micelle. This may hinder the binding, thereby decreasing the association constant, K_{mic}.

To model the presence of a competitive inhibitor, a third binding reaction is included in the theoretical description. Specifically:

$$P + I \rightleftharpoons PI \tag{7.12}$$

where I denotes the inhibitor and PI denotes the protein-inhibitor complex. The equilibrium association constant for the inhibitor is defined as follows:

$$K_I = \frac{[PI]}{[P]\,[I]} \tag{7.13}$$

Using the definitions of the association constants given in Eqs. (7.10), (7.11), and (7.13), the total protein concentration, $[P]^{tot}$, in any phase can be written as follows:

$$[P]^{tot} = [P]\,(1 + K_{mon}\,[S_{mon}] + K_{mic}\,[S_{mic}] + K_I\,[I]) \tag{7.14}$$

The protein partition coefficient, K_p, can then be obtained by applying Eq. (7.14) in both phases. The following expression is obtained:

$$K_p \equiv \frac{[P]_\alpha^{tot}}{[P]_\beta^{tot}} = \left(\frac{[P]_\alpha}{[P]_\beta}\right)\left(\frac{1 + K_{mon,\alpha}\,[S_{mon}]_\alpha + K_{mic,\alpha}\,[S_{mic}]_\alpha + K_{I,\alpha}\,[I]_\alpha}{1 + K_{mon,\beta}\,[S_{mon}]_\beta + K_{mic,\beta}\,[S_{mic}]_\beta + K_{I,\beta}\,[I]_\beta}\right) \tag{7.15}$$

where the subscripts α and β denote the micelle-rich and the micelle-poor phases, respectively . Note that in Eq. (7.15), the ratio $[P]_\alpha/[P]_\beta$ represents the baseline protein partition coefficient when no ligand (surfactant or inhibitor) for the protein is present, that is, when $[S_{mon}] = [S_{mic}] = [I] = 0$. As discussed above, this baseline protein partition coefficient essentially corresponds to the excluded-volume contribution to K_p, that is:

$$K_p^{EV} = \frac{[P]_\alpha}{[P]_\beta} \tag{7.16}$$

A comparison of Eq. (7.7) with Eqs. (7.15) and (7.16) shows that:

$$K_p^{aff} = \frac{1 + K_{mon,\alpha}\,[S_{mon}]_\alpha + K_{mic,\alpha}\,[S_{mic}]_\alpha + K_{I,\alpha}\,[I]_\alpha}{1 + K_{mon,\beta}\,[S_{mon}]_\beta + K_{mic,\beta}\,[S_{mic}]_\beta + K_{I,\beta}\,[I]_\beta} \tag{7.17}$$

Several additional assumptions can be made to further simplify Eq. (7.17) to predict K_p^{aff}. First, provided that the ligands are present in great excess compared to the protein, as was the case in the experiments reported, the unbound ligand concentrations $[S_{mon}]$, $[S_{mic}]$, and $[I]$ in each phase can be approximated by their total concentrations, $[S_{mon}]^{tot}$, $[S_{mic}]^{tot}$, and $[I]^{tot}$, all of which can be measured or estimated experimentally. Although

the protein concentration used in this study was quite low (on the order of 0.01 μM), it is important to note that even if the protein concentration is on the order of 1 g/L (that is, on the order of 10 μM), which corresponds to the upper end of the typical protein titer achievable in *E. coli* fermentation processes [101], the ligands would still be far from being saturated, and this assumption would still be valid. Second, since both the micelle-rich and the micelle-poor phases are largely aqueous, and the micelles in both phases are both cylindrical in shape (as predicted by a molecular-thermodynamic theory of micellization [21, 102], the microenvironments in which the binding takes place are similar. It is therefore reasonable to assume that the association constants are the same in either phase, that is, that $K_{mon,\alpha} = K_{mon,\beta}$, $K_{mic,\alpha} = K_{mic,\beta}$, and $K_{I,\alpha} = K_{I,\beta}$. Third, if the inhibitor is a small molecule like D-glucose, and does not interact specifically with the surfactant, it is expected to partition more or less evenly between the two phases, that is, $[I]_{\alpha}^{tot} = [I]_{\beta}^{tot}$. Utilizing these assumptions, and dropping the phase subscripts when the values corresponding to the two phases are identical, we can rewrite Eq. (7.17) as follows:

$$K_p^{aff} = \frac{1 + K_{mon}\,[S_{mon}]_{\alpha}^{tot} + K_{mic}\,[S_{mic}]_{\alpha}^{tot} + K_I\,[I]^{tot}}{1 + K_{mon}\,[S_{mon}]_{\beta}^{tot} + K_{mic}\,[S_{mic}]_{\beta}^{tot} + K_I\,[I]^{tot}} \tag{7.18}$$

The concentrations can usually be measured experimentally, for example, by mapping the surfactant phase diagram and by estimating the CMC of the surfactant. Therefore, the only unknown parameters in Eq. (7.18) are the three association constants, K_{mon}, K_{mic}, and K_I. If these three association constants are known, Eqs. (7.5), (7.7), and (7.18) can be used to predict the overall protein partition coefficient, K_p, for any protein in a given two-phase aqueous micellar system.

7.4.4 Discussion and Comparison to Experiments

First, the value of K_p^{EV} predicted using Eq. (7.5) is compared with the measured baseline protein partition coefficient. The relevant physical parameters needed are estimated as follows. For the surfactant $C_{10}G_1$, the calculated micellar cross-sectional radius, R_0, is

19 $\AA$, obtained by adding together the optimal micellar core radius (11 $\AA$), evaluated using a molecular-thermodynamic theory of micellization [21, 102], and the length of the glycosyl head group (8 $\AA$), estimated from the bond lengths and angles . At the operating temperature of 29 $°C$, the $C_{10}G_1$/buffer phase diagram indicates that the total (monomeric and micellar) surfactant mole fractions in the micelle-rich and the micelle-poor phases are 0.00616 and 8.46×10^{-5}, respectively (see Figure 7-2). The corresponding surfactant weight fractions are 0.0992 and 0.00150 for the micelle-rich and the micelle-poor phases, respectively, calculated by using the molecular weights of water and $C_{10}G_1$. Since the molar volumes of both phases are approximately equal to that of water, the surfactant volume fraction is equal to the surfactant weight fraction. Accordingly, the difference in surfactant volume fractions between the two phases, $\Delta\phi$, is 0.0977 at 29 $°C$.

Hink and coworkers estimated the hydrodynamic radius of GFP to be 23 $\AA$, which was calculated from the translational diffusion coefficient measured by fluorescence correlation spectroscopy [103]. Approximating GFP as a sphere of radius 23 $\AA$, the theory predicts that $K_p^{EV} = 0.62$ for GFP under the experimental conditions reported, which is in excellent agreement with the measured value of 0.66. As for CBM9-GFP, whose tertiary structure has not yet been solved, one needs to make some educated guesses. The likely shape of CBM9-GFP should be two globules (CBM9 and GFP) joined by a long, flexible linker, assuming that CBM9 and GFP fold independently of each other. The present theory is not capable of dealing with such a shape, and its extension to model a shape of such complexity is beyond the scope of this thesis. The average radius of the CBM9 domain is 26 $\AA$, estimated from the dimensions of its crystal structure [104]. Considering that the effective radius of CBM9-GFP should be somewhere between 49 $\AA$ (the sum of the radii of the two domains) and 26 $\AA$ (the radius of the larger, CBM9 domain), the predicted K_p^{EV} should be between 0.29 and 0.58, according to Eq. (7.5). The measured value of 0.47 falls between these two bounds. The lower bound corresponds to the case when CBM9-GFP essentially behaves as the smallest possible sphere that can contain the two domains in it. (The linker, given its flexibility, is not expected to contribute to

the effective radius of the protein.) The upper bound corresponds to the case when the two domains essentially partition independently of each other, which may be possible given that the linker is sufficiently long and flexible.

The prediction of K_p^{aff} using Eq. (7.18) requires the values of the three association constants, K_{mon}, K_{mic}, and K_I, as inputs. Of these three, only K_I (for glucose as the competitive inhibitor) is known from independent measurements. Boraston and coworkers [90] used two methods to measure the association constant between CBM9 and glucose. Fluorescence titration yielded a value of $1.3 \times 10^4\ M^{-1}$ for K_I, whereas isothermal titration calorimetry yielded a value of $0.3 \times 10^4\ M^{-1}$ [90]. In this thesis, the average of these two values, $0.8 \times 10^4\ M^{-1}$, is used as an estimate of K_I.

Since the values of K_{mon} and K_{mic} are unknown, their values were extracted from the experimental partitioning data, as depicted in Figure 7-3, by nonlinear regression, using the model described in Eq. (7.18). First, the values of the surfactant concentrations, $[S_{mon}]_\alpha^{tot}$, $[S_{mic}]_\alpha^{tot}$, $[S_{mon}]_\beta^{tot}$, and $[S_{mic}]_\beta^{tot}$ were estimated. The total (monomeric and micellar) surfactant concentration in each phase can be read off the phase diagram by noting the intersections of the fitted coexistence curve and the operating tie line at 29 $°C$ (see Figure 7-2). At total surfactant concentrations above the CMC, the monomeric surfactant concentration is very well approximated by the critical micelle concentration (CMC) irrespective of the total surfactant concentration [14]. The micellar surfactant concentration can be calculated by subtracting the CMC from the total surfactant concentration in each phase. Utilizing a molecular-thermodynamic theory of micellization developed by the Blankschtein group, the CMC of $C_{10}G_1$ at 29 $°C$ is estimated to be 1.2 mM [21, 102]. Note that experimentally determined CMC values of $C_{10}G_1$ range from 0.8 mM to 2.2 mM at a slightly lower temperature [94]. The estimated values of the surfactant concentrations used in this chapter are summarized in Table 7.1.

Nonlinear regression was performed on the values of K_p^{aff}, which are calculated by dividing the experimentally determined values of K_p by the baseline K_p (which is equal to K_p^{EV}) of 0.473, according to Eq. (7.7). Performing nonlinear regression using the

Phase	$[S]^{tot}$ (mM)	$[S_{mon}]^{tot}$ (mM)	$[S_{mic}]^{tot}$ (mM)
Micelle-rich phase (α)	342.2	1.2	341.0
Micelle-poor phase (β)	4.7	1.2	3.5

Table 7.1: Estimated values of the surfactant concentrations in each coexisting micellar phase at 29^oC.

software package NLREG (www.nlreg.com), one obtained the following values for the association constants (with their respective 95% confidence intervals generated by the regression procedure):

$$K_{mon} = (800 \pm 220)\ M^{-1} \tag{7.19}$$

and

$$K_{mic} = (36 \pm 4.1)\ M^{-1} \tag{7.20}$$

The best fit generated using these values of K_{mon} and K_{mic} is plotted as the dotted line in Figure 7-3, with $R^2 = 0.9994$. The high quality of the fit suggests that the CBM9-GFP partitioning behavior in the presence of glucose does follow what is expected in the case of competitive inhibition.

As expected from the arguments presented in the Section 7.4.3, the estimated value of K_{mon} is about 20 times higher than that of K_{mic}. It is also important to note that the affinity between the protein and a $C_{10}G_1$ monomer is about an order-of-magnitude weaker than that between the protein and glucose. This is also expected, because the attachment of the surfactant tail at the 1 position of the glucose moiety deprives it of a key hydrogen bonding site believed to be important to the sugar-binding ability of CBM9 [90]. Therefore, the theoretical description is certainly consistent with the experimental partitioning data and with the current understanding of the sugar-binding domain CBM9.

Isothermal titration calorimetry was also attempted to measure the values of K_{mon} and K_{mic} independently. However, it was found that the affinity is too weak to be detected if the association constant is below 1000 M^{-1} (results not shown).

An interesting, and original, feature of the theoretical framework described above is

Phase	% CBM9-GFP bound to micelles	% CBM9-GFP bound to monomers	% CBM9-GFP free
Micelle-rich phase (α)	6.8	86.2	7.0
Micelle-poor phase (β)	46.0	6.0	48.0

Table 7.2: Binding status of CBM9-GFP in each coexisting phase at 29^oC in the absence of glucose, calculated based on the values of the association constants, K_{mon} and K_{mic}, extracted from the partitioning data.

that it accounts explicitly for the role of the surfactant monomers. Often, because one typically works at surfactant concentrations that are much higher than the CMC, the micellar surfactants tend to outnumber the monomeric surfactants considerably, such that any effect associated with the monomers can be safely neglected. However, in the case of affinity-enhanced partitioning in two-phase aqueous micellar systems, because the monomeric surfactants possess a much stronger affinity for the protein than the micellar surfactants ($K_{mon} \simeq 20K_{mic}$), the monomeric contribution to partitioning becomes at least comparable to the micellar contribution, in spite of the fact that there are considerably more micellar surfactants than monomeric surfactants. To illustrate the importance of the monomeric surfactants, Table 7.2 shows a break-down of the binding status of the protein in each phase. In the micelle-rich phase, the monomeric contribution is minimal, since over 86% of the protein residing in that phase is bound to the micelles. On the other hand, nearly half of the protein in the micelle-poor phase is bound to the monomers, which clearly suggests that if the monomeric contribution were ignored, it would not have been possible to explain the observed partitioning results.

Furthermore, since the monomeric surfactant concentrations are approximately equal in the two coexisting micellar phases, the surfactant monomers do not help to promote the partitioning of the tagged protein into the micelle-rich phase. Consequently, the observed increase in K_p must be due solely to the difference in micellar surfactant concentrations between the two coexisting micellar phases. As a matter of fact, the monomeric surfactants act rather as competitive inhibitors, similar to glucose, and in effect hinder the extractive ability of the affinity attractions between the protein and the micelles. This

observation has important practical implications, because unlike glucose, whose concentration can be adjusted, the surfactant monomers are always present in equilibrium with the micelles. This explains partly why the protein partition coefficient is only 3.1, in spite of the about two order-of-magnitude difference in surfactant concentrations that exists between the two coexisting micellar phases. This also suggests that a surfactant having a lower CMC, and hence, a lower monomer concentration, would be a better candidate to implement affinity-enhanced partitioning of the type described in this chapter.

7.5 Conclusions

In this chapter, the successful realization of the concept of affinity extraction in a simple, single-surfactant two-phase aqueous micellar system was presented. The effectiveness of the novel CBM9 sugar-binding protein tag was demonstrated. The results show that the fusion protein CBM9-GFP was extracted preferentially into the micelle-rich phase, with more than a six-fold increase in the protein partition coefficient, due to the specific affinity interactions between the CBM9 domains and the $C_{10}G_1$ surfactants.

A theoretical framework was developed to rationalize and quantify the phenomenon of affinity-enhanced partitioning in two-phase aqueous micellar systems. This theoretical framework, which accounts for both excluded-volume interactions and affinity interactions between the protein and the surfactant, was shown to be consistent with the experimental protein partitioning data, as well as with the current understanding of the sugar-binding domain CBM9. The theoretical framework suggests that the surfactant monomers need to be accounted for as a distinct binding partner for the protein, and that in effect, they behave as competitive inhibitors which are always present in the system. This observation could have important practical implication in the design and development of an industrial unit operation based on affinity extraction in two-phase aqueous micellar systems.

Lastly, it should be noted that the observed affinity between CBM9 and $C_{10}G_1$ is

rather weak, compared to that commonly seen in other affinity bioseparation applications [81, 82]. It is encouraging that even with such a weak affinity (K_{mic} is on the order of 10 M^{-1}), it was still possible to effectively extract the tagged protein into the micelle-rich phase using the method described in this paper. Various ways to further improve the separation, by optimizing the operating temperature, by reducing the monomeric surfactant concentration, as well as by using stronger ligands, will be discussed in Chapter 9.

Chapter 8

Affinity-Enhanced Purification of CBM9-GFP Directly from *E. coli* Cell Lysate

8.1 Introduction

Validating the effectiveness of decontamination and disinfection treatments utilized in many industrial and hospital environments is an important and often challenging task. A biological indicator is a molecule that enables the detection of biological activity, and as such, permits the validation of decontamination or disinfection treatments [105, 106, 107]. The biological indicator can be a specific microorganism suspension (microbiological test system) with a defined resistance to a particular decontamination treatment. Enzymes and proteins have also been used as biological indicators to evaluate the immediate efficacy of industrial procedures, such as blanching, pasteurization, and disinfection treatments, as well as to monitor the satisfactory preservation of a product subjected to disinfection or sterilization [107, 108, 109, 110, 111, 112].

It has recently been proposed that green fluorescent protein (GFP) can be utilized as a biological indicator, due to its simple assay by spectrofluorimetry or by visual inspec-

tion using a hand-held UV lamp [107]. Moreover, GFP has been shown to be extremely resistant to thermal and chemical degradation [107]. The high resistance of GFP to harsh thermal and chemical conditions implies that one can validate the lack of biological activity in the vicinity of the GFP, and therefore, the effectiveness of a particular decontamination or disinfection treatment, when no GFP fluorescence is observed.

A recombinant form of the green fluorescent protein, GFPuv, can be successfully expressed in bacteria, such as *E. coli*, and can be mass-produced by fermentation. However, in order to utilize GFP as a biological indicator, it would be desirable to develop a simple and cost-effective downstream purification process. Currently, GFP is purified on a laboratory scale by three-phase partitioning or by hydrophobic-interaction chromatography [113, 114]. However, these methods only allow the production of a small amount of GFP at high costs. Therefore, it is desirable to develop an alternative separation method which is better suited for the large-scale production of GFP.

With that in mind, it is hoped that affinity-enhanced protein partitioning in two-phase aqueous micellar systems can be utilized to purify GFP. As demonstrated in Chapter 7, CBM9-GFP, that is, GFP fused to a CBM9 affinity tag, can be preferentially and specifically extracted to the micelle-rich phase of the two-phase aqueous micellar system generated by the nonionic surfactant, decyl β-D-glucopyranoside ($C_{10}G_1$), which acts simultaneously as the affinity ligand and as the phase-forming surfactant. At the same time, other hydrophilic biomolecules, including the protein impurities, should partition to the micelle-poor phase and away from the target protein, CBM9-GFP, by virtue of excluded-volume interactions between the impurities and the micelles [47, 48, 49]. Accordingly, the method developed in Chapter 7 should represent an effective separation method to purify and concentrate CBM9-GFP.

In this chapter, the successful preferential extraction of CBM9-GFP (the target protein) from a clarified *E. coli* cell lysate, with the simultaneous removal of protein impurities away from the target protein, will be presented. In so doing, one demonstrates proof-of-principle that affinity-enhanced partitioning in two-phase aqueous micellar sys-

tems can be utilized in a real dirty mixture, which represents an important first step in developing a cost-effective separation method for GFP, a protein that needs to be produced on a large scale in order to be used as a biological indicator. The results also show, for the first time, that affinity-enhanced protein partitioning in two-phase aqueous micellar systems can indeed be utilized in the context of a complex mixture to purify a target protein of interest.

The reminder of the chapter is organized as follows. First, in Section 8.2, the materials and experimental methods utilized in this investigation are described. Next, in Section 8.3, the experimental results are presented and discussed. Finally, concluding remarks are presented in Section 8.4.

8.2 Materials and Methods

8.2.1 Materials

The nonionic surfactant $C_{10}G_1$ (decyl β-D-glucopyranoside, lot no. 012K5028), and all the other reagents used in the partitioning experiments were purchased from Sigma (St. Louis, MO). All reagents were of analytical grade and were used as received. All solutions were prepared at pH 7.2 using 16.4 mM disodium phosphate and 1.82 mM citric acid [64] in water purified through a Millipore Milli-Q ion-exchange system (Bedford, MA). The BCA Protein Assay Kit was purchased from Pierce (Rockford, IL). The glassware used in all the experiments were washed in a 50 : 50 ethanol : $1M$ sodium hydroxide bath for at least 24 h, followed by a $1M$ nitric acid bath for at least 24 h, then rinsed copiously with Milli-Q water, and finally dried in an oven.

8.2.2 Protein Production and Clarified Cell Lysate Preparation

The cloning of the fusion protein CBM9-GFP and the production of the protein in *E. coli* were carried out as described in Kavoosi et al. [91]. Briefly, overnight cultures of *E.*

coli strain BL21 harboring the pET28-GFP plasmid or the pET28-CBM9-GFP plasmid were diluted 100-fold in a tryptone-yeast extract-phosphate (TYP) medium supplemented with 50 $\mu g/mL$ of kanamycin. Cells were grown at 37 $^{\circ}C$ to a cell density (OD_{600nm}) of about 1.0, and protein production was induced with the addition of isopropyl-1-thio-β-D-galactoside (IPTG) to a final concentration of 0.3 mM. Incubation was continued for an additional 10 to 12 h at 30 $^{\circ}C$. The cells were harvested by centrifugation at $8500 \times g$ for 20 min at 4 $^{\circ}C$, resuspended in high salt buffer (1 M NaCl, 50 mM potassium phosphate, pH 7.0), and ruptured by two passages through a French pressure cell at a pressure of 21,000 $lb\ in^{-2}$. Cell debris was removed by centrifugation at $27,000 \times g$ for 30 min at $4^{\circ}C$ to yield the clarified cell lysate used in all the subsequent experiments.

8.2.3 Determination of CBM9-GFP Concentrations by Fluorimetry

The determination of CBM9-GFP concentrations in aqueous surfactant solutions was carried out by fluorimetry in a QuantaMaster luminescence spectrofluorimeter (Photon Technology International, Inc., NJ). The excitation wavelength at 395 nm and the emission wavelength at 508 nm were used. Purified CBM9-GFP, prepared as described in Kavoosi et al. [91], was used to determine the calibration curves. Specifically, solutions of known CBM9-GFP concentrations and surfactant concentrations that matched those of the micelle-rich or the micelle-poor phases were analyzed by fluorimetry, and the fluorescence values were plotted against the CBM9-GFP concentrations. It was observed that the calibration curves were linear at the protein concentrations investigated. The accuracy of the assay was confirmed by measuring the protein concentrations in both micellar phases, and determining the overall material balance on the protein.

8.2.4 Determination of Total Protein Concentrations

Total protein concentrations were determined using the bicinchoninic acid (BCA) method [115]. This method is based on the reaction between the peptide bonds in the vicinity of four particular amino acids (cysteine, cystine, tryptophan, and tyrosine) with Cu^{2+} to form Cu^{+}, which forms a purple complex with BCA. This water-soluble complex exhibits a strong absorbance at 562 nm, which is then measured using a Shimadzu UV-160U spectrophotometer. The assays were conducted following the manufacturer's instructions. The calibration curve was determined using bovine serum albumin (BSA) as the standard. Note that the micelle-rich phase could not be analyzed using this method, due to interference by the high $C_{10}G_1$ concentration (10 $wt\%$) in that phase (the manufacturer's instructions stipulated a maximum allowable concentration of 5 $wt\%$ for C_8G_1, a close analog of $C_{10}G_1$). Therefore, the total protein concentration in the micelle-rich phase was calculated by subtracting the total amount of protein measured in the micelle-poor phase from the initial total amount of protein in the cell lysate.

8.2.5 Determination of the $C_{10}G_1$ Phase Diagram by the Cloud-Point Method

The phase diagram of $C_{10}G_1$ in the presence of the clarified cell lysate was measured by the cloud-point method [47, 98]. For three dilution levels of the clarified cell lysate (5x, 10x, and 40x), $C_{10}G_1$ solutions of known concentrations were prepared and placed in a transparent thermo-regulated device whose temperature was controlled to within 0.02 $°C$. A magnetic stirrer was used to ensure temperature and concentration homogeneity. The temperature was first lowered such that the solution exhibited a single, clear phase. Subsequently, the temperature was raised slowly, and the temperature at which the solution first became cloudy, indicating the onset of phase separation, was recorded. The procedure was repeated at least three times for each data point to ensure reproducibility. The $C_{10}G_1$ concentration in each coexisting micellar phase, corresponding to a specific

temperature, can be read off the resulting phase diagram by noting the intersections of the operating tie-line at that temperature with the coexistence curve.

8.2.6 Partitioning CBM9-GFP in the $C_{10}G_1$ Two-Phase Aqueous Micellar System

Buffered solutions, each with a total volume of 3 mL, were prepared in graduated 10-mL test tubes. The $C_{10}G_1$ surfactant at a final concentration of 0.05 g $C_{10}G_1/g$ total (5 $wt\%$) was mixed with the diluted clarified cell lysate. The resulting solutions were well mixed. Subsequently, the solutions were placed in a thermo-regulated device, previously set at a temperature of 29 $°C$. The observed phase ratio at this temperature was 1 : 1, which also confirmed the accuracy of the measured phase diagram (see Section 8.3), since a surfactant concentration of 0.05 g $C_{10}G_1/g$ total lies at the mid-point of the tie-line at 29 $°C$. Solutions were maintained at that temperature for at least 6 h to attain partitioning equilibrium.

After partitioning equilibrium was attained, the two coexisting micellar phases formed were withdrawn separately with great care, using syringe and needle sets, and the CBM9-GFP and total protein concentrations in each phase were determined as described above. Each partitioning experiment was repeated at least 3 times to ensure reproducibility.

8.3 Results and Discussion

Before partitioning, the CBM9-GFP concentration and the total protein concentration of the clarified cell lysate were determined by fluorimetry and by BCA protein assay, respectively. The CBM9-GFP concentration was (1.81 ± 0.03) mg CBM9-GFP/g total, and the total protein concentration was (25.7 ± 0.4) mg protein/g total. Because of its high viscosity and turbidity, the undiluted cell lysate was difficult to work with using the well-established protocols described in Section 8.2.5. Specifically, it was not possible

to determine the cloud-point temperature accurately, since the clear-to-cloudy transition was blurred by the inherent turbidity of the undiluted cell lysate. Following partitioning, it was also challenging to withdraw the two coexisting micellar phases cleanly using a syringe and needle set, due to the high viscosity of the undiluted cell lysate. Therefore, experiments involving the cell lysate were carried out with a diluted cell lysate. To probe the effect of the dilution levels of the cell lysate on the phase behavior and the partitioning behavior, three different dilution levels (40x, 10x, and 5x) of the cell lysate were investigated.

Since it is often observed that the phase behavior of aqueous micellar solutions can be sensitive to the presence of impurities [94], it was necessary to study how the $C_{10}G_1$/buffer phase diagram, that is, the temperature versus $C_{10}G_1$ concentration coexistence curve, changes in the presence of such a complex mixture. The phase diagram of the $C_{10}G_1$/buffer system in the presence of the cell lysate was therefore mapped for the three dilution levels considered, and the results are presented in Figure 8-1. The experimentally measured coexistence curve, as well as the theoretical fit of the data, in the absence of any cell lysate, as shown in Figure 7-2, are also presented for comparison purposes. As can be seen, the coexistence curves in the presence of the diluted cell lysate (at the three dilution levels considered) are indistinguishable from each other and from the one in the absence of the cell lysate. This somewhat surprising result can be confirmed if the observed phase ratios corresponding to the resulting two-phase aqueous micellar systems are accurately predicted by the lever rule [10]. Specifically, as predicted by the lever rule, for the three partitioning experiments corresponding to the three cell lysate dilution levels, a $1:1$ phase ratio was indeed observed for a 5 $wt\%$ $C_{10}G_1$ solution at 29 $^{\circ}C$.

The partitioning behavior of the target protein CBM9-GFP can be quantified in terms of its partition coefficient, defined as:

$$K_{CBM9-GFP} = \frac{[CBM9-GFP]_{\alpha}}{[CBM9-GFP]_{\beta}}$$

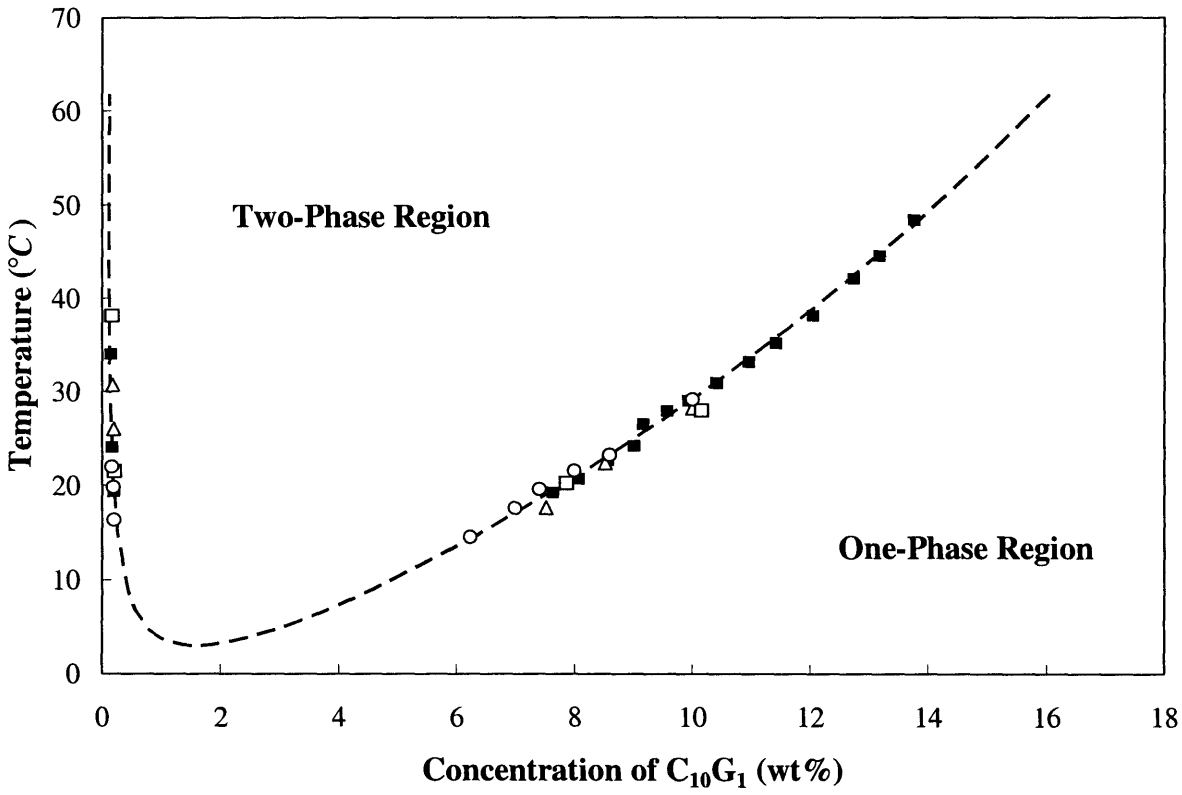

Figure 8-1: Experimentally measured phase diagram of the $C_{10}G_1$/buffer system in the absence and in the presence of the cell lysate. The solid squares (■) represent experimentally measured cloud points in the absence of the cell lysate. The open circles (○), open squares (□), and open triangles (△) represent experimentally measured cloud points of the $C_{10}G_1$/buffer system in the presence of the cell lysate diluted 40x, 10x, and 5x, respectively. The errors for the cloud points are about 0.1 $°C$ (within the size of the symbols). The dotted line (- - -) represents the theoretical best-fit of the experimental cloud points, as presented in Figure 7-2. The two-phase region, and the one-phase region are indicated.

where $[CBM9-GFP]_\alpha$ and $[CBM9-GFP]_\beta$ are the measured CBM9-GFP concentrations in the micelle-rich (α) and in the micelle-poor (β) phases, respectively. To quantify the effectiveness of the separation method in removing unwanted impurities, it is helpful to define the overall partition coefficient of other proteins present in the clarified cell lysate, K_{OP}, where:

$$K_{OP} = \frac{[P]_\alpha - [CBM9-GFP]_\alpha}{[P]_\beta - [CBM9-GFP]_\beta}$$

where $[P]_\alpha$ and $[P]_\beta$ are the measured total protein concentrations in the micelle-rich and micelle-poor phases, respectively. The results of the partitioning experiments, in terms of the measured partition coefficients, $K_{CBM9-GFP}$ and K_{OP}, are presented in Figures 8-2 and 8-3, respectively.

In Figure 8-2, the experimentally measured CBM9-GFP partition coefficients corresponding to the three cell lysate dilution levels considered are shown along with the partition coefficient value corresponding to the partition of CBM9-GFP in the absence of the cell lysate, as discussed in Chapter 7. Under the same experimental conditions (29 $°C$, 5 $wt\%$ $C_{10}G_1$), the CBM9-GFP partition coefficients corresponding to the three cell lysate dilution levels are statistically indistinguishable ($K_{CBM9-GFP} \simeq 3$). The greater than unity $K_{CBM9-GFP}$ values clearly demonstrate the effectiveness of the concept of affinity-enhanced partitioning in this simple two-phase aqueous micellar system, since the affinity-tagged CBM9-GFP protein was successfully extracted into the micelle-rich phase, despite the opposing tendency of the excluded-volume effects, which serve to drive any biomolecule into the micelle-poor phase based on its size [47, 48, 49]. Moreover, the observed similar $K_{CBM9-GFP}$ values at the three cell lysate dilution levels considered suggests that the affinity ligands available on the surface of the $C_{10}G_1$ micelles are not saturated, and are effective in of handling an industrially relevant concentration (0.36 mg CBM9-GFP/g total) of the target protein. Lastly, the fact that the $K_{CBM9-GFP}$ values in the presence of the diluted cell lysate closely match those obtained for CBM9-GFP in the absence of the cell lysate is also very encouraging from a practical point of view, since it

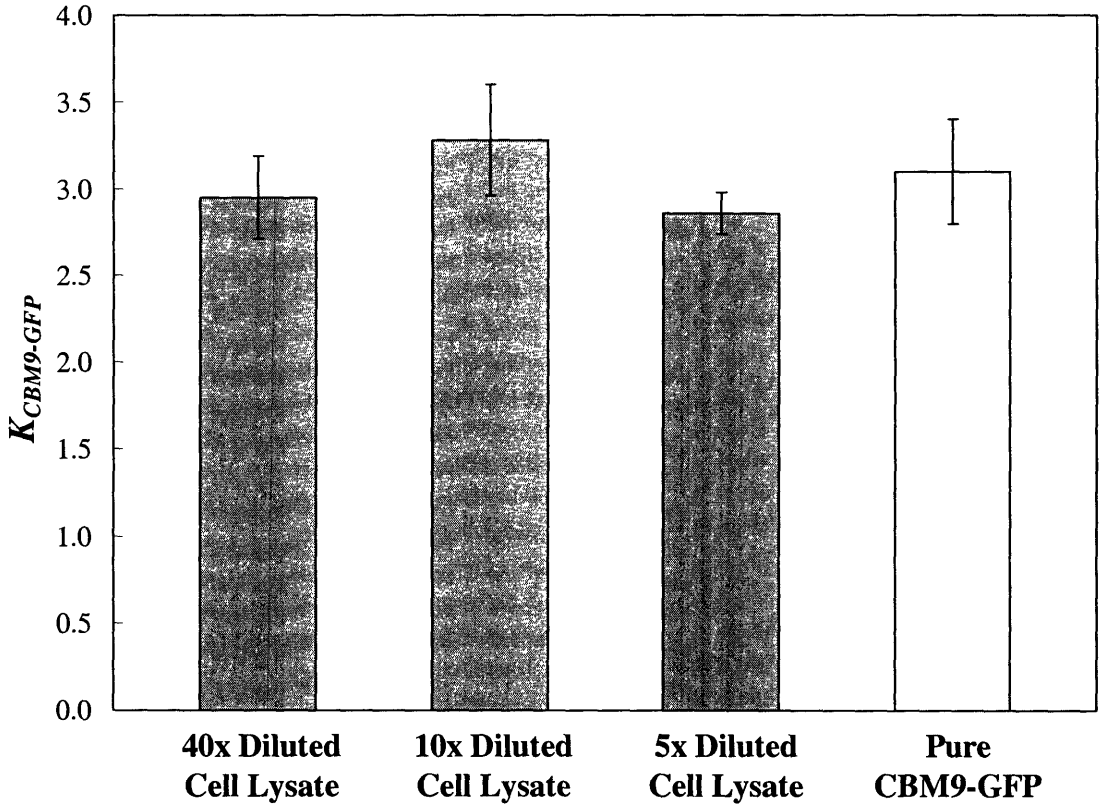

Figure 8-2: Experimentally measured partition coefficients of the target protein CBM9-GFP, $K_{CBM9-GFP}$, at the three different cell lysate dilution levels considered: 40x, 10x, and 5x (gray bars). The $K_{CBM9-GFP}$ value corresponding to the partitioning of the purified CBM9-GFP (see Chapter 7), under the same experimental conditions (29 $^{\circ}C$, 5 $wt\%$ $C_{10}G_1$), is shown (white bar) for comparison purposes. The error bars represent 95% confidence limits for the measurements.

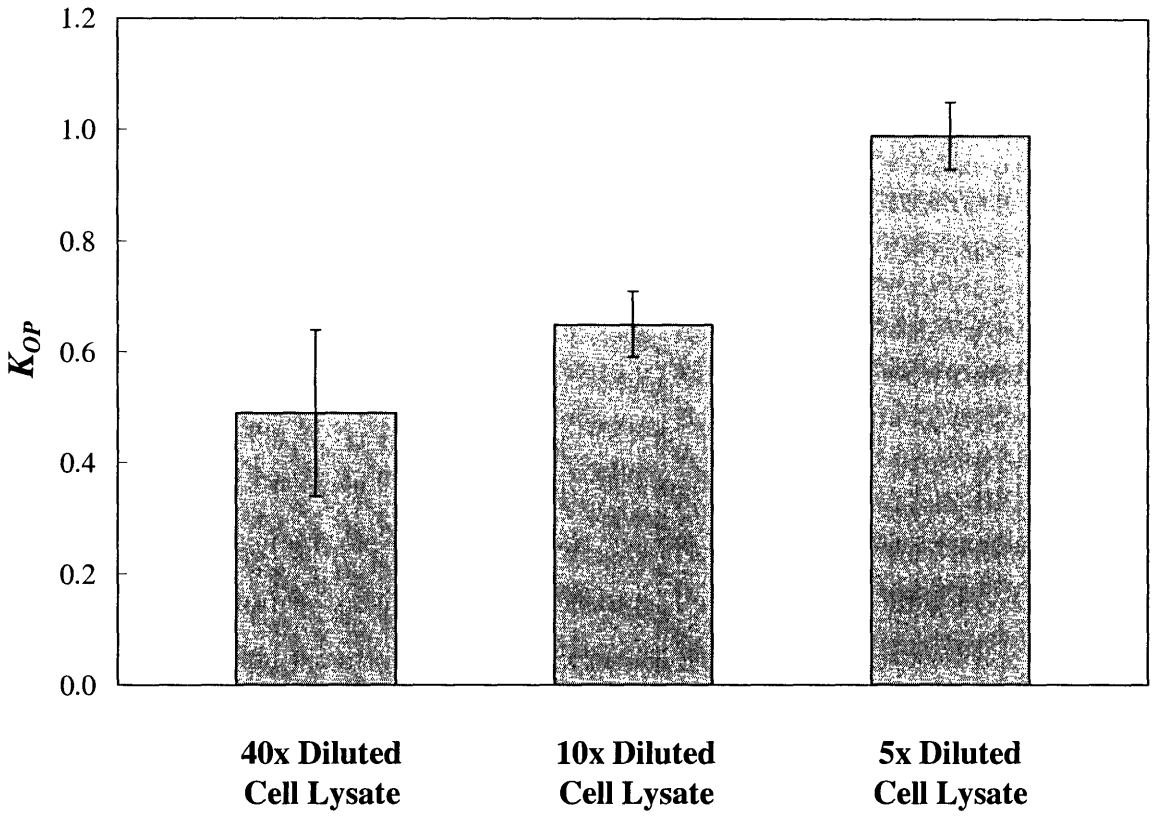

Figure 8-3: Experimentally measured partition coefficients of other proteins present in the cell lysate, K_{OP}, at the three cell lysate dilution levels considered: 40x, 10x, and 5x, under the same experimental conditions (29 $°C$, 5 $wt\%$ $C_{10}G_1$).

suggests that the presence of the cell lysate does not interfere with the affinity-enhanced extraction of the target protein. Furthermore, the independence of the CBM9-GFP partition coefficient on the presence of the impurities also implies that the theoretical framework formulated to describe affinity-enhanced protein partitioning in two-phase aqueous micellar systems, as discussed in Section 7.4, should apply equally well to an affinity-tagged protein in a complex mixture, because the theoretical model has been validated in the case of the purified protein.

The experimental overall partition coefficients of the protein impurities present in the cell lysate, K_{OP}, are shown in Figure 8-3. Contrary to what is observed in the case

of the partition coefficients of the target protein (see Figure 8-2), there appears to be a greater variation in the K_{OP} values at different cell lysate dilution levels, with K_{OP} at 40x dilution having the lowest value (0.49 ± 0.15), followed by K_{OP} at 10x dilution (0.65 ± 0.06), and finally by K_{OP} at 5x dilution having the highest value, (0.99 ± 0.09). In principle, one expects hydrophilic protein impurities to partition preferentially to the micelle-poor phase, due to excluded-volume interactions between the proteins and the micelles, resulting in a protein partition coefficient value below 1. Considering that a large amount of hydrophobic, membrane-bound proteins should have been removed along with the cell debris when the cell lysate was clarified, the majority of the remaining protein impurities in the cell lysate should be mostly hydrophilic. Therefore, based on excluded-volume considerations, one would expect that the total partition coefficient of these proteins, K_{OP}, should be less than 1, and this is indeed the case for the 10x and the 40x diluted cell lysates (see Figure 8-3). From a practical view point, this also implies that the separations method was indeed capable of extracting the tagged protein into the micelle-rich phase ($K_{CBM9-GFP} > 1$), while removing the majority of the protein impurities to the micelle-poor phase ($K_{OP} < 1$).

Because of the complexity of the cell lysate, and the inability of the BCA total protein assay to measure individual impurity concentrations, we were not able to rigorously investigate the observed variation of K_{OP} at the three cell lysate dilution levels considered (see Figure 8-3). Intuitively, however, one may conjecture that the observed variation is the result of slow, but gradual, denaturation of the protein impurities in the two-phase aqueous micellar system, an effect which is likely to be more pronounced at higher protein concentrations. Indeed, it has been well documented that proteins are more prone to denaturation at higher concentrations [116, 117, 118]. While the target protein CBM9-GFP, which consists of the two highly robust domains, CBM9 and GFP, did not seem to undergo denaturation during the course of the experiments, the less stable protein impurities in the cell lysate may undergo gradual denaturation, a process which occurs spontaneously in any cell lysate, but which may be accelerated in the presence of a

surfactant at an elevated temperature. The denatured protein impurities, which typically have a stronger hydrophobic character due to the exposure of more hydrophobic amino acid residues as the protein denatures (unfolds), may be more attracted to the micelle-rich phase than they would be in their native, non-denatured, state. This would lead to a higher partition coefficient than what would be expected based solely on excluded-volume considerations, which in turn, would increase K_{OP} values. An experimental observation which is consistent with this conjecture was the appearance of a visible amount of white precipitate, which is likely to correspond to denatured protein aggregates that precipitated out of solution, at the interface between the two coexisting micellar phases when the partitioning experiment was allowed to proceed for a longer time.

8.4 Conclusions

In this chapter, proof-of-principle of the affinity-enhanced extraction of an affinity-tagged protein directly from a cell lysate using two-phase aqueous micellar systems was demonstrated. The effective separation of the target protein, CBM9-GFP, from other protein impurities present in the cell lysate, was attained using a simple two-phase aqueous micellar system formed by only a single nonionic surfactant, $C_{10}G_1$, which acts simultaneously as the phase-forming surfactant and as the affinity ligand.

To probe the effect of the dilution levels of the cell lysate on the phase behavior and on the protein partitioning behavior, three different dilution levels (40x, 10x, and 5x) of the cell lysate were investigated. The target protein partition coefficient ($K_{CBM9-GFP}$) was found to be independent of the cell lysate dilution levels, and statistically identical to the value obtained with purified CBM9-GFP. The results suggest that the presence of the impurities does not interfere with the partitioning of the target protein, and that the system is effective in handling industrially relevant protein concentrations. The protein impurities present in the cell lysate, on the other hand, were found to partition preferentially to the micelle-poor phase, where they experience less steric, or excluded-

volume, interactions. Interestingly, a more even partitioning of the protein impurities was observed at higher cell lysate concentrations. Gradual denaturation of the protein impurities was proposed as a possible explanation for their partitioning behavior.

In conclusion, the successful implementation of affinity-enhanced protein partitioning in two-phase aqueous micellar systems directly from a cell lysate, presented in this chapter, represents an important first step towards developing a cost-effective separation method for GFP, and more generally, for other proteins of interest.

Chapter 9

Improving Affinity-Enhanced Protein Partitioning in Two-Phase Aqueous Micellar Systems

9.1 Introduction

Now that proof-of-principle of affinity-enhanced protein partitioning in two-phase aqueous micellar systems has been successfully demonstrated in Chapters 7 and 8, it is practically relevant to investigate how to improve the partitioning performance by optimizing various aspects of the system. Fortunately, because a theoretical framework to model the partitioning behavior has already been developed (see Section 7.4), one can address this need by pursuing a rational design approach, based on the fundamental understanding of the phase behavior of micellar solutions and of the protein partitioning behavior. It is hoped that the theoretical framework presented in Section 7.4 can assist the process engineer in finding the optimal operating conditions for the separation, as well as in designing the process in a manner that is best suited for the specific purification needs.

In general, the process engineer who attempts to implement affinity-enhanced partitioning in two-phase aqueous micellar systems has the ability to manipulate various

aspects of the system, some more easily than others. For example, the operating temperature and pH, as well as the initial surfactant and protein concentrations, can all be easily changed, subject to the limitations imposed by the micellar phase behavior and by the ability of the protein not to undergo denaturation at those conditions. More generally, the process engineer can also: (i) choose a different phase-forming surfactant-ligand, (ii) use a surfactant mixture of adjustable composition, (iii) modify the protein tag to improve affinity, or (iv) exploit a completely different type of affinity interaction. There are no doubt a great deal of choices and a vast parameter space that the process engineer can explore to improve the separation, in the context of affinity-enhanced partitioning in two-phase aqueous micellar systems.

Not every modification will impact the separation efficiency, let alone lead to a significant improvement. For example, it has been shown both experimentally and theoretically that the protein partition coefficient does not depend on the initial surfactant concentration (in the case of a single surfactant) [10, 11], since this only affects the phase ratio, but not the surfactant concentrations of the micelle-rich and the micelle-poor phases However, note that changing the phase ratio does allow one to optimize other important separation characteristics, such as yields and concentration factors. As long as the proteins remain relatively dilute so that they do not interact with each other or saturate the ligands, the initial protein concentration also does not affect the protein partition coefficient, as has been frequently observed experimentally [47, 12]. On the other hand, most other modifications to the operating parameters and to the system components can potentially influence various aspects of the micellar phase behavior and of the protein partitioning behavior, thus providing opportunities for the process engineer to improve the separation.

With the above in mind, this chapter discusses various strategies to improve the target protein separation by *slightly perturbing* the basic system considered in Chapters 7 and 8. In other words, these strategies represent an exploration of the "lower-hanging fruits" of a vast optimization space, in order to illustrate some practical approaches that the

process engineer may adopt, as well as some potential pitfalls that the process engineer may encounter, in the rational design and optimization of the separation. It should be emphasized that the strategies discussed here do by no means exhaust all the possible ways to improve the separation, due to their limited scope. In this chapter, three specific strategies will be discussed and investigated (see Sections 9.3.1, 9.3.2, and 9.3.3), following a description of the materials and methods used in these investigations in Section 9.2.

Based on the theoretical model described in Section 7.4, one can identify several possible strategies to improve the separation. First, the tie-line length has a great impact on the separation. Mechanistically, the tie-line length can affect partitioning in several ways. In terms of the target protein partition coefficient, K_p, the excluded-volume contribution, K_p^{EV}, is clearly a strong function of the tie-line length $(\phi_\alpha - \phi_\beta)$ [see Eq. (7.5)]. In addition, the affinity contribution, K_p^{aff}, also depends on the tie-line length by virtue of its dependence on the surfactant concentrations in either of the coexisting micellar phases [see Eq. (7.18)]. Moreover, the tie-line length also affects the steric exclusion of the impurities into the micelle-poor phase, the extent of which influences the overall quality of the separation. Intuitively, the selectivity of the separation should improve when the two coexisting micellar phases are more dissimilar (corresponding to longer tie-lines), although practical considerations, such as yield maximization, may ultimately drive the design decision. In Section 9.3.1, the effect of changing the operating tie-line length, by changing the operating temperature, will be discussed.

A second strategy to improve the separation is to minimize the monomeric surfactant concentrations, as suggested by the theoretical model presented in Section 7.4. Specifically, the monomeric surfactants, despite their low concentrations, are capable of binding the target protein with an affinity that is higher than that of the micellar surfactants. Accordingly, because the monomeric surfactants are distributed evenly between the two coexisting micellar phases, they essentially act as competitive inhibitors. In a way, minimizing the monomeric surfactant concentrations also increases the dissimilarity between the two coexisting micellar phases, which, in turn, should improve the selectivity of the

separation. In Section 9.3.2, the effect of varying the monomeric surfactant concentration on protein partitioning will be discussed.

A third strategy to improve the separation is to increase the strength of the affinity interactions. A stronger affinity ligand would result in a decreased amount of unbound protein at equilibrium, which should lead to an improved target protein partition coefficient. The affinity between the CBM9 tag and the surfactant-ligand $C_{10}G_1$ is quite weak ($K_{mic} \simeq 36M^{-1}$), and therefore, there should be ample room for improvement, either by choosing a better surfactant-ligand or by engineering the protein tag. Nevertheless, it should be noted that despite the low affinity, the observed enhancement of the target protein partition coefficient is already quite high (more than 6-fold; see Figure 7-3), sufficient for an effective separation if the extraction is run continuously in a countercurrent, multi-equilibrium-stage manner [9]. This is due to the fact that the weak affinity is compensated by the extremely large surface area covered by the affinity ligands, due to the small size of the $C_{10}G_1$ micelles. In Section 9.3.3, the effect of varying the affinity strength on protein partitioning will be discussed.

9.2 Materials and Methods

9.2.1 Materials

The target fusion protein, CBM9-GFP, was produced and purified by the procedure described in Section 7.2. The surfactant decyl β-D-glucopyranoside ($C_{10}G_1$, lot no. 012K5028), the lyophilized protein horse heart cytochrome c (lot no. 77H7052), sodium L-ascorbate (lot no. 46H02965), as well as the buffer salts, were purchased from Sigma (St. Louis, MO), and were used as received. All solutions used in the cloud-point temperature measurements and in the partitioning experiments were prepared at pH 7.2 using a solution of 16.4 mM dissodium phosphate and 1.82 mM citric acid (derived from McIlvaine's buffer [64]) in water purified through a Millipore Milli-Q ion-exchange system (Bedford, MA). The glassware used in all the experiments was washed in a 50 : 50

ethanol : $1M$ sodium hydroxide bath for at least 24 h, then in a $1M$ nitric acid bath for at least 24 h, rinsed with copious amounts of Milli-Q water, and finally dried in an oven.

9.2.2 Partitioning CBM9-GFP and Cytochrome c Simultaneously in the $C_{10}G_1$/Buffer Two-Phase Aqueous Micellar System

To demonstrate the capability of the method to purify the target protein, CBM9-GFP, from a model impurity, cytochrome c, with adequate selectivity, the two proteins were partitioned simultaneously in the $C_{10}G_1$/buffer two-phase aqueous micellar system, using the same procedures described in Section 7.2.6. The partitioning experiments were conducted at three different temperatures, namely, 19.6 $°C$, 29.0 $°C$, and 37.0 $°C$. The initial surfactant concentrations were 0.04 g $C_{10}G_1/g$ total (at 19.6 $°C$), 0.05 g $C_{10}G_1/g$ total (at 29.0 $°C$), and 0.06 g $C_{10}G_1/g$ total (at 37.0 $°C$). Under the three solution conditions considered, a phase volume ratio of approximately 1 was obtained, which was the expected value based on applying the lever-rule to the respective tie-lines at the three temperatures considered. The initial protein concentrations used were 0.01 mg CBM9-GFP/g total (0.19 μM) and 0.32 mg cytochrome c/g total (26.0 μM) at the three conditions.

The cytochrome c concentrations of the micelle-rich and the micelle-poor phases were determined by spectrophotometry using a Shimadzu UV-160U UV-Visible Recording Spectrophotometer (Columbia, MD), according to a protocol developed by Kamei et al. [10]. Following the addition of L-ascorbate to the sample in the cuvette to ensure that all the cytochrome c was in its reduced form, the absorbance of the sample was measured at 549.5 nm. The CBM9-GFP concentrations of the micelle-rich and the micelle-poor phases were determined by fluorimetry, as described in Section 7.2.4. Calibration curves were determined using prepared solutions of known protein concentrations and surfactant concentrations that matched those of the micelle-rich or the micelle-poor phases. Due to

the presence of a high concentration of cytochrome c, which has significant absorbance at 395 nm (the excitation wavelength for CBM9-GFP), a different calibration curve was determined for CBM9-GFP at each cytochrome c concentration encountered. The cytochrome c assay was found not to be affected by the presence of CBM9-GFP at very low concentrations. It was observed that the calibration curves were linear at the protein concentrations investigated. The accuracy of the assay was confirmed by measuring the protein concentrations in both coexisting micellar phases and determining the overall material balance on the protein.

9.3 Results and Discussion

9.3.1 Optimizing the Tie-Line Length

According to the phase diagram of the $C_{10}G_1$/buffer system, shown in Figure 7-2, the tie-line length increases as the operating temperature is increased. The manner in which this happens can be predicted, given the relevant temperature-dependent parameters $C(T)$ and $\Delta\mu(T)$, using the theory for micellar phase behavior discussed in Section 7.4.1. Therefore, the operating temperature is a convenient experimental parameter that one can vary to control the tie-line length. For the $C_{10}G_1$/buffer system, the variation of the tie-line length with temperature is shown in Figure 9-1.

Note, however, that varying the operating temperature does more than just vary the tie-line length. The monomeric surfactant concentration, $[S_{mon}]$, which is approximately the same in both coexisting micellar phases (that is, $[S_{mon}] = [S_{mon}]_\alpha = [S_{mon}]_\beta$), is also a function of temperature. As discussed in Section 7.4, the monomeric surfactants affect the protein partition coefficient because they act as competitive inhibitors. Using the molecular-thermodynamic theory of micellization developed by the Blankschtein group [21, 102], the monomeric surfactant concentration can be predicted at different temperatures, and the results are shown in Figure 9-2.

As shown in Figure 9-2, $[S_{mon}]$ increases slowly as the temperature is increased. This is

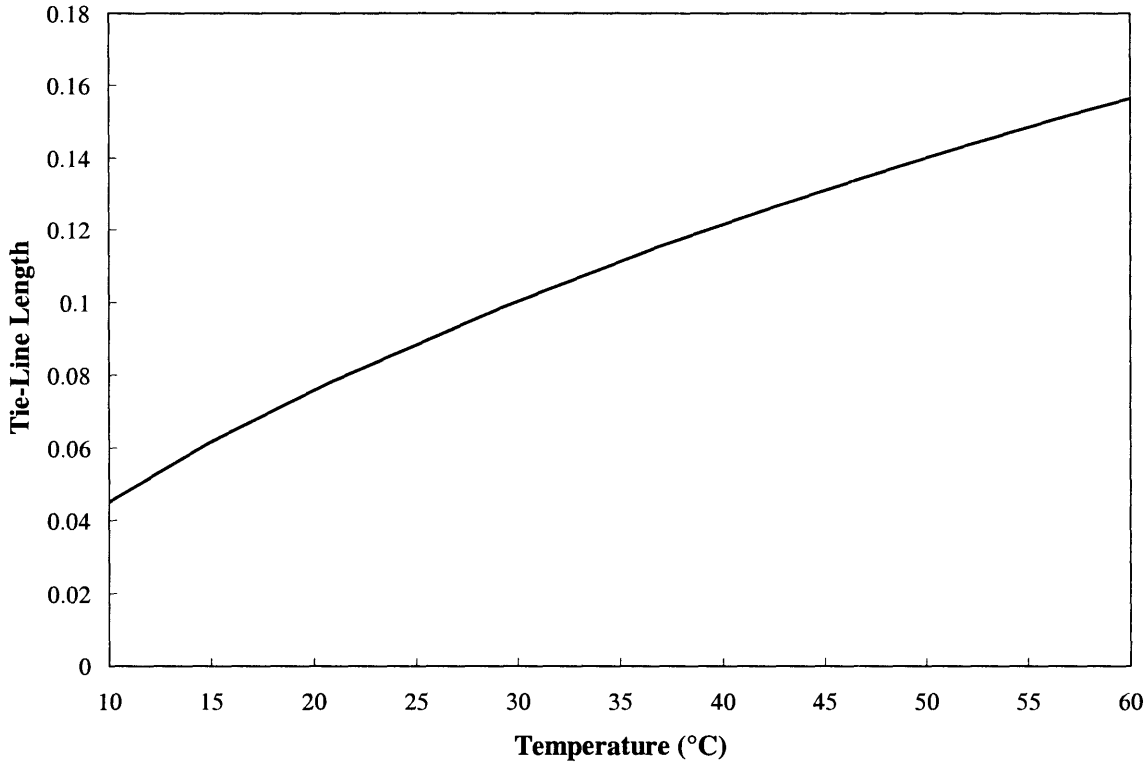

Figure 9-1: The tie-line length ($\Delta\phi = \phi_\alpha - \phi_\beta$) as a function of temperature, for the $C_{10}G_1$/buffer two-phase aqueous micellar system, obtained from the theoretical best-fit of the phase diagram presented in Figure 7-2.

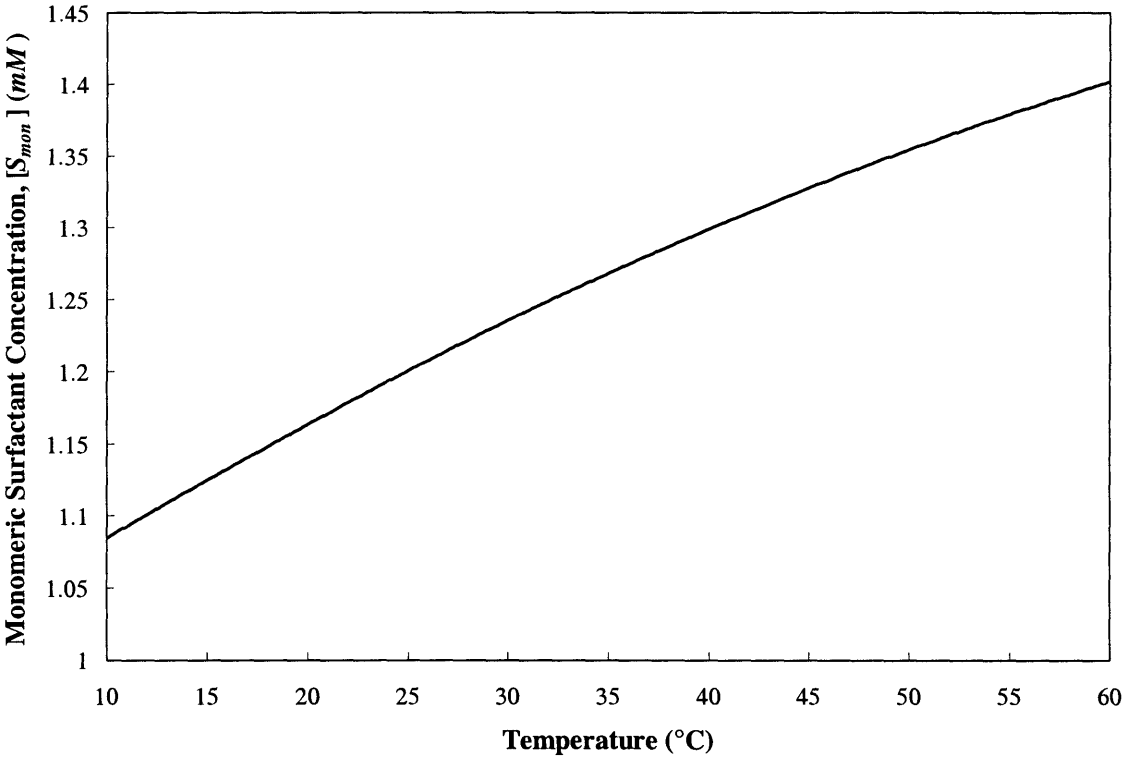

Figure 9-2: The monomeric surfactant concentration, $[S_{mon}]$, as a function of temperature, for the $C_{10}G_1$/buffer system, as estimated using a molecular-thermodynamic theory of micellization [21, 102].

expected, as the hydrophobicity of the surfactant tail, which is the predominant driving force for micellization, decreases as the temperature is increased. Consequently, more surfactant molecules remain in the monomeric form at higher temperatures.

In addition to the monomeric surfactant concentration, the equilibrium association constants, K_{mon} and K_{mic}, may also vary with temperature (see Section 7.4.3). However, for CBM9, Boraston et al. have established that the association constant between CBM9 and cellobiose, an oligosaccharide that has a significant affinity for CBM9, does not vary with temperature [90]. More specifically, the entropic component of the affinity interaction increases, as expected, with temperature, but the enthalpic component decreases as the temperature increases, balancing out the entropy increase. The authors reasoned that since CBM9 is derived from a thermophilic organism that lives at extreme temperature conditions, the temperature-independence of the association constant of CBM9 for its substrate is perhaps necessary for the corresponding enzyme to function properly at those temperatures [90]. Although we do not have direct experimental evidence that the association constant of CBM9 for $C_{10}G_1$ will follow the same trend as that for cellobiose, it is reasonable to assume, as a first-order approximation, that K_{mon} and K_{mic} should be temperature-invariant as well.

The theoretically predicted values of K_p^{EV}, K_p^{aff},and K_p corresponding to the partitioning of CBM9-GFP in the $C_{10}G_1$/buffer two-phase aqueous micellar system, computed using Eqs. (7.5), (7.18), and (7.7), respectively, as a function of temperature, are presented in Figure 9-3. For the predictions shown in Figure 9-3, a value of 33.5 $\AA$ was used for the effective radius, R_p, of CBM9-GFP. This value, which is within the plausible range of 26 $\AA$ to 57 $\AA$, suggested in Section 7.4.4, is the one that most closely predicts the observed baseline partition coefficient of 0.47. As shown in Figure 9-3, the excluded-volume contribution, K_p^{EV}, decreases as the temperature increases, reflecting the increasing steric exclusion of the proteins from the micelle-rich phase for longer tie-lines. On the other hand, K_p^{aff} increases as the temperature increases, suggesting that the greater difference in the ligand concentrations between the two coexisting micellar phases more than com-

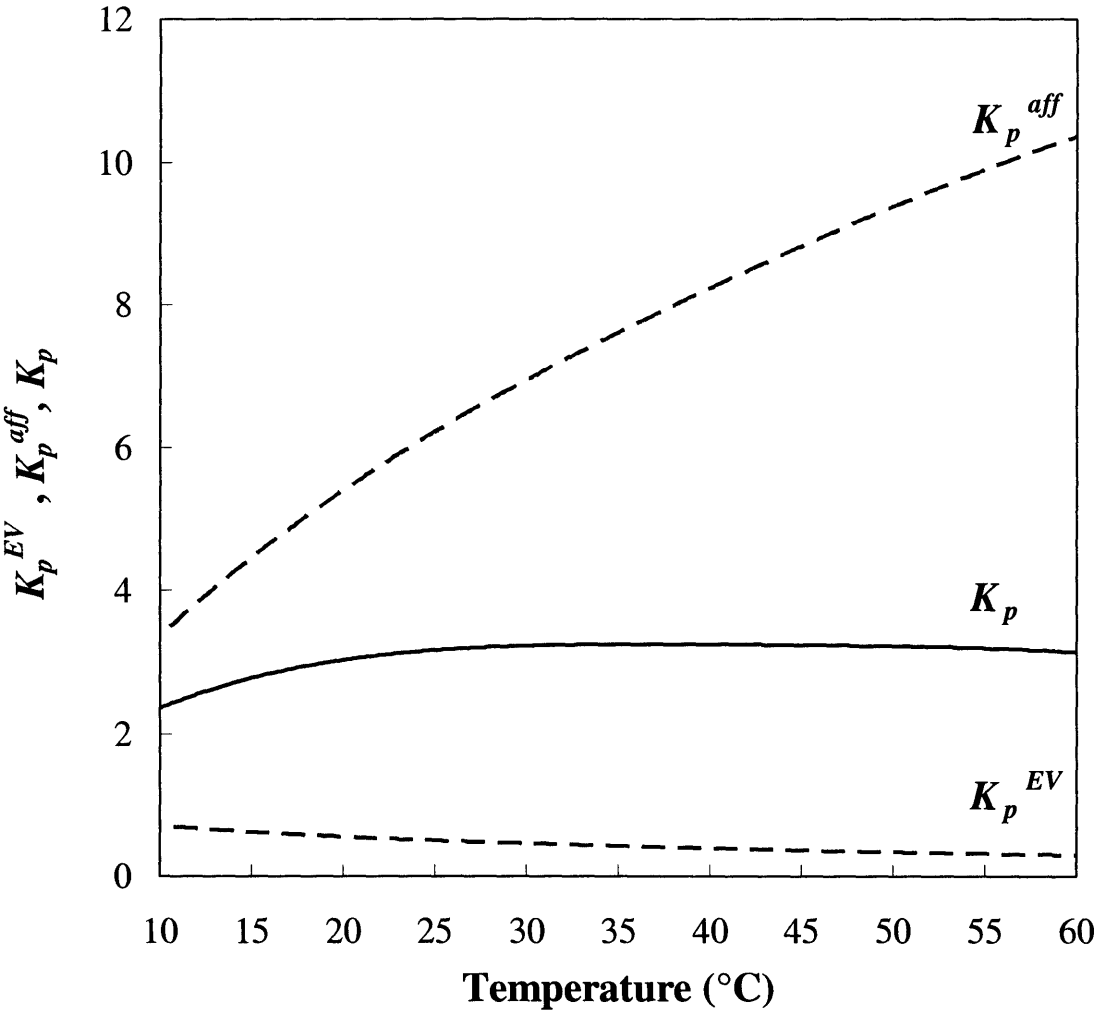

Figure 9-3: Theoretically predicted excluded-volume contribution, K_p^{EV}, affinity contribution, K_p^{aff}, and overall CBM9-GFP partition coefficient, K_p, in the $C_{10}G_1$/buffer two-phase aqueous micellar system, as a function of temperature. The curves were predicted using the theory presented in Section 7.4.

pensates for the increase in monomeric surfactant (inhibitor) concentration at increasing temperatures. The overall K_p, however, shows an interesting and important trend: it first increases, reaches a maximum at about 37 $^{\circ}C$, and then gradually decreases, as the temperature, or the tie-line length increases. The excluded-volume interactions gradually outcompete the affinity-interactions at the very long tie-line lengths corresponding to the higher temperatures. This clearly indicates that there is an optimal operating temperature at which the target protein CBM9-GFP is most effectively extracted into the micelle-rich phase.

However, the picture that emerges is different if one considers the selectivity of the separation of CBM9-GFP from a protein impurity, which is a measure of how effectively the target protein can be purified from a mixture. Figure 9-4 shows the theoretically predicted partition coefficients of CBM9-GFP, $K_{CBM9-GFP}$, and of a model impurity – cytochrome c, K_{cytc}, as a function of temperature. Note that $K_{CBM9-GFP}$ is the same as K_p presented in Figure 9-3. The theoretical partition coefficient of cytochrome c, K_{cytc}, which only accounts for excluded-volume interactions, is predicted using Eq. (2.4) utilizing an R_p value of 16 $\AA$ [52]. The experimentally measured partition coefficients of CBM9-GFP and cytochrome c, which were partitioned simultaneously in the same two-phase aqueous micellar system, at three different temperatures (19.6 $^{\circ}C$, 29.0 $^{\circ}C$, and 37.0 $^{\circ}C$) are also shown for comparison purposes. The results in Figure 9-4 indicate that the theoretical $K_{CBM9-GFP}$ and K_{cytc} predictions closely match the experimental values, and that, as expected, the two proteins partition independently of each other, similar to the case with the cell lysate discussed in Chapter 8. The predicted selectivity, defined as the ratio $K_{CBM9-GFP}/K_{cytc}$, as a function of temperature, is shown in Figure 9-5. As can be seen and as expected, the selectivity of the separation does increase as the two coexisting micellar phases become more dissimilar at the higher temperatures.

The results presented in Figure 9-5 reveal, perhaps not surprisingly, that one should be able to obtain better separation selectivities at higher temperatures. With a different set of design criteria, in which the goal is to obtain the highest target protein partition

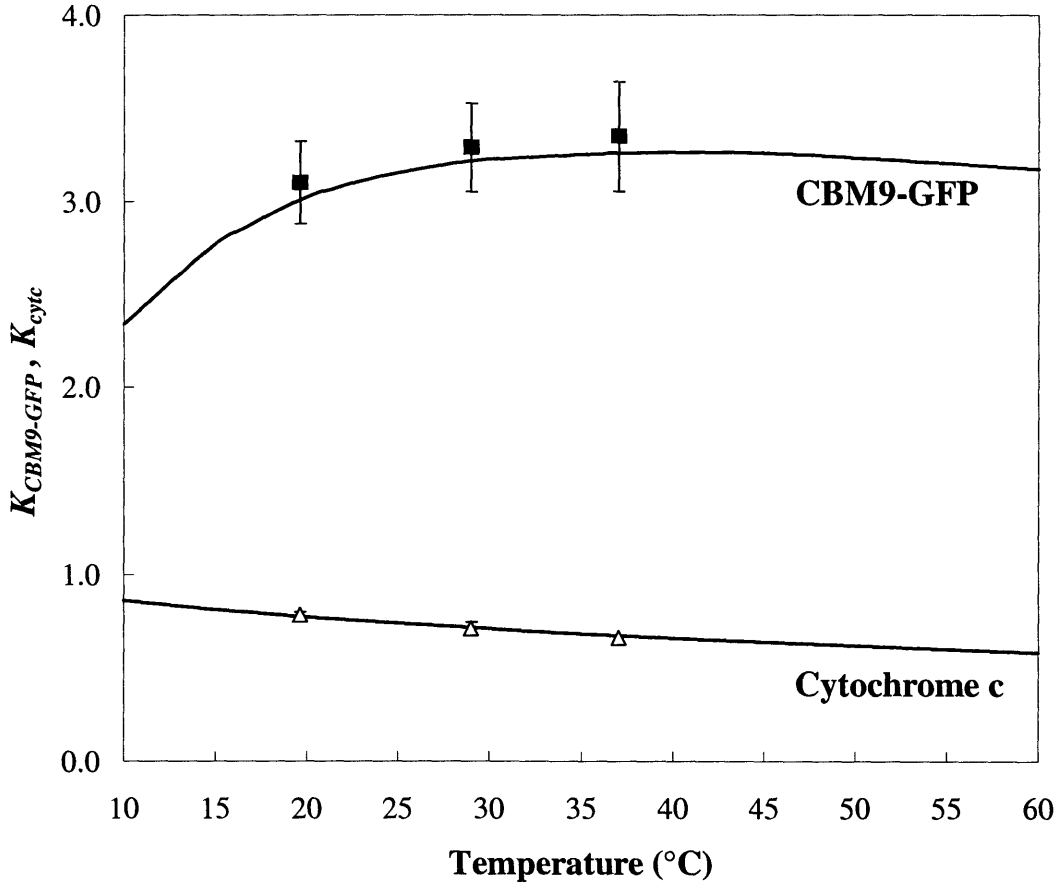

Figure 9-4: Theoretically predicted protein partition coefficients of the target protein, CBM9-GFP, $K_{CBM9-GFP}$, and of a model impurity, cytochrome c, K_{cytc}, as a function of temperature. The experimentally measured values at three temperatures (19.6 $°C$, 29.0 $°C$, and 37.0 $°C$) are shown for comparison purposes (■: CBM9-GFP, △: cytochrome c). The error bars represent 95% confidence intervals for triplicate experiments. For cytochrome c, the 95% confidence interval is within the size of the symbol.

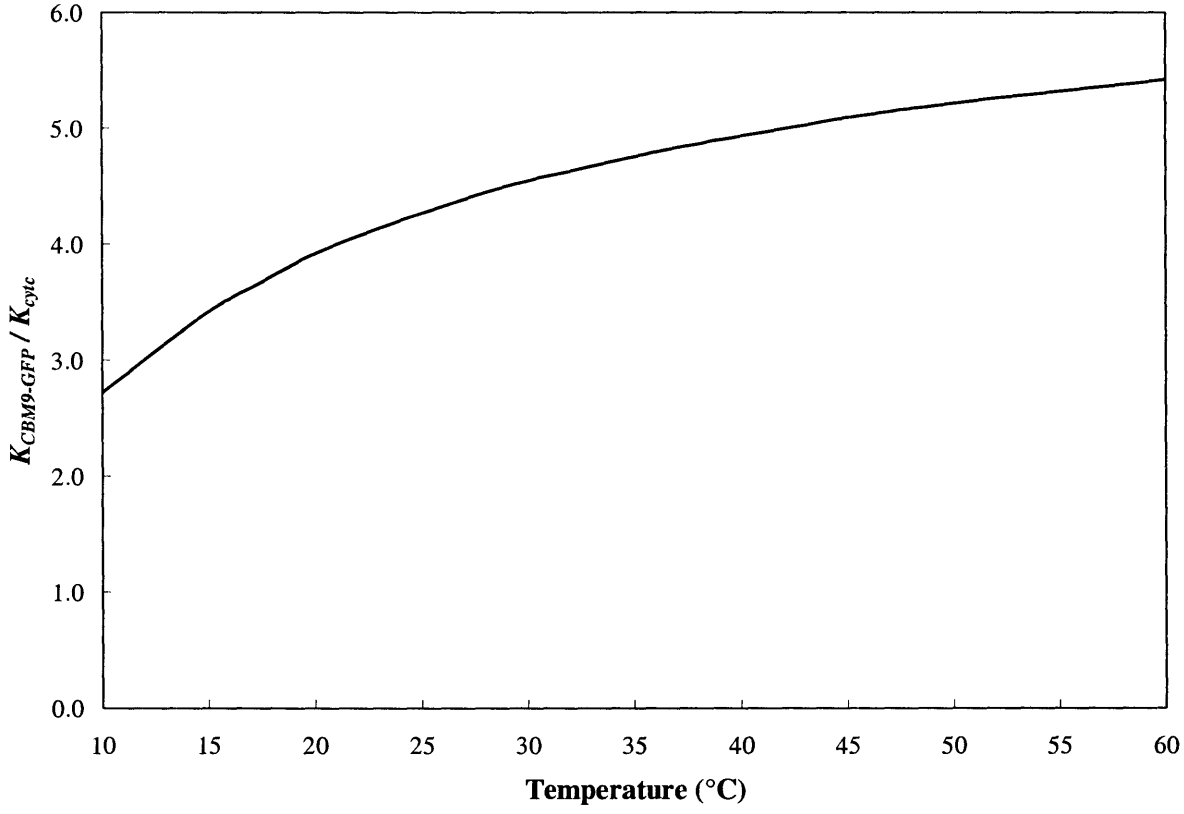

Figure 9-5: The selectivity of the separation of CBM9-GFP from cytochrome c, $K_{CBM9-GFP}/K_{cytc}$, as a function of temperature, in the $C_{10}G_1$/buffer two-phase aqueous micellar system.

coefficient, the results in Figure 9-3 should be kept in mind, because they reveal that the maximum target protein partition coefficient is obtained at a lower temperature, where the separation selectivity is not the highest. Clearly, the ability to access higher temperatures, and hence longer tie-lines, is restricted by the thermal stability of the proteins. As a result, there may be a compromise between obtaining a higher separation selectivity and maintaining a satisfactory recovery of the active target protein. It should also be stressed that it may be possible to obtain longer tie-lines by using a different surfactant system having a lower critical temperature, rather than by simply raising the operating temperature.

9.3.2 Reducing the Monomeric Surfactant Concentration

As discussed in Section 7.4, reducing the monomeric surfactant concentration should also improve the partition coefficient of the target protein. Figure 9-6 shows the theoretically predicted K_p^{aff} as a function of the monomeric surfactant concentration, for different K_{mon} and K_{mic} values, calculated using Eq. (7.18). Note that for the predictions shown in Figure 9-6, the tie-line length is kept constant at a value of 0.0977. In addition, for comparison purposes, the ratio of K_{mic} to K_{mon}, which is a measure of the steric penalty for a micellar surfactant to bind the protein, was also held constant at 0.045 (see Section 7.4.4).

As shown in Figure 9-6, the theory suggests that the monomeric surfactant concentration indeed has a profound effect on protein partitioning, with K_p^{aff} increasing dramatically as $[S_{mon}]$ decreases. For the actual system studied, where $[S_{mon}] = 1.2$ mM, $K_{mon} = 800$, and $K_{mic} = 36$, K_p^{aff} would increase by about 50% if $[S_{mon}]$ were an order-of-magnitude lower. For systems with stronger affinity, the effect of the monomeric surfactant concentration would be even more pronounced. This observation should have key implications for the future design of the affinity surfactant.

Unfortunately, because the monomeric surfactants are in equilibrium with the micelles in any micellar system, one cannot independently vary the monomeric surfactant con-

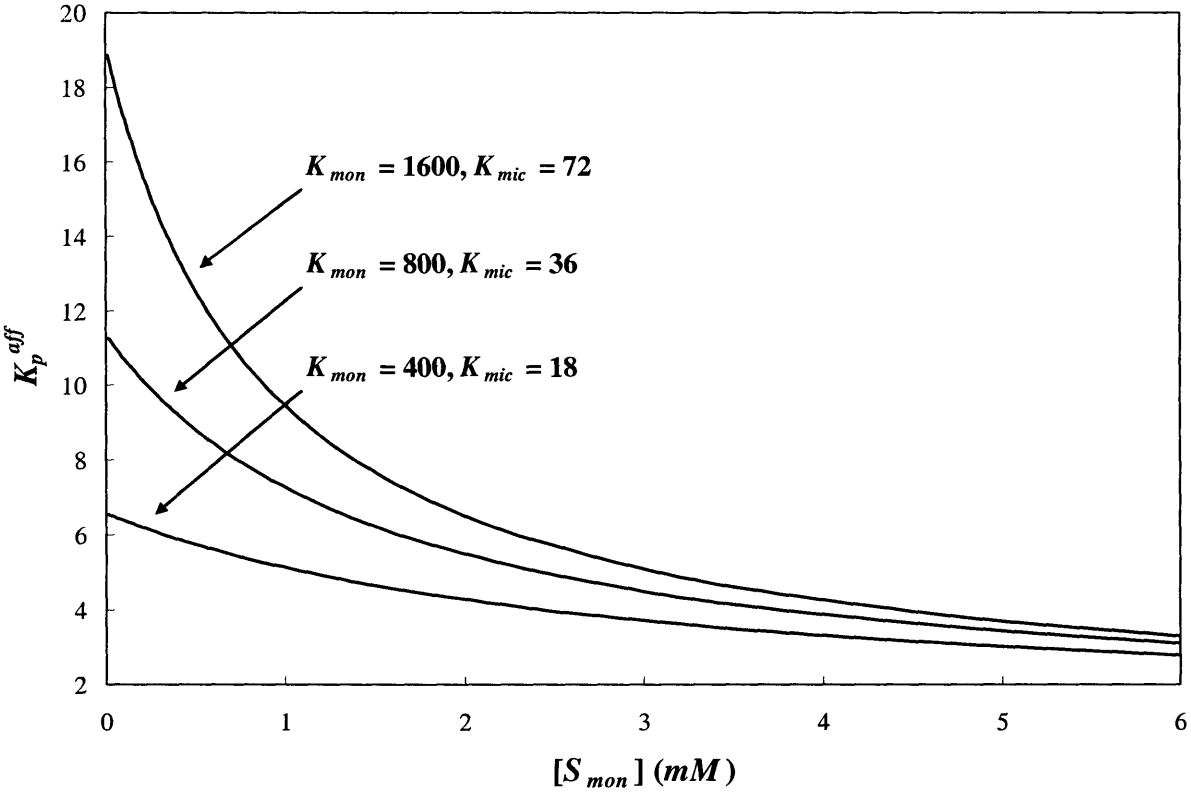

Figure 9-6: Theoretically predicted affinity contribution to the CBM9-GFP partition coefficient, K_p^{aff}, as a function of the monomeric surfactant concentration, $[S_{mon}]$, for various levels of protein-surfactant affinities. The ratio K_{mic}/K_{mon} was held constant at 0.045.

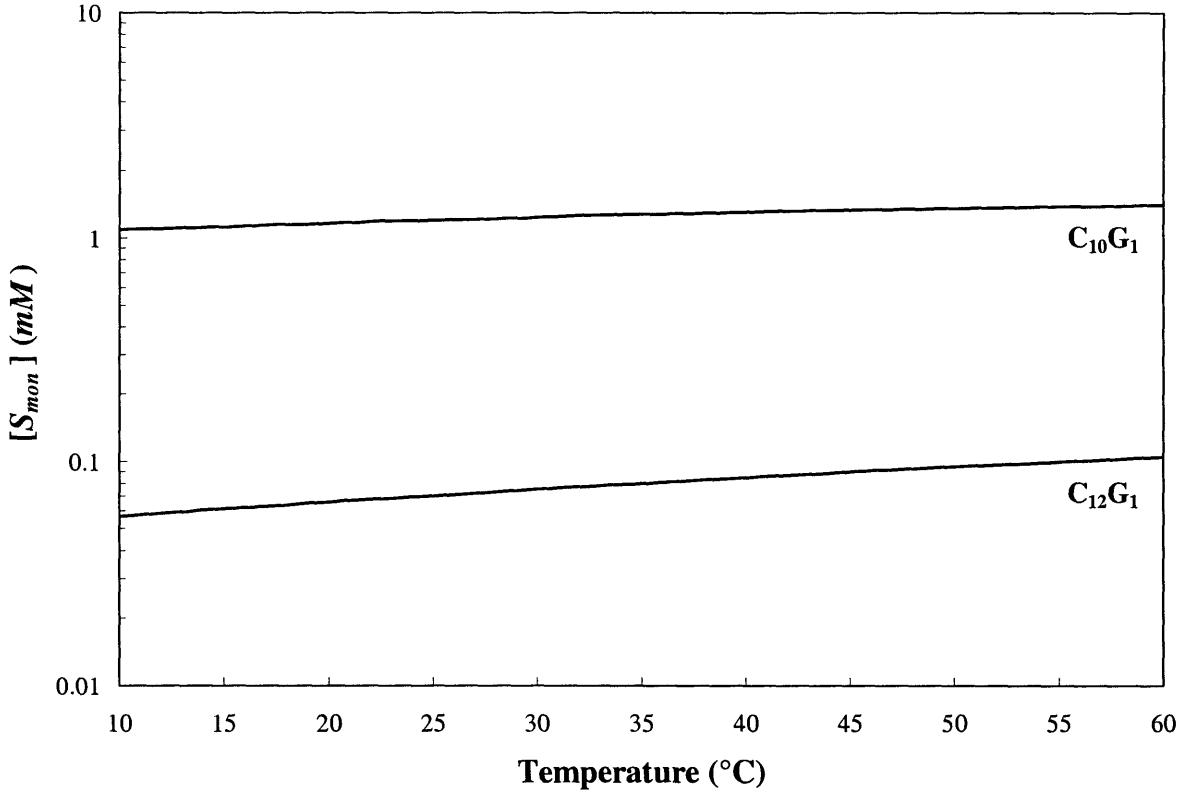

Figure 9-7: The monomeric surfactant concentrations, $[S_{mon}]$, of the $C_{10}G_1$/buffer and the $C_{12}G_1$/buffer systems, as a function of temperature, as estimated by the molecular-thermodynamic theory developed by the Blankschtein group [21, 102].

centration without also changing various aspects of the micellization process and of the micellar solution phase separation. As a result, it is difficult to study experimentally the effect of the monomeric surfactant concentration on protein partitioning. The best strategy to vary the monomeric surfactant concentration by a significant amount would be to use a longer surfactant tail. With this in mind, Figure 9-7 shows the monomeric surfactant concentrations of $C_{10}G_1$ and $C_{12}G_1$, predicted using the molecular-thermodynamic theory of micellization developed by the Blankschtein group [21, 102], as a function of temperature.

As shown in Figure 9-7, the monomeric surfactant concentration in the $C_{12}G_1$/buffer

system is about an order-of-magnitude lower than that in the $C_{10}G_1$/buffer system. Assuming that the glucosyl head of $C_{12}G_1$ behaves similarly to that of $C_{10}G_1$ in terms of its affinity interaction with the target protein, and that the micellar surfactants are similarly constrained sterically, one should expect the protein partition coefficient of the target protein to increase, by about 50%, according to Figure 9-6, if the tie-line length is held constant. Of course, $C_{10}G_1$ and $C_{12}G_1$ will not exhibit the same phase behavior under the same conditions, and therefore, cloud-point temperature measurements were carried out to locate the coexistence curve of the $C_{12}G_1$/buffer system. Unfortunately, these cloud-point temperature measurements revealed that the $C_{12}G_1$/buffer system has a very low critical temperature, such that even at a $C_{12}G_1$ concentration of 30% by weight, the system remains in the two-phase region within the workable temperature range (about 10 $°C$ to 37 $°C$). This, in turn, implies that the tie-line at room temperature is very long, and that the micelle-rich phase is very concentrated. Although a long tie-line is convenient for the separation, attempts to partition the protein CBM9-GFP in the $C_{12}G_1$/buffer system failed, because the very high viscosity and the almost solid-like nature of the micelle-rich phase prevented the successful analysis of the protein partitioning behavior. It is also doubtful that the micelle-rich phase, at such a high surfactant concentration, would remain as an isotropic liquid phase, which is the condition for which the theoretical description presented in Section 7.4 is valid. Other approaches to lower the monomeric surfactant concentration, including using surfactant mixtures instead of a single surfactant, will require considerable modification of the system studied so far, and will also complicate the application of the theoretical model presented in Section 7.4. Therefore, an experimental investigation of the effect of the monomeric surfactant concentration on the protein partitioning behavior was not pursued any further.

9.3.3 Using a Stronger Ligand

Another strategy to improve the efficiency of the separation is to use a stronger ligand. The affinity of the protein CBM9-GFP for the surfactant $C_{10}G_1$ is quite weak, and

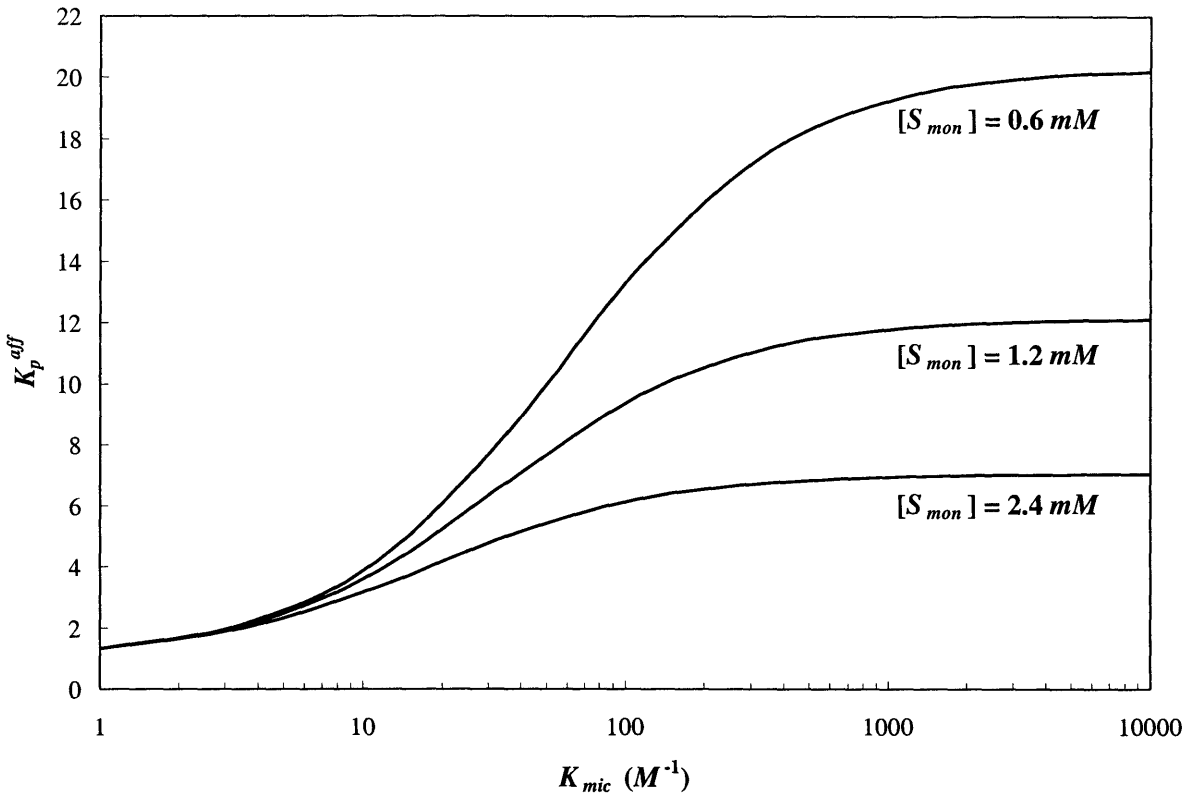

Figure 9-8: Theoretically predicted affinity contribution to the CBM9-GFP partition coefficient, K_p^{aff}, as a function of the protein-micellar surfactant association constant, K_{mic}, for three different monomeric surfactant concentrations, $[S_{mon}]$.

consequently, there should be ample room for improvement, either by choosing a better surfactant-ligand or by engineering the protein tag.

Figure 9-8 shows how the predicted affinity contribution to the protein partition coefficient, K_p^{aff}, varies as the protein-micellar surfactant association constant, K_{mic}, is increased, for three different monomeric surfactant concentrations. To generate Figure 9-8, it was assumed that the ratio K_{mic}/K_{mon}, which is a measure of the steric penalty for protein binding incurred by the micellar surfactant, as opposed to a monomeric surfactant, is constant. (Note that this conceptually reasonable assumption was made for simplicity, but it is possible that for a different protein tag-ligand pair, K_{mic}/K_{mon} will be

different due to a different configuration of the binding surface.) The protein partitioning behavior illustrated in Figure 9-8 has important implications for the process engineer who is interested in designing a protein tag-ligand pair for use in affinity-enhanced protein partitioning in two-phase aqueous micellar systems. Because of the presence of the monomeric surfactants as inhibitors, K_p^{aff} plateaus above a certain K_{mic} value, such that further improvement of the affinity has no effect on the partition coefficient. For example, for the monomeric surfactant concentration encountered in the study presented in Chapter 7 ($[S_{mon}] = 1.2\ mM$), the value of K_p^{aff} will be capped off at about 12 beyond a K_{mic} value of about 1000 M^{-1}. This can be understood in view of the fact that any affinity improvement that one may achieve will likely apply to both the micellar surfactant and the monomeric surfactant. The stronger-binding monomeric surfactants will also become stronger inhibitors, thus negating the benefit of the increased affinity of the micellar surfactants for the target protein. Considering the great impact of the monomeric surfactant concentration on affinity-enhanced protein partitioning, efforts to lower the monomeric surfactant concentration may prove to be more productive than those aimed at creating stronger binders. In addition, modifying the binding surface such that the micellar surfactants do not experience as great a steric penalty, that is, increasing the ratio K_{mic}/K_{mon}, may also yield a significant improvement. This can potentially be achieved by introducing a spacer between the affinity moiety and the surfactant hydrophobic tail, in order to allow more configurational freedom for the micellar surfactants to bind the proteins.

Because it is known that maltose (the dimer of glucose) binds the protein tag CBM9 more strongly than glucose does ($K_{maltose} = 290,000\ M^{-1}$ whereas $K_{glucose} = 8,000\ M^{-1}$, based on measurements by fluorescence titration and isothermal titration calorimetry) [90], a preliminary experimental investigation was carried out to determine whether one can obtain improved partition coefficients by using the corresponding surfactant-ligands, the alkyl β-D-maltopyranosides (C_iG_2, where i is the number of carbon atoms in the surfactant hydrocarbon tail). Because of the increased hydrophilicity of the C_iG_2's over the

corresponding C_iG_1's, the phase-separation temperatures of the C_iG_2's in buffer should be much higher than those of the C_iG_1's in buffer. As a result, one can only generate two-phase aqueous micellar systems using the C_iG_2's at elevated temperatures. Unfortunately, cloud-point temperature measurements revealed that even $C_{16}G_2$, the most hydrophobic of the commercially available alkyl β-D-maltopyranosides, and hence the easiest to phase-separate, does not exhibit phase separation even up to 65 $^{\circ}C$, certainly out of the workable temperature range for proteins. Additional experimental studies on this front were prevented by the complication of having to design and synthesize a novel surfactant, or surfactant mixture, that has the suitable phase behavior and strong CBM9-GFP binding affinity. Because of the sensitive nature of the phase behavior of two-phase aqueous micellar systems, it may in fact be simpler to improve the affinity by engineering the protein tag, than by designing *de novo* a surfactant-ligand that has stronger affinity and that also exhibits the required phase-forming characteristics.

9.4 Conclusions

In this chapter, various strategies for improving the affinity-enhanced partitioning of the target protein, CBM9-GFP, in two-phase aqueous micellar systems were explored. It was found that the tie-line length, which can be controlled by varying the operating temperature or by selecting a different phase-separating micellar system, provides an opportunity for optimization. Another promising strategy is to reduce the monomeric surfactant concentration, which can yield significant enhancements even in the case of moderate affinity. Increasing the strength of the affinity interactions should also enhance the protein partitioning. However, because the increased affinity would likely apply to both the micellar surfactants and the monomeric surfactants, the extent of the enhancement will be limited by the monomeric surfactant concentration.

It is worth stressing again that there are many choices, both in terms of system components and operating conditions, that the process engineer can explore to improve

affinity-enhanced protein partitioning in two-phase aqueous micellar systems. In order to have a well-defined and manageable scope for this thesis, the theoretical and the experimental investigations discussed in Sections 9.3.1 through 9.3.3 were limited to modifications that did not drastically alter the basic system studied in Chapters 7 and 8. The use of surfactant mixtures, for example, was avoided due to the experimental and theoretical challenges associated with mixed micellar systems. However, the general applicability of affinity-enhanced protein partitioning in two-phase aqueous micellar systems, as demonstrated by the simple and elegant system developed in this thesis, should be recognized. The theoretical description developed in Section 7.4 should also provide a good starting point for the process engineer to venture into the vast parameter space in search of a superior system that best suits the purification needs.

Part IV

Concluding Remarks

Chapter 10

Conclusions and Future Research Directions

10.1 Thesis Summary

This thesis was motivated by the need for developing a cost-effective separation method for low-cost, high-volume protein products. As discussed in Chapter 1, this unmet challenge can potentially be addressed by the use of extraction in two-phase aqueous micellar systems (cloud-point extraction). Although cloud-point extractions have been utilized in the past to address various separation needs (see Chapter 2), the efficient purification of industrially relevant hydrophilic proteins requires the introduction of new modes of interactions between the protein and the micelles, in order to obtain desired levels of yield and specificity. With that in mind, the central goal of this thesis was to explore various ways of enhancing protein partitioning in two-phase aqueous micellar systems, by the incorporation of electrostatic and affinity interactions, to purify industrially relevant proteins. In addition to demonstrating proof-of-principle of these approaches to enhance protein partitioning in two-phase aqueous micellar systems, this thesis also sought to develop a fundamental understanding of the underlying principles behind the phenomena of electrostatically-enhanced and affinity-enhanced partitioning.

In Part II of the thesis, electrostatically-enhanced partitioning in two-phase aqueous micellar systems was discussed. Chapter 4 first provided an overview of electrostatically-enhanced partitioning in two-phase aqueous micellar systems, and reviewed the relevant literature in this area, especially the work of Daniel Kamei in the Blankschtein group. The work of Kamei et al. in the area of electrostatic enhancement was then extended in important ways in Chapter 5. The electrostatically-enhanced partitioning of an industrially relevant enzyme, glucose 6-phosphate dehydrogenase (G6PD), using two-phase aqueous mixed (nonionic/cationic) micellar systems was investigated experimentally and theoretically. The study reported in Chapter 5 demonstrated the successful enhancement of the partitioning of G6PD, a negatively-charged protein, by adding the positively-charged surfactant alkyltrimethylammonium bromide (C_nTAB) to form charged mixed micelles with the phase-forming surfactant, $C_{10}E_4$. In the best-performing system studied, the measured G6PD partition coefficients in the $C_{10}E_4/C_n$TAB/buffer systems were improved as much as 22-fold, compared to those obtained in the corresponding $C_{10}E_4$/buffer system, clearly demonstrating the enormous potential of electrostatic enhancement. In addition, the effect of the tail length of the positively-charged surfactant added was investigated for the first time. The experimental results revealed that: (i) the propensity of the positively-charged C_nTAB surfactant to denature the enzyme follows the trend C_{12}TAB $>$ C_{10}TAB $>$ C_8TAB, and (ii) the ability of C_nTAB to enhance the partitioning of the enzyme also follows the trend C_{12}TAB $>$ C_{10}TAB $>$ C_8TAB. Hence, an optimal balance must be sought for which satisfactory enhancement can be obtained without causing unacceptable loss of product. The surfactant compositions of the two coexisting micellar phases were also measured experimentally, and used as inputs to a theory for electrostatic enhancement developed by Kamei et al., in order to rationalize the observed G6PD partition coefficients. It was shown that the theoretically predicted protein partition coefficients are in reasonable agreement with the experimentally measured values, suggesting that the theory can indeed be used as a predictive tool for the optimal design of these systems.

Affinity-enhanced partitioning was discussed in Part III of this thesis. Chapter 6 first provided an overview of affinity-enhanced partitioning in two-phase aqueous micellar systems, and reviewed the relevant literature in this area. In Chapter 7, proof-of-principle of the affinity-enhanced partitioning of an engineered affinity-tagged protein, CBM9-GFP, using two-phase aqueous micellar systems generated by a single surfactant, decyl β-D-glucopyranoside ($C_{10}G_1$), was demonstrated. The experimental results showed that the partition coefficient of the target protein, CBM9-GFP, can be improved more than 6-fold, by virtue of the affinity interactions, and that the enhancement was indeed specific to the target protein. Not only was the system utilized the simplest and easiest to implement among others considered in the past, but it also represented the first successful attempt to achieve significant and specific affinity enhancement for a protein with a fusion tag that can, in principle, be generally applied to any protein of interest. An important practical advantage of the method developed is that glucose, a safe and inexpensive reagent, can be used to elute the protein from the surfactants once the extraction is completed. The simplicity of the system also allowed the development and validation of an original theoretical framework to describe affinity-enhanced partitioning in two-phase aqueous micellar systems. The theoretical framework, which accounts for both excluded-volume interactions and affinity interactions between the proteins and the surfactant molecules (in both monomeric and micellar forms), was shown to be consistent with the experimental protein partitioning data, as well as with the current understanding of the sugar-binding domain CBM9. One important implication of the theoretical description is that the surfactant monomers need to be accounted for as a distinct binding partner for the proteins, and that in effect, they behave as competitive inhibitors which are always present in the system.

In Chapter 8 of Part III, the method developed in Chapter 7 was tested in terms of its ability to handle a complex protein mixture – a real *E. coli* cell lysate. It was successfully demonstrated, for the first time, that affinity-enhanced partitioning in two-phase aqueous micellar systems can indeed be applied to a complex mixture, with predictable results.

Partitioning experiments were conducted at three different dilution levels of the cell lysate. The phase diagram of the $C_{10}G_1$/buffer two-phase aqueous micellar system was not altered by the presence of the cell lysate at the three dilution levels studied. The partition coefficient of the target protein, CBM9-GFP, was also found to be independent of the cell lysate dilution level, and to be statistically identical to the value obtained with purified CBM9-GFP. The results suggest that the presence of the protein impurities in the cell lysate does not interfere with the partitioning of the target protein, and that the separation method is indeed capable of handling industrially relevant protein concentrations. The protein impurities present in the cell lysate, on the other hand, were simultaneously concentrated away from the target protein, into the micelle-poor phase, by virtue of excluded-volume interactions, resulting in an effective purification of the target protein CBM9-GFP.

In Chapter 9, various strategies for improving the affinity-enhanced partitioning of the target protein, CBM9-GFP, in two-phase aqueous micellar systems were explored. It was found that the tie-line length, which can be controlled by the operating temperature or by selecting a different phase-separating micellar system, provides an opportunity for optimization. Another promising strategy is to reduce the monomeric surfactant concentration, which can yield significant enhancement even in the case of moderate affinity. Increasing the strength of the affinity interactions should also enhance the partitioning of the target protein. However, because the increased affinity would likely apply to both the micellar surfactant and the monomeric surfactant, the extent of the enhancement will be limited by the monomeric surfactant concentration. The theoretical description developed in Chapter 7 should provide the necessary guidelines for the process engineer to venture into the vast parameter space in search of a superior system that best suits the purification needs.

10.2 Future Research Directions

10.2.1 Attaining Greater Partition Coefficients of the Target Protein Experimentally

Although the enhancements of the target protein partition coefficients attained by incorporating electrostatic effects, discussed in Chapter 5, were already quite remarkable, there is still room for further improvement. The studies conducted so far in the Blankschtein group only made use of common and well-known ionic surfactants, such as sodium dodecyl sulfate (SDS) and alkyltrimethylammonium bromide (C_nTAB), but there are other types of ionic surfactants in the market that remain to be tested in order to optimize the separation. A more thorough study of the denaturation effect of charged surfactants on the target protein of interest would also be valuable in the search for superior surfactants for use in electrostatically-enhanced partitioning.

Although several possible strategies to improve the target protein partition coefficient were identified and discussed in Chapter 9, it was not possible to investigate each of the proposed strategies experimentally, without significantly modifying the basic system used in Chapters 7 and 8. The issue often encountered was that the many factors that control the protein separation efficiency are all intertwined and cannot be studied independently. In addition, the phase behavior of the two-phase aqueous micellar system proved to be highly sensitive to changes in the solution conditions, which complicates any attempt to modify the system as desired. However, considering the great number of surfactants and surfactant mixtures that one can choose from, there should be other surfactants or surfactant mixtures that are capable of performing better than the systems that were studied so far. For example, one can imagine that an alkyl maltopyranoside (C_iG_2) surfactant that has a long enough tail (perhaps, having $i > 20$), which unfortunately is not commercially available, may be able to phase-separate at ambient temperatures, while having a lower monomeric surfactant concentration than $C_{10}G_1$ and possibly having a higher affinity for CBM9. Introducing a spacer between the protein-binding moiety and

the hydrophobic surfactant tail may also increase the configurational flexibility of the micelle-bound ligand to interact with the protein, thereby lessening the steric penalty that the micellar surfactant experiences. Furthermore, mixing surfactants will also provide much greater flexibility to alter the system properties for improved partitioning (see Section 10.2.2).

10.2.2 Using Surfactant Mixtures in Affinity-Enhanced Partitioning

For the work on affinity enhancement of protein partitioning presented in Part III, mixing surfactants was avoided because of the experimental and theoretical challenges encountered with mixed micellar systems. However, it is clear that mixing surfactants should provide much greater flexibility to alter the system properties, in order to attain improved partitioning. Moreover, from a practical point of view, using surfactant mixtures is also advantageous economically, because most inexpensive, technical-grade surfactants in the market are, in effect, surfactant mixtures with polydispersity in both the surfactant head and the surfactant tail. It is also possible to use less of the more expensive affinity surfactant, if it can provide a similar separation performance when mixed with a cheaper surfactant.

The use of surfactant mixtures, however, poses several challenges. For polydisperse surfactants, the phase behavior can be considerably different than what is observed in the case of pure surfactants. Moreover, the very large number of thermodynamic degrees of freedom makes it very difficult to analyze the phase behavior of the surfactant mixture by using simple phase diagrams as discussed in this thesis. Although the theory for affinity-enhanced partitioning developed in Chapter 7 provided some important design criteria for these systems, it remains a challenge to identify the proper surfactant mixture that maintains the two-phase aqueous micellar system at ambient temperatures and yields the desired micellar solution properties. Without the insight provided by a robust theory to model the phase behavior of the mixed micellar system of interest, a more em-

pirical approach, based on trial-and-error, will probably be needed. For example, various technical-grade alkyl polyglucoside surfactants will have to be tested experimentally: (i) to determine their phase-separating temperature range, (ii) to measure the relevant solution properties, such as the surfactant concentrations in each coexisting micellar phases, and (iii) to locate the optimal operating temperature.

10.2.3 Acquiring a Fundamental Understanding of the Phase Behavior of Mixed Micellar Systems

For the work on electrostatic enhancement of protein partitioning presented in Part II, a surfactant mixture consisting of $C_{10}E_4$ and C_nTAB was used to generate the two-phase aqueous micellar system consisting of charged mixed micelles. Although the phase behavior of the mixed micellar systems was successfully measured experimentally by mapping the isothermal cross sections of the three-dimensional phase diagrams, the experiments were extremely tedious, and did not allow one to sample many different surfactant mixtures to attain better performance in a reasonable amount of time. Similarly, for affinity enhancement of protein partitioning studied in Part III, mixing surfactants should provide more flexibility to better optimize the protein separation. For both electrostatic and affinity enhancements, the use of surfactant mixtures should also likely become important practically due to economic considerations. Accordingly, it would be highly desirable if a fundamental understanding of the phase behavior of mixed micellar systems could be formulated to guide the search for a suitable surfactant mixture without the need to test each potential mixture experimentally.

A theoretical framework to describe the phase behavior of binary surfactant mixtures was developed by Puvvada et al. [26, 27]. Unfortunately, unlike the phase behavior theory for single surfactants, which was utilized effectively in this thesis to analyze the phase behavior of the $C_{10}G_1$/buffer system, the corresponding theoretical framework for binary surfactant mixtures is considerably more involved mathematically. More importantly, the parameters needed as inputs to the theory in order to predict the phase behavior

of a given mixed micellar system cannot be as readily extracted from the experimental data. Furthermore, few studies were conducted in the past in applying the theoretical framework to study the experimental phase behavior of different classes of surfactant mixtures. Ideally, one would like to be able to predict the phase behavior of any mixed micellar system given the chemical structures of the various surfactant components and the relevant solution conditions. However, the inherent intricacies of the phenomena of mixed micellization and mixed micellar solution phase behavior, coupled with the increased number of available thermodynamic degrees of freedom associated with mixtures, may require the use of computer simulations or semi-empirical approaches, such as group-contribution methods.

10.2.4 Partitioning CBM9-GFP in Two-Phase Aqueous Polymer Systems with Affinity Ligands

Although, as explained in Chapter 6, two-phase aqueous micellar systems have important advantages over two-phase aqueous polymer systems with respect to bioseparations, it may be worthwhile to attempt the partitioning of CBM9-GFP in a two-phase aqueous polymer system loaded with affinity ligands. The reason is that in two-phase aqueous polymer systems, there is no competitive inhibition effect from the monomeric surfactants, and therefore, the resulting partition coefficient of the affinity-tagged protein may be more extreme. The challenge with this approach involves the loading of the affinity ligands in the polymer system. Many carbohydrate polymers, such as dextran, are routinely used to create two-phase aqueous polymer systems, and may already serve as an effective ligand for CBM9-GFP. However, in the prototypical PEG/dextran two-phase aqueous polymer systems, most hydrophilic proteins partition preferentially to the dextran-rich phase [9, 53], which implies that CBM9-GFP will not be concentrated away from the protein impurities. As a result, PEG/dextran two-phase aqueous polymer systems may not be the most suitable candidate. On the other hand, various kinds of PEG/salt two-phase

aqueous polymer systems, which have important practical and economical advantages over the PEG/dextran systems, may be more suitable, provided that the PEG polymer can be derivatized with the affinity ligand by organic synthesis. The use of other types of phase-separating polymer systems, such as those involving the use of di-block copolymers, may also be explored.

10.2.5 Exploring the Use of Other Types of Affinity Interactions

As discussed in Section 6.1, there are currently many types of affinity interactions being exploited in bioseparations, both in the laboratory and in the biotechnology industry. Each type has its own pros and cons, and is more suitable to a certain application than the others. Therefore, it should be beneficial to explore ways to incorporate these other types of affinity interactions into two-phase aqueous micellar systems, in order to broaden the applicability of these systems and to capitalize on the already-developed familiarity with the existing affinity technologies. It will also be interesting to verify if the fundamental understanding gained from this thesis, including the many lessons learned, will indeed apply generally to all types of affinity interactions.

The important advantages of exploiting the affinity interaction between the sugar-binding CBM9 and a glucose-like moiety were discussed in Chapter 7. The most valuable attribute of this particular type of affinity interaction is the fact that it is readily exploited by using the *commercially available* surfactant $C_{10}G_1$ as the ligand, which conveniently, also serves simultaneously as the phase-forming surfactant for the two-phase aqueous micellar system. It is unlikely that for other types of affinity interactions, one will be able to find such an ideal surfactant-ligand as readily. More likely, the surfactant-ligand will have to be designed and synthesized *de novo*, and more than one surfactant will be needed to create the two-phase aqueous micellar systems containing the ligand-decorated micelles.

10.2.6 Partitioning Other Types of Biomolecules

The primary focus of this thesis has been the purification of hydrophilic proteins. However, partitioning in two-phase aqueous micellar systems has also been utilized in the past to separate other types of biomolecules, including hydrophobic proteins [42], antibiotics [96], and viruses [11]. As more and more biomolecules find their ways to the market, separation methods such as those studied in this thesis could also find applications in the purification of whole cells, plasmid DNA, virus-like particles, small peptides, biosurfactants, pigments, and so on. The use of electrostatic and affinity enhancement methods discussed in this thesis should also be exploited to maximize the separation performance of these other biomolecules.

10.2.7 Developing an Integrated Downstream Process

There is certainly sufficient evidence that partitioning in various types of two-phase aqueous complex-fluid systems can provide a highly effective method for separating biomolecules in a laboratory scale, often outperforming the current separation methods. It is also well established that liquid-liquid extraction can be easily scaled up and run in a continuous, efficient manner [7, 9, 53]. The natural next step for making these separation methods appealing to the process engineer would be: (i) to develop real unit operations based on these methods, and (ii) to demonstrate that they will indeed perform well at a large scale and be as good as, if not better than, the currently used separation methods. The question of how these unit operations fit into the big picture of the entire downstream process also needs to be addressed. In other words, an integrated downstream process that makes use of partitioning in two-phase aqueous micellar systems will have to be developed.

Many aspects of the integrated process remain to be worked out. For example, the requirements on the feed stream, in terms of, say, its solid content and salt concentration, have to be determined, and any necessary upstream steps needed to prepare the feed stream for the extraction operation have to be implemented. The extraction should be

run continuously for maximum efficiency, and the manner in which that is achieved, including what equipment to use and how to optimize the process, has to be worked out. In this regard, several aspects of the two-phase aqueous micellar systems which were not addressed as part of this thesis, including the viscosity and the settling time of the micellar phases, will likely become important. Following the extraction, one will have to recover the target protein of interest and to remove the surfactant(s) from the output stream. Preferably, for economical reasons, the surfactant(s) should be recycled as much as possible. This necessitates the development of an operation to separate the surfactant(s) from the protein. Finally, there needs to be a quality-control protocol to ensure that the target protein of interest indeed survives the purification process without unacceptable changes to its desired properties. In summary, there is a great need, from a practical point of view, to develop an integrated downstream process that incorporates partitioning in two-phase aqueous micellar systems seamlessly into the entire bioprocess. Only then will one be able to demonstrate the technological advantages and the economic benefits of these extraction systems in comparison to the currently used technologies.

10.3 Concluding Remarks

In conclusion, liquid-liquid extraction in two-phase aqueous micellar systems indeed holds great promise as an alternative purification method for hydrophilic proteins. The effectiveness of the various means of enhancing protein separations in these systems by introducing electrostatic and affinity interactions were clearly demonstrated in this thesis. A basic fundamental understanding of electrostatic and affinity enhancements was also developed to guide the process engineer in the design and optimization of the separation process. Although there remains work to be done before such systems can reach their full potential and be eventually commercialized, this thesis nevertheless represents an essential starting point for future efforts to improve, extend, and commercialize this promising bioseparation method.

Bibliography

Bibliography

[1] National Research Council Committee On Biobased Industrial Products. *Biobased industrial products: priorities for research and commercialization.* National Academy Press, Washington, DC, 2000.

[2] K. Keller, T. Friedmann, and A. Boxman. The bioseparation needs for tomorrow. *Trends in Biotechnology*, 19(11):438–441, 2001.

[3] N. Kosaric. *Biosurfactants: production, properties, applications.* Surfactant science series ; v. 48. Marcel Dekker, New York, NY, 1993.

[4] A. Pandey. *Concise encyclopedia of bioresource technology.* Food Product Press, New York, NY, 2004.

[5] S. M. Wheelwright. *Protein purification: design and scale up of downstream processing.* Wiley-Interscience, New York, NY, 1994.

[6] J. A. Howell, V. Sanchez, and R. W. Field. *Membranes in bioprocessing: theory and applications.* Chapman and Hall, Glasgow, UK, 1993.

[7] J. Rydberg. *Solvent extraction: principles and practice.* Marcel Dekker, New York, NY, 2nd edition, 2004.

[8] W. L. Hinze and E. Pramauro. A critical review of surfactant-mediated phase separations (cloud-point extractions): theory and applications. *Critical Reviews in Analytical Chemistry*, 24(2):133–177, 1993.

[9] H. Walter, D. E. Brooks, and D. Fisher. *Partitioning in aqueous two-phase systems: theory, methods, uses, and application to biotechnology.* Academic Press, Orlando, FL, 1985.

[10] D. T. Kamei. *Protein and viral partitioning in two-phase aqueous micellar systems.* PhD thesis, Massachusetts Institute of Technology, Cambridge, MA, June 2000.

[11] D. T. Kamei, J. A. King, D. I. C. Wang, and D. Blankschtein. Separating lysozyme from bacteriophage P22 in two-phase aqueous micellar systems. *Biotechnology and Bioengineering*, 80(2):233–236, 2002.

[12] C. L. Liu, D. T. Kamei, J. A. King, D. I. C. Wang, and D. Blankschtein. Separation of proteins and viruses using two-phase aqueous micellar systems. *Journal of Chromatography B*, 711(1-2):127–138, 1998.

[13] F. H. Quina and W. L. Hinze. Surfactant-mediated cloud point extractions: an environmentally benign alternative separation approach. *Industrial and Engineering Chemistry Research*, 38(11):4150–4168, 1999.

[14] J. N. Israelachvili. *Intermolecular and surface forces: with applications to colloidal and biological systems.* Academic Press, London ; Orlando, FL, 1985.

[15] J. C. Berg. *Wettability.* Surfactant science series ; v. 49. Marcel Dekker, New York, NY, 1993.

[16] D. R. Ekserova and Kruglyakov P. M. *Foam and foam films: theory, experiment, application.* Surfactant science series ; v. 5. Marcel Dekker, New York, NY, 1998.

[17] W. G. Cutler and E. Kissa. *Detergency: theory and technology.* Surfactant science series ; v. 20. Marcel Dekker, New York, NY, 1987.

[18] J. Sjoblom. *Emulsions and emulsion stability.* Surfactant science series ; v. 61. Marcel Dekker, New York, NY, 1996.

[19] C. Tanford. *The hydrophobic effect: formation of micelles and biological membranes.* Wiley-Interscience, New York, NY, 2nd edition, 1978.

[20] M. J. Schick. *Nonionic surfactants: physical chemistry.* Surfactant science series ; v. 23. Marcel Dekker, New York, NY, 1987.

[21] N. J. Zoeller and D. Blankschtein. Development of user-friendly computer programs to predict solution properties of single and mixed surfactant systems. *Industrial and Engineering Chemistry Research*, 34(12):4150–4160, 1995.

[22] Y. Nibu and T. Inoue. Solid-liquid phase behavior of binary mixture of tetraethylene glycol decyl ether and water. *Journal of Colloid and Interface Science*, 205:231–240, 1998.

[23] D. Blankschtein, G. M. Thurston, and G. B. Benedek. Theory of phase-separation in micellar solutions. *Physical Review Letters*, 54(9):955–958, 1985.

[24] D. Blankschtein, G. M. Thurston, and G. B. Benedek. Phenomenological theory of equilibrium thermodynamic properties and phase-separation of micellar solutions. *Journal of Chemical Physics*, 85(12):7268–7288, 1986.

[25] C. L. Liu, Y. J. Nikas, and D. Blankschtein. Novel bioseparations using two-phase aqueous micellar systems. *Biotechnology and Bioengineering*, 52(2):185–192, 1996.

[26] S. Puvvada and D. Blankschtein. Thermodynamic description of micellization, phase behavior, and phase separation of aqueous solutions of surfactant mixtures. *Journal of Physical Chemistry*, 96(13):5567–5579, 1992.

[27] S. Puvvada and D. Blankschtein. Theoretical and experimental investigations of micellar properties of aqueous solutions containing binary mixtures of nonionic surfactants. *Journal of Physical Chemistry*, 96(13):5579–5592, 1992.

[28] H. Watanabe and H. Tanaka. A nonionic surfactant as a new solvent for liquid-liquid extraction of zinc(II) with 1-(2-pyridylazo)-2-naphthol. *Talanta*, 25(10):585–589, 1978.

[29] S. Igarashi and K. Endo. Room temperature phosphorescence of palladium (II)-coproporphyrin III complex in a precipitated nonionic surfactant micelle phase: determination of traces of palladium (II). *Analytica Chimica Acta*, 320(1):133–138, 1996.

[30] C. G. Pinto, J. L. P. Pavon, B. M. Cordero, E. Romero Beato, and S. Garcia Sanchez. Cloud point preconcentration and flame atomic absorption spectrometry: application to the determination of cadmium. *Journal of Analytical Atomic Spectrometry*, 11(1):37–41, 1996.

[31] C. Wang, D. F. Martin, and B. B. Martin. Cloud point extraction of chromium(III) ion with 8-hydroxyquinoline derivatives. *Journal of Environmental Science and Health A*, 34(3):705–719, 1999.

[32] S. Akita and H. Takeuchi. Cloud-point extraction of organic compounds from aqueous solutions with nonionic surfactant. *Separation Science and Technology*, 30(5):833–846, 1995.

[33] A. E. Fernandez, Z. S. Ferrera, and J. J. S. Rodriguez. Determination of polychlorinated biphenyls by liquid chromatography following cloud point extraction. *Analytica Chimica Acta*, 358(2):145–155, 1998.

[34] Sirimanne S. R., J. R. Barr, D. G. Patterson, and L. Ma. Quantification of polycyclic aromatic hydrocarbons and polychlorinated dibenzo-p-dioxins in human serum by combined micelle-mediated extraction (cloud point extraction) and HPLC. *Analytical Chemistry*, 68(9):1556–1560, 1996.

[35] A. Bockelen and R. Niessner. Combination of micellar extraction polycyclic aromatic hydrocarbons from aqueous media with detection by synchronous fluorescence. *Fresenius Journal of Analytical Chemistry*, 346(4):435–440, 1993.

[36] C. G. Pinto, J. L. P. Pavon, and B. M. Cordero. Cloud point preconcentration and high-performance liquid chromatographic determination of polycyclic aromatic hydrocarbons with fluorescence detection. *Analytical Chemistry*, 66(6):874–881, 1994.

[37] C. G. Pinto, J. L. P. Pavon, and B. M. Cordero. Cloud point preconcentration and high-performance liquid chromatographic determination of organophosphorus pesticides with dual electrochemical detection. *Analytical Chemistry*, 67(15):2606–2612, 1995.

[38] R. C. Martinez, E. R. Gonzalo, M. G. G. Jimenez, C. G. Pinto, J. L. P. Pavon, and J. H. Mendez. Determination of the fungicides Folpet, Captan and Captafol by cloud-point preconcentration and high-performance liquid chromatography with electrochemical detection. *Journal of Chromatography A*, 754:85–96, 1996.

[39] R. A. Ramelmeier, G. C. Terstappen, and M.-R. Kula. The partitioning of cholesterol oxidase in Triton X-114-based aqueous two-phase systems. *Bioseparation*, 2:315–324, 1991.

[40] G. C. Terstappen, R. A. Ramelmeier, and M.-R. Kula. Protein partitioning in detergent-based aqueous two-phase systems. *Journal of Biotechnology*, 28:263–275, 1993.

[41] T.-F. Zhang and L. P. Hager. A single-step large-scale purification or pyruvate oxidase. *Archives of Biochemistry and Biophysics*, 257(2):485–487, 1987.

[42] C. Bordier. Phase-separation of integral membrane-proteins in Triton X-114 solution. *Journal of Biological Chemistry*, 256(4):1604–1607, 1981.

[43] K. J. Clemetson, D. Bienz, M.-L. Zahno, and E. F. Luscher. Distribution of platelet glycoproteins and phosphoproteins in hydrophobic and hydrophilic phases in Triton X-114 phase partition. *Biochimica et Biophysica Acta*, 778:463–469, 1984.

[44] S. R. Sirimanne, D. G. Patterson, L. Ma, and J. B. Justice. Application of cloud-point extraction/reversed-phase high performance liquid chromatography: a preliminary study of the extraction and quantification of vitamins A and E in human serum and whole blood. *Journal of Chromatography B*, 716:129–137, 1998.

[45] T. Saitoh and W. L. Hinze. Concentration of hydrophobic organic compounds and extraction of protein using alkylammoniosulfate zwitterionic surfactant mediated phase separations (cloud point extractions). *Analytical Chemistry*, 63(21):2520–2525, 1991.

[46] A. Schwarz, G. C. Terstappen, and A. H. Futerman. Isolation of gangliosides by cloud-point extraction with a nonionic detergent. *Analytical Biochemistry*, 254(2):221–225, 1997.

[47] Y. J. Nikas, C. L. Liu, T. Srivastava, N. L. Abbott, and D. Blankschtein. Protein partitioning in two-phase aqueous nonionic micellar solutions. *Macromolecules*, 25(18):4797–4806, 1992.

[48] C. L. Liu, Y. J. Nikas, and D. Blankschtein. Partitioning of proteins using two-phase aqueous surfactant systems. *AIChE Journal*, 41(4):991–995, 1995.

[49] L. Lue and D. Blankschtein. A liquid-state theory approach to modeling solute partitioning in phase-separated solutions. *Industrial and Engineering Chemistry Research*, 35(9):3032–3043, 1996.

[50] D. T. Kamei, J. A. King, D. I. C. Wang, and D. Blankschtein. Understanding viral partitioning in two-phase aqueous micellar systems: 1. role of attractive interactions between viruses and micelles. *Biotechnology and Bioengineering*, 78(2):190–202, 2002.

[51] D. T. Kamei, J. A. King, D. I. C. Wang, and D. Blankschtein. Understanding viral partitioning in two-phase aqueous micellar systems: 2. effect of entrained micelle-poor domains. *Biotechnology and Bioengineering*, 78(2):203–216, 2002.

[52] D. T. Kamei, D. I. C. Wang, and D. Blankschtein. Fundamental investigation of protein partitioning in two-phase aqueous mixed (nonionic/ionic) micellar systems. *Langmuir*, 18(8):3047–3057, 2002.

[53] P.-Å. Albertsson. *Partition of cell particles and macromolecules.* Wiley-Interscience, New York, NY, 3rd edition, 1986.

[54] A. Shiloach and D. Blankschtein. Predicting micellar solution properties of binary surfactant mixtures. *Langmuir*, 14(7):1618–1636, 1998.

[55] Cosgrove M. S., C. Taylor, S. Paludan, M. J. Adams, and H. R. Levy. On the mechanism of the reaction catalyzed by glucose-6-phosphate dehydrogenase. *Biochemistry*, 37:2759–2767, 1998.

[56] Özer. N., Y Aksoy, and H. Ögus. Kinetic properties of human placental glucose-6-phosphate dehydrogenase. *International Journal of Biochemistry and Cell Biology*, 33:221–226, 2001.

[57] P. Rowland, A. K. Basak, S. Gover, H. R. Levy, and M. J. Adams. The three-dimensional structure of glucose-6-phosphate dehydrogenase from *Leuconostoc mesenteroides* refined at 2.0 Å resolution. *Structure*, 2(11):1073–1087, 1994.

[58] F. H. Lojudice, D. P. Silva, N. I. T. Zanchin, C. C. Oliveira, and A. Pessoa Jr. Overexpression of glucose-6-phosphate dehydrogenase in genetically modified *Saccharomyces cerevisiae*. *Applied Biochemistry and Biotechnology*, 91-93:161–169, 2001.

[59] B. Champluvier and M.-R. Kula. Dye-ligand membranes as selective adsorbents for rapid purification of enzymes: a case study. *Biotechnology and Bioengineering*, 40(1):33–40, 1992.

[60] Y. K. Chang, G. E. McCreath, and H. A. Chase. Development of an expanded bed technique for an affinity purification of G6PDH from unclarified yeast cell homogenates. *Biotechnology and Bioengineering*, 48(4):355–366, 1995.

[61] Y. K. Chang and H. A. Chase. Ion exchange purification of G6PDH from unclarified yeast cell homogenates using expanded bed adsorption. *Biotechnology and Bioengineering*, 49(2):204–216, 1996.

[62] E. L. Gelamo and M. Tabak. Spectroscopic studies on the interaction of bovine (BSA) and serum (HSA) albumins with ionic surfactants. *Spectrochimica Acta A*, 56(11):2255–2271, 2000.

[63] M. Sen, S. P. Mitra, and D. K. Chattoraj. Thermodynamics of binding cationic detergents to bovine serum albumin. *Colloid Surface*, 2:259–275, 1981.

[64] T. C. McIlvaine. A buffer solution for colorimetric comparison. *Journal of Biological Chemistry*, 49:183–186, 1921.

[65] H. U. Bergmeyer. *Methods of Enzymatic Analysis*, volume 2. Verlag Chemie, Weinheim, Germany, 3rd edition, 1983.

[66] M. Tsubouchi, H. Mitsushio, and N. Yamasaki. Determination of cationic surfactants by two-phase titration. *Analytical Chemistry*, 53:1957–1959, 1981.

[67] M. Cardamone, N. K. Puri, W. H. Sawyer, R. J. Capon, and M. R. Brandon. A spectroscopic and equilibrium binding analysis of cationic detergent-protein interactions using soluble and insoluble recombinant porcine growth hormone. *Biochimica et Biophysica Acta*, 1206:71–82, 1994.

[68] E. D. Goddard and K. P. Ananthapadmanabhan. *Interactions of surfactants with polymers and proteins.* CRC Press, Boca Raton, FL, 1993.

[69] J. R. Brown and P. Shockley. *Lipid-protein interactions*, volume 1. Wiley-Interscience, New York, NY, 1982.

[70] P. A. Alred, A. Kozolowski, M. Harris, and F. Tjerneld. Application of temperature-induced phase partitioning at ambient temperature for enzyme purification. *Journal of Chromatography A*, 659:289–298, 1994.

[71] A. A. Bhide, R. M. Patel, J. B. Joshi, and V. G. Pangarkar. Affinity partitioning of enzymes using unbound triazine dyes in PEG/phosphate system. *Separation Science and Technology*, 30:2989–3000, 1995.

[72] P. Bailon, G. K. Ehrlich, Fung W.-J., and W. Berthold. *Affinity chromatography: methods and protocols.* Methods in molecular biology; v. 147. Humana Press, Totowa, NJ, 2000.

[73] L. Stryer. *Biochemstry.* W. H. Freeman, New York, NY, 4th edition, 1995.

[74] P. Cuatrecasas, M. Wilchek, and C. B. Anfinsen. Selective enzyme purification by affinity chromatography. *Proceedings of the National Academy of Science, U. S. A.*, 61:636–643, 1968.

[75] M. N. Gupta. *Methods for affinity-based separations of enzymes and proteins.* Birkhauser Verlag, Basel, Switzerland, 2002.

[76] G. Lilius, M. Persson, L. Bülow, and K. Mosbach. Metal affinity precipitation of proteins carrying genetically attached polyhistidine affinity tails. *European Journal of Biochemistry*, 198:499–504, 1991.

[77] B. Mattiasson and M. Rampstorp. Ultrafiltration affinity purification: isolation of concanavalin A from seeds of *Canavalia ensiformis*. *Journal of Chromatography*, 283:323–330, 1984.

[78] B. D. Kelley, D. I. C. Wang, and T. A. Hatton. Affinity-based reversed micellar protein extraction. 1. principles and protein ligand systems. *Biotechnology and Bioengineering*, 42(10):1199–1208, 1993.

[79] T. Abudiab and R. R. Beitle Jr. Preparation of magnetic immobilized metal affinity separation media and its use in the isolation of proteins. *Journal of Chromatography A*, 795:211–217, 1998.

[80] G. E. Wuenschell, E. Naranjo, and F. H. Arnold. Aqueous two-phase metal affinity extraction of heme proteins. *Bioprocess Engineering*, 5(5):199–202, 1990.

[81] J. Turkovâa. *Bioaffinity chromatography.* Journal of chromatography library ; v. 55. Elsevier, New York, NY, 2nd edition, 1993.

[82] M. T. W. Hearn and D. Acosta. Applications of novel affinity cassette methods: use of peptide fusion handles for the purification of recombinant proteins. *Journal of Molecular Recognition*, 14:323–369, 2001.

[83] S. D. Flanagan and S. H. Barondes. Affinity partitioning: method for purification of proteins using specific polymer-ligands in aqueous polymer two-phase systems. *Journal of Biological Chemistry*, 250(4):1484–1489, 1975.

[84] U. Sivars, J. Abramson, S. Iwata, and F. Tjerneld. Affinity partitioning of a poly(histidine)-tagged integral membrane protein, cytochrome bo(3) ubiquinol oxidase, in a detergent-polymer aqueous two-phase system containing metal-chelating polymer. *Journal of Chromatography B*, 743:307–316, 2000.

[85] T. Saitoh and W. L. Hinze. Use of surfactant-mediated phase-separation (cloud point extraction) with affinity ligands for the extraction of hydrophilic proteins. *Talanta*, 42(1):119–127, 1995.

[86] M. B. Linder, M. Qiao, F. Laumen, K. Selber, T. Hyytiä, T. Nakari-Setälä, and M. E. Penttilä. Efficient purification of recombinant proteins using hydrophobins

as tags in surfactant-based two-phase systems. *Biochemistry*, 43(37):11873–11882, 2004.

[87] K. Selber, F. Tjerneld, A. Collén, T. Hyytiä, T. Nakari-Setälä, M. Bailey, R. Fagerström, J. Kan, J. van der Laan, M. Penttilä, and M.-R. Kula. Large-scale separation and production of engineered proteins, designed for facilitated recovery in detergent-based aqueous two-phase extraction systems. *Process Biochemistry*, 39:889–896, 2004.

[88] K. Terpe. Overview of tag protein fusions: From molecular and biochemical fundamentals to commercial systems. *Applied Microbiology and Biotechnology*, 60(5):523–533, 2003.

[89] C. Winterhalter, P. Heinrich, A. Candussio, G. Wich, and W. Liebl. Identification of a novel cellulose-binding domain within the multidomain 120 kDa xylanase XynA of the hyperthermophilic bacterium *Thermotoga maritima*. *Molecular Microbiology*, 15(3):431–444, 1995.

[90] A. B. Boraston, A. L. Creagh, M. M. Alam, J. M. Kormos, P. Tomme, C. A. Haynes, R. A. J. Warren, and D. G. Kilburn. Binding specificity and thermodynamics of a family 9 carbohydrate-binding module from *Thermotoga maritima* xylanase 10A. *Biochemistry*, 40(21):6240–6247, 2001.

[91] M. Kavoosi, J. Meijer, E. Kwan, A. L. Creagh, D. G. Kilburn, and C. A. Haynes. Inexpensive one-step purification of polypeptides expressed in *Escherichia coli* as fusions with the family 9 carbohydrate-binding module of xylanase 10A from *T. maritima*. *Journal of Chromatography B*, 807(1):87–94, 2004.

[92] Crameri A., E. A. Whitehorn, E. Tate, and W. P. Stemmer. Improved green fluorescent protein by molecular evolution using DNA shuffling. *Nature Biotechnology*, 14(3):315–319, 1996.

[93] O. Shimomura, F. H. Johnson, and Y. Saiga. Extraction, purification and properties of aequorin, a bioluminescent protein from the luminous *hydromedusan, Aequorea*. *Journal of Cell and Comparative Physiology*, 59:223–239, 1962.

[94] D. Balzer and H. Lüders. *Nonionic surfactants: alkyl polyglucosides*. Surfactant science series ; v. 91. Marcel Dekker, New York, NY, 2000.

[95] R. M. Garavito and D. Picot. Crystallization of membrane proteins: a minireview. *Journal of Crystal Growth*, 110(1-2):89–95, 1991.

[96] C. K. Lee and W. D. Su. Nonionic surfactant-mediated affinity cloud-point extraction of vancomycin. *Separation Science and Technology*, 34(16):3267–3277, 1999.

[97] J. Sambrook and D. W. Russell. *Molecular cloning: a laboratory manual*. Cold Spring Harbor Laboratory Press, Cold Spring Harbor, NY, 2001.

[98] G. Briganti, S. Puvvada, and D. Blankschtein. Effect of urea on micellar properties of aqueous solutions of nonionic surfactants. *Journal of Physical Chemistry*, 95(22):8989–8995, 1991.

[99] A. Cordes, J. Flossdorf, and M. R. Kula. Affinity partitioning: development of mathematical model describing behavior of biomolecules in aqueous two-phase systems. *Biotechnology and Bioengineering*, 30(4):514–520, 1987.

[100] S. S. Suh and F. H. Arnold. A mathematical model for metal affinity protein partitioning. *Biotechnology and Bioengineering*, 35(7):682–690, 1990.

[101] M. L. Shuler and F. Kargi. *Bioprocess engineering: basic concepts*. Prentice Hall, Upper Saddle River, NJ, 2nd edition, 2002.

[102] S. Puvvada and D. Blankschtein. Molecular-thermodynamic approach to predict micellization, phase behavior and phase separation of micellar solutions: 1. application to nonionic surfactants. *Journal of Chemical Physics*, 92(6):3710–3724, 1990.

[103] M. A. Hink, R. A. Griep, J. W. Borst, A. van Hoek, M. H. M. Eppink, A. Schots, and A. J. W. G. Visser. Structural dynamics of green fluorescent protein alone and fused with a single chain Fv protein. *Journal of Biological Chemistry*, 275(23):17556–17560, 2000.

[104] V. Notenboom, A. B. Boraston, D. G. Kilburn, and D. R. Rose. Crystal structures of the family 9 carbohydrate-binding module from *Thermotoga maritima* xylanase 10A in native and ligand-bound forms. *Biochemistry*, 40(21):6248–6256, 2001.

[105] T. C. V. Penna, P. G. Mazzola, and A. M. S. Martins. The efficacy of chemical agents in cleaning and disinfection programs. *BMC Infectious Diseases*, 1:16, 2001.

[106] P. G. Mazzola, T. C. V. Penna, and A. M. S. Martins. Determination of decimal reduction time (D value) of chemical agents used in hospitals for disinfection purposes. *BMC Infectious Diseases*, 3:24, 2003.

[107] T. C. V. Penna, M. Ishii, L. O. Nascimento, A. Pessoa Jr., and O. Cholewa. Thermal stability of recombinant green fluorescent protein (GFPuv) at various pH values. *Applied Biochemistry and Biotechnology*, 114(16):469–484, 2004.

[108] B. A. Eagerman and A. H. Rouse. Heat inactivation temperature-time relationships for pectinesterase inacvation in citrus juices. *Journal of Food Science*, 41:1396–1297, 1976.

[109] M. Villamiel, R. López-Fandino, N. Corzo, and A. Olano. Denaturation of beta-lactoglobulin and native enzymes in the plate exchanger and holding tube section during continuous flow pasteurization of milk. *Food Chemistry*, 58:49–52, 1997.

[110] P. Piyasena, S. Liou, and McKellar R. C. Predictive modeling of inactivation of *Listeria ssp.* in bovine milk during high-temperature short-time pasteurization. *International Journal of Food Microbiology*, 39:167–173, 1998.

[111] J. L. Forsyth, R. K. O. Apenten, and D. S. Robinson. The thermostability of purified isoperoxidases from *Brassica oleracea var. gemmifera*. *Food Chemistry*, 65:99–109, 1999.

[112] L. M. M. Tijskens, P. S. Rodis, M. L. A. T. M. Hertog, N. Proxenia, and C. van Dijk. Actvity of pectin methyl esterase during blanching of peaches. *Journal of Food Engineering*, 39:167–177, 1999.

[113] C. Dennison and R. Lovrien. Three phase partitioning: concentration and purification of proteins. *Protein Expression and Purification*, 11:149–161, 1997.

[114] T. C. V. Penna, M. Ishii, A. Pessoa Jr., L. C. de Souza, and O. Cholewa. Evaluation of recombinant green fluorescent protein (GFPuv) purification with various HiTrap HIC resins. *Applied Biochemistry and Biotechnology*, 114(16):453–468, 2004.

[115] P. K. Smith, R. I. Krohn, G. T. Hermanson, A. K. Mallia, F. H. Gartner, M. D. Provenzano, E. K. Fujimoto, N. M. Goeke, Olson B. J., and D. C. Klenk. Measurement of protein using bicinchoninic acid. *Analytical Biochemistry*, 150(1):76–85, 1985.

[116] G. B. Fields, D. O. V. Alonso, D. Stigter, and K. A. Dill. Theory for the aggregation of proteins and copolymers. *Journal of Physical Chemistry*, 96:3974–3981, 1992.

[117] L. R. Young, A. L. Fink, and K. A. Dill. Aggregation of globular proteins. *Accounts of Chemical Research*, 26:614–620, 1993.

[118] P. Gupta, C. K. Hall, and A. C. Voegler. Effect of denaturant and protein concentrations upon protein refolding and aggregation: a simple lattice model. *Protein Science*, 7:2642–2652, 1998.